GEOLOGY AND GEOCHEMISTRY OF THE MAYO-DARLÉ TIN
DEPOSIT, WEST-CENTRAL CAMEROON, CENTRAL AFRICA

By

François Roger Nguene

Submitted in Partial Fulfillment of
the Requirements for the Degree of
Doctor of Philosophy

New Mexico Institute Of Mining And Technology
Socorro, New Mexico
April 1982

ACKNOWLEDGMENTS

ABSTRACT

The Mayo-Darlé complex occurs along the Cameroon Line (a strike-slip zone) and intrudes Pan-African orogenic belt metasediments and metavolcanics. The complex consists of a differentiated alkalic suite of rocks including benmoreite, alkali syenite (nordmarkite), rhyolite, alkali biotite granite and granite porphyry. Whole rock Rb-Sr studies indicate that the complex intruded the metasediments 73 ± 6 m.y. ago with a $^{87}Sr/^{86}Sr$ initial ratio of 0.7030 ± 0.0035 based on the syenite isochron. The surrounding metasediments were dated to 614 ± 20 m.y. with a $^{87}Sr/^{86}Sr$ initial ratio of 0.7059 ± 0.0007.

Tin mineralization occurs as porphyry-type stockwork veinlets with grades up to 0.3% SnO_2, and as high-grade (2-20% SnO_2) vertical and horizontal greisen veins within the host alkali biotite granite. Secondary ore is restricted to paleofluvial and/or lacustrine conglomerates directly overlying the granite, and residual occurrences due to in situ weathering of the mineralized stockwork veinlets within the granite.

Primary mineralization occurs as sub-millimeter to meter-wide vertical quartz-cassiterite lodes and horizontal or subhorizontal quartz-cassiterite veins (up to 30 cm thick) with minor topaz and zinnwaldite. The vertical veins are centered around highly silicified breccia pipes. These breccia pipes are barren of cassiterite. Alteration consists of greisenization, silicification, chloritization,

and hematization. Zones of intense kaolinization up to hundreds of meters in diameter occur nearby, but they are not centered on primary tin mineralization.

Fluid inclusion studies indicate mineralization by Na-Cl-F rich brines up to 65 eq. wt. % NaCl over temperature ranges of 550 to 300°C. Episodic boiling of mineralizing fluids, probably due to periods of pressure changes, occurred over temperature ranges of 520 to 320°C. Periodic fluctuations of pressures between lithostatic and hydrostatic conditions caused by episodic magma overpressures caused the fracturing of the solidified granite. It is postulated that the fracture system was reactivated by a late intrusive at depth. Fluids evolving from such an intrusive ascended through the host granite, scavenging tin from tin-bearing minerals (biotite, amphiboles, magnetite, ilmenite, sphene). The mineralizing fluids interacted with the granite imparting upon it the special features which commonly characterize granites associated with tin mineralization (high SiO_2, high K, high Rb, and high $^{87}Sr/^{86}Sr$ initial ratios).

TABLE OF CONTENTS

LIST OF ILLUSTRATIONS

LIST OF TABLES

CHAPTER 1. INTRODUCTION

1.1 STATEMENT OF PROBLEMS

Because of its young age and good surface exposure, the Mayo-Darlé tin deposit provides an opportunity for a thorough investigation of the process of Sn mineralization as related to granite magmatism. This study was undertaken with the following objectives in mind:

1. This virtually unstudied deposit was to be described. Primary mineralization at Mayo-Darlé remains undisturbed by either mining activities or weathering processes; this facilitates the evaluation of processes which brought about Sn deposition in this setting.

2. The genesis of the granite and its relationship with Sn mineralization were to be determined. The genetic link between primary tin deposits and granitoids and their volcanic equivalents has gained worldwide acceptance (Taylor, 1979). Sn mineralization relates to granitoids both spatially and temporally. The understanding of mineralization processes at Mayo-Darlé must parallel the deciphering of the genetic characteristics of the granite associated with tin mineralization. Was the source material of mantle or crustal origin? Which processes were responsible for magma generation: partial melting or fractional crystallization or both? Why do some special features such as high SiO_2, K, Rb, and high $^{87}Sr/^{86}Sr$

initial ratios occur in granites associated with tin mineralization?

3. Conditions prevailing during mineralization were to be determined. Which role do high-temperature, high-salinity "magmatic" fluids play in the deposition of tin ores?

4. The relationship between tin mineralization and tensional tectonics was to be investigated.

1.2 REGIONAL GEOLOGICAL SETTING

Cameroon forms a link between the regions of west and central Africa. The geology of Cameroon is summarized by Cahen and Snelling (1966). A folded and metamorphosed basement is unconformably overlain by a practically horizontal sedimentary cover of Lower Cretaceous to Quaternary age. The basement may be subdivided into three major units (Fig. 1): 1)the Lower Precambrian consists of mica-schists, charnockite gneisses, and granites which form the Cameroon-Gabon Archean-Proterozoic nucleus of 2.8 to 1.8 billion years (Lasserre, 1964, 1975, 1976, 1978, 1981), which extends over 20,000 km^2 in southern Cameroon (Fig. 1); 2)the undifferentiated Precambrian formations, and 3)the Late Precambrian-Early Cambrian granites, metasediments, and metavolcanics of 550 ± 100 m.y. (Lasserre, 1964; Lasserre and Soba, 1976) which extend from the south-central plateau to the Chad basin (Fig. 1). Post-tectonic intrusions of

Paleocene-Eocene age, 60 to 40 m.y., occur as granite-syenite complexes in West-Cameroon along the Cameroon-Nigeria border. Tertiary to Recent-aged magmatism in Cameroon is associated with zones of epeirogenic uplift accompanied by intrusions of alkalic composition. These intrusions have been interpreted as being localized along preexisting faults (Black and Girod, 1970).
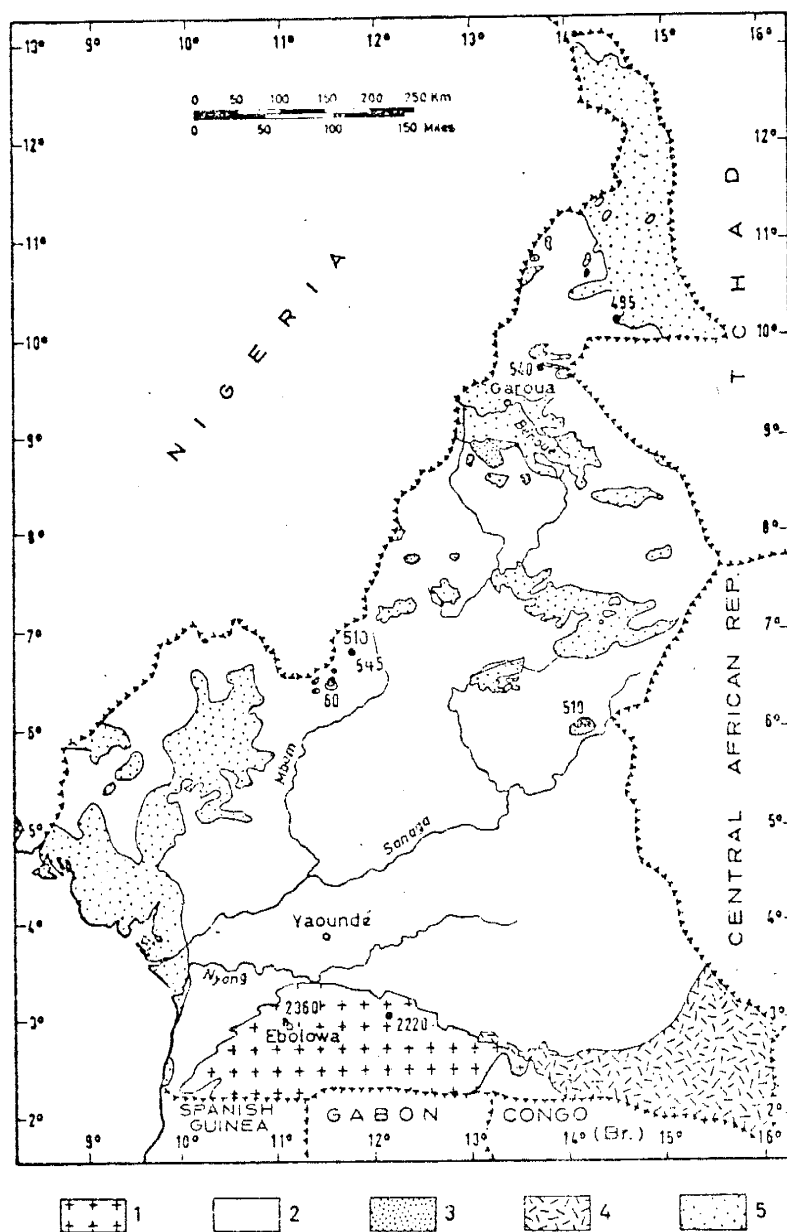
Fig. 1. Location and age of basement units in Cameroon. 1: Charnockitic massif; 2: Undifferentiated Precambrian, 560 $\pm$ 20 m.y.; 3: Post-tectonic granites; 4: Upper Precambrian beds; 5: Cretaceous and Younger (Adapted from Cahen and Snelling, 1966).

Tertiary-aged caldera complexes form a NNE trend of high heat flow indicated by the presence of oceanic islands Sao Thome and Fernando Po, and the active volcano Mount Cameroon on the continent. This trend is known as the "Cameroon Line," a strike-slip shear zone (Fig. 2). The Cameroon volcanic zone is considered a zone of incipient rifting (Burke et al., 1971). Intrusive complexes along the Cameroon Line are similar to the Jurassic-aged, alkali complexes in Nigeria (Wright, 1970; Black, 1957), and consist of gabbros, diorites, syenites, granites, and their extrusive equivalents. A major regional tectonic feature, the "Benue Trough", occurs west of the Cameroon Line (Fig. 3). The Benue Trough was formed during the Cretaceous Period as a failed arm of the three arm rift developed as a triple junction joining South America and Africa (Burke et al., 1971). Geophysical studies suggest that The Benue Trough, filled by over 5000 m of Cretaceous sediments, was initially a rift valley bounded by east-northeasterly faults, a direction which coincides with that of preexisting transcurrent faulting (Cratchley and Jones, 1965).
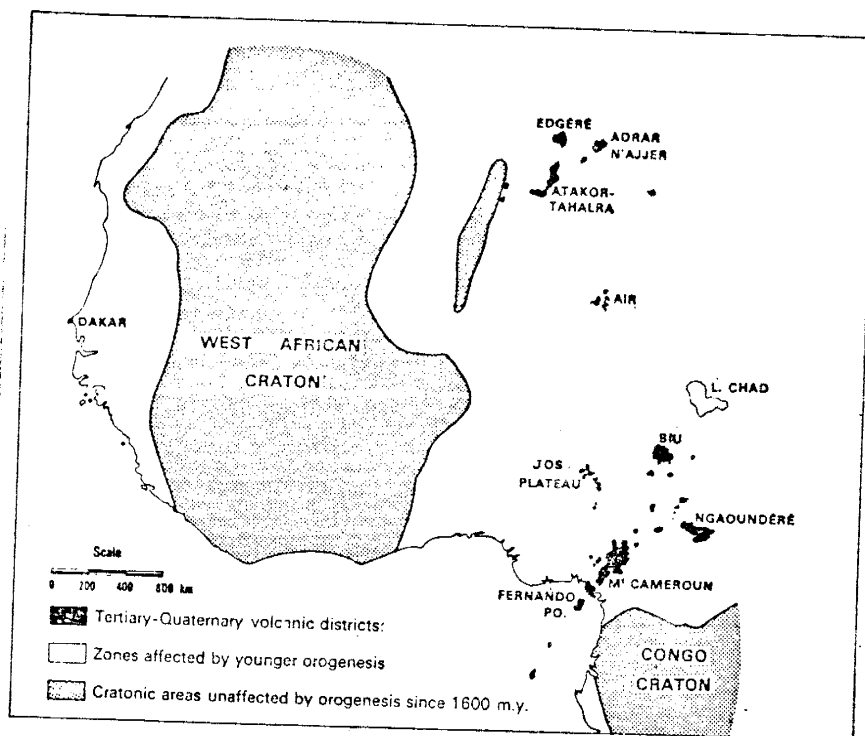
Fig. 2. Distribution of Tertiary volcanism in West-Africa. Location of the "Cameroon Line" (Adapted from Clifford, 1970).
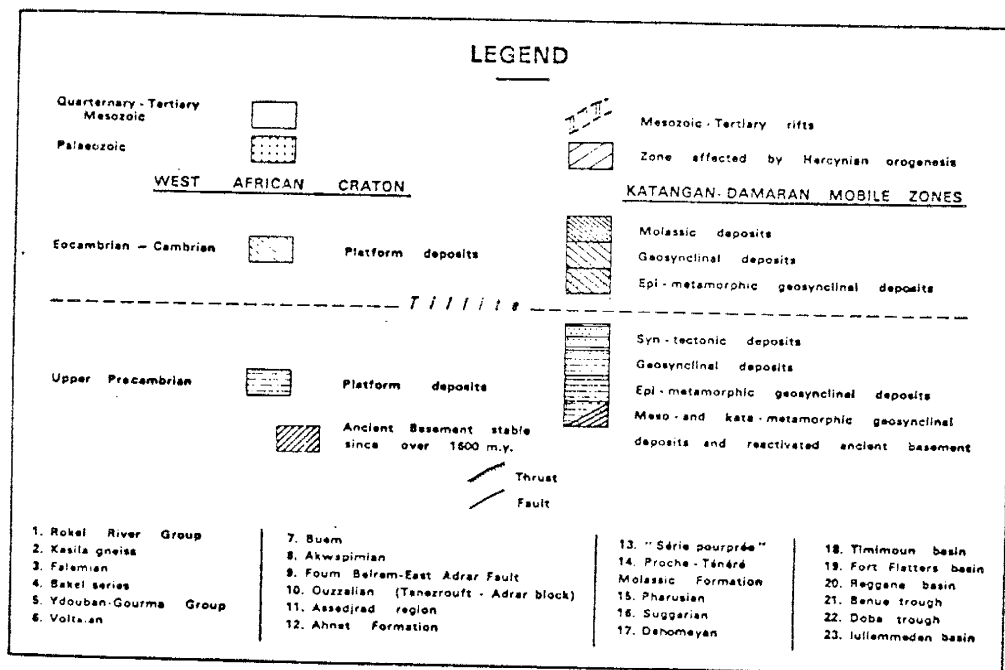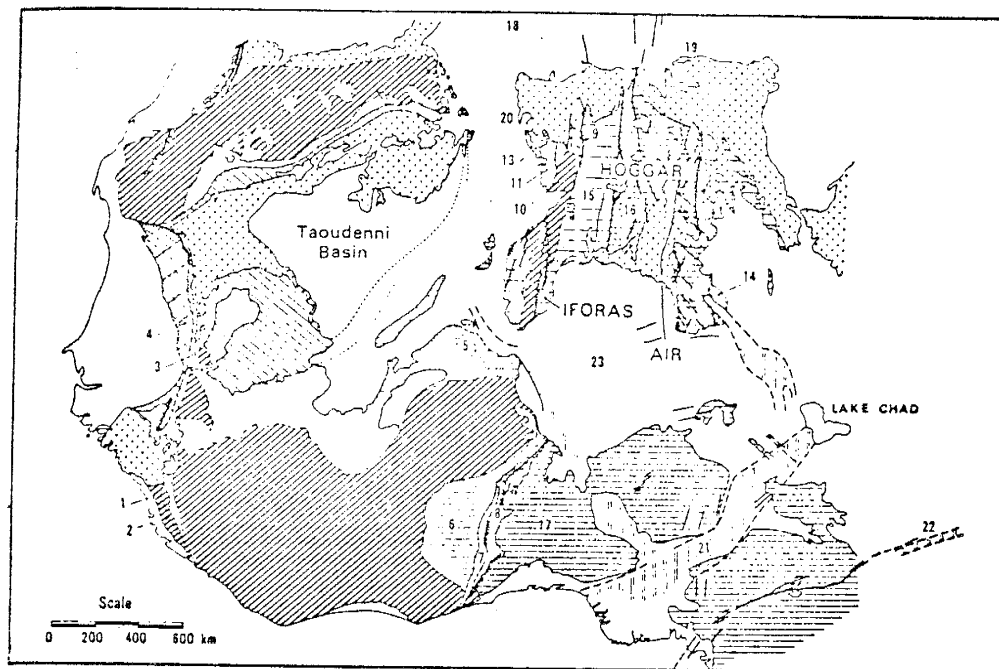
Fig. 3. Structural Map of West-Africa (Adapted from Clifford, 1970).

1.3   HISTORY OF MINING AT MAYO-DARLÉ

The Mayo-Darlé tin mine is located on the Cameroon Line, 165 km NE of Foumban and 60 km SW of Banyo, on the hinge of the Adamaoua plateau in West Central Cameroon. The Mayo-Darlé complex is composed of NE-NNE oriented, interconnected heights which form a large massif. The altitude of the Mayo-Darlé massif is 1700 m. The difference in elevation between the Tikar plains in the south is 900 m.

Mineralization at Mayo-Darlé was first reported in 1927; production began in 1933 and peaked from 1965 to 1967 at a yearly output of 58.71 tons of SnO_2 concentrate from mainly placer and residual deposits. Through December 1980, the mine yielded about 5000 tons of cassiterite concentrate (Archives of the Cameroon Ministry of Mines and Power, Mayo-Darlé mine record books). Reconnaissance prospecting surveys were carried out in the immediate vicinity of the mine, but no further economic placer discoveries were made. Current mining activity is reduced to a small artisanal operation. Large volumes of soils and weathered granites are abated and water-washed; the concentrate amounts to about 70% SnO_2. Other mineralization associated with the Cameroon Line is molybdenum, tungsten, fluorite, niobium, tantalum, and minor gold (Laplaine, 1969).

1.4   PREVIOUS STUDIES AT MAYO-DARLE

A reconnaissance geology survey of West-Central Cameroon was carried out by Koch (1953, 1959). The scope of his studies encompassed all crystalline rocks of the region. Thus there was no detailed investigation at any given locality. Even though Mayo-Darlé is the most discussed of the "younger granites" of Cameroon, reference to its geology still refers to Koch's (1959) sketchy descriptions. Koch (1959) described a medium to coarse-grained, pinkish to white, biotite granite which intrudes the metamorphic rocks. A minor peralkaline variety, riebeckite granite, occurs in association with biotite granite. Minor porphyry phases occur in association with the main granite body. Microscopic examinations revealed perthitic microcline as the main potassium feldspar. Accessories identified were fluorite, zircon, sphene (rare), and magnetite.

Koch (1959) inferred that Sn mineralization was related to the host granite. He identified two types of greisen veins on the basis of abundance of zinnwaldite and chlorite in the veins. Structurally, Koch (1959) distinguished horizontal, inclined and vertical mineralized veins cross-cutting the granite.

Gazel, Lasserre, Limasset, and Vachette (1963) determined an age of 65 $\pm$ 12 m.y. for the granite associated with tin mineralization by a non-isochron Rb-Sr method. Cantagrel et al. (1978) determined a K/Ar age of 49 $\pm$ 1 m.y. for the Mayo-Darlé granite. Lasserre (1978) determined a whole-rock Rb-Sr isochron age of 63.3 $\pm$ 1.3 m.y. with a $^{87}Sr/^{86}Sr$

initial ratio of 0.7027 ± 0.0011 from samples from Mayo-Darlé and Mba Namboé, 35 km SW of Mayo-Darlé. A mantle source for these granites was inferred from this low isotopic strontium initial ratio.

Many exploration projects have been carried out around Mayo-Darlé (Archives, Cameroon Ministry of Mines and Power). The lastest project was undertaken by Morawietz (1968). In his conclusions Morawietz (1968) recommended a more detailed investigation of the geology around the deposit if further developments in the mine were to be realized.

1.5 METHODS OF INVESTIGATION

Five months were spent on field studies to produce a geologic map with sufficient detail to help in sorting out the relations between the various rock units of the complex. Field studies also encompassed the investigation of the spatial and temporal links between the granite and tin mineralization. Special emphasis was put on the description of physical features of the deposit such as the nature of mineralization, structural controls, and alteration. Samples were collected for petrographic and geochemical studies.

Samples of the various rock units were studied in thin sections and were analyzed for major and trace elements by x-ray fluorescence and atomic absorption, and instrumental

neutron activation, respectively. Mineralogy as inferred from thin section studies and chemical variation diagrams were used to classify the various rock types. Rb-Sr whole rock analyses were carried out on the metasediments and the igneous rocks. Isochrons were determined for all rock units.

Major element chemistry, trace elements, and strontium isotope data were used in modeling studies to determine the processes responsible for magma generation, the source of the magma and the degree of crustal contamination.

Fluid inclusion microthermometry analyses were carried out on quartz from mineralized veins and on quartz from the granite. Conditions during mineralization, such as temperature and salinities of mineralizing fluids, pressure, and depth during entrapment of these fluids, were inferred from microthermometry analyses. Rb-Sr isotope measurements were made on inclusion waters in quartz.

CHAPTER 2. GEOLOGY OF THE MAYO-DARLÉ COMPLEX

2.1 PETROGRAPHY

2.2.1 Late Precambrian Basement rocks

Late Precambrian basement rocks cover about two-thirds of the study area (Fig. 4). The basement rocks consist mainly of biotite gneiss and quartz diorite gneiss. Local varieties such as biotite-hornblende gneiss and garnet gneiss are present.

Biotite gneiss and biotite-hornblende gneiss

Biotite gneiss composes about half of the exposed metamorphic rocks around Mayo Darlé. The rocks are medium to coarse grained. Gneissic foliation is well developed. Light, quartz-feldspathic layers, few millimeters to 2 cm wide alternate with dark, mostly micaceous (biotite) layers. The direction of foliation is NE-NNE and the dips average 35° to the NW. Massive to slightly foliated varieties occur sparsely. The texture varies locally to "sub-augen" with rimmed quartz and feldspar eyes up to 2 cm in diameter. The biotite gneiss is locally cut by quartz and diabase veins. Quartz veins are observed in abundance near the contacts with the intruding granite. Modal composition is 20 to 30 percent quartz, 15 to 30 percent K-feldspar, 5 to 40 percent plagioclase, 10 to 15 percent biotite and 5 percent

hornblende; no kyanite or sillmanite was observed in thin sections. Accessory minerals are zircon, magnetite, and apatite.

Thin section examinations show the overall percentage of quartz and K-feldspar to increase near the contact with the granite body. Alteration of biotite and hornblende to chlorite and magnetite is common. K-feldspar commonly alters to sericite. Samples of the GN-X-80 series in the northern part of the study area are relatively poor in plagioclase (5 to 10 percent), while the MDJ-X-80 series, outcropping in the southeast corner, are relatively rich in plagioclase (20 to 40 percent). Plagioclase porphyroblasts show well to poorly developed albite twinning. Estimated composition of plagioclase ranges from An_{15-25} to An_{45}. K-feldspar and plagioclase occur as euhedral to subhedral crystals. Both orthoclase and microcline are present. Most microcline exhibits microperthitic textures. Braided and string microperthites are common. Quartz occurs as rounded to stretched crystals exhibiting undulatory extinction and microfracturing. Locally quartz occurs as xenoblastic crystals intergrown with plagioclase and K-feldspar. Quartz also occurs as lenticular inclusions in plagioclase. Biotites occur as platy, elongate crystals showing a preferred orientation. Hornblende is present as large (110) and (100) sections. The overall texture in thin section is porphyroblastic.

Quartz-diorite gneiss and garnet gneiss

In the eastern part of the study area, a fairly homogeneous white-grey to greenish, massive to slightly foliated, fine to medium-grained, quartz-diorite gneiss is in contact with the granite. This homogeneous body occurs over a lateral distance of at least 3 km. Locally spheroidal weathering patterns obscure the foliation direction. The apparent homogeneity of this unit (PG-X-80 sample suites) does locally grade to a more pronounced gneissic texture. This texture is characterized by alternating layers and/or lenticles, 2 to 3 cm thick, of felsic and mafic composition. Some of these interlayered felsic and mafic units have 2 to 3 percent garnet and were termed garnet gneiss. Locally, and most frequently near the contact with intrusive rocks, the quartz-diorite gneiss is cut by small quartz- filled veinlets. The quartz diorite gneiss is cut by sulfide- rich, diabase veins. The sulfide phase seems to be localized in diabase veins cross-cutting the country rocks. No sulfide phase has been observed in association with tin mineralization.

The quartz-diorite gneisses are composed chiefly of 25 to 40 percent quartz, 25 to 50 percent plagioclase, 5 percent K-feldspar, and 3 percent hornblende. Accessory minerals are zircon, magnetite, apatite, and sillimanite. Zircon is evident in biotite by pleochroic haloes. Rounded, detrital zircon is also noticed. Sillimanite occurs as needle-like

crystals. In thin section the texture is porphyroblastic. Preferred orientation of biotite is not evident. Quartz occurs as anhedral to subhedral grains exhibiting undulatory extinction. Plagioclase is present as subhedral to euhedral crystals showing well developed albite twinning. Plagioclase averages An_{30} in composition, and myrmekitic fringes are present on some plagioclase grains. K-feldspar, mostly microcline, is very perthitic. String microperthites are common. Sericitization of plagioclase is common. Biotite alters to chlorite and magnetite. In the garnet gneiss sericitization of plagioclase is well pronounced, and minor muscovite is present.

Fig. 4. Geologic Map of the Mayo-Darlé complex.

THE MAYO-DARLE COMPLEX

EXPLANATION

Late Cretaceous Formations

- ▨ Granite Porphyry
- ▨ Biotite Granite
- ▨ Biotite-Riebeckite Granite
- ▨ Volcanics—Rhyolite dikes
- ▨ Volcanics—Rhyolite
- ▨ Syenite
- ▨ Quartz Syenite Porphyry

Precambrian Basement Complex

- ☐ Quartz-diorite Gneiss
- ☐ Garnet Gneiss (Leptite)
- ☐ Hornblende Biotite Gneiss
- ☐ Biotite Gneiss and undifferentiated

- ▨ Zone of intense chloritization
- ▨ Zone of intense kaolinization
- ▨ Zone of greisenization and disseminated mineralization
  Fz = Hydrothermal feeder zone
  Q = Quartz filled veins
- ✕ Vein system associated with major structural trend directions
- ▬ Diabase dikes
- ▬ Diabase dikes with sulphides
- ⌐40 Contact, showing dip
- ⌐40 Strike and dip of foliations
- ✛ Strike of vertical foliations
- ╱ Fault, dashed when inferred
- ⌇⌇⌇ Fault zone with evidence of shearing

Fig. 5.   NNW – SSE section across the Mayo-Darlé complex.

NNW
A

NYENINGA PETE
RIVER

RESERVOIR

HOSSERE DJANGA

HOSSERE GOMDJO

SSE
B

ELEVATION
(m)

2000
1500
1000

0   1   2 km

EXPLANATION

LATE CRETACEOUS FORMATIONS

GRANITE PORPHYRY

BIOTITE GRANITE

NORDMARKITE , QUARTZ SYENITE PORPHYRY

LATE PRECAMBRIAN METASEDIMENTS

BIOTITE AND QUARTZ DIORITE GNEISS

QUARTZ VEINS

PRESUMED PALEO-SURFACE
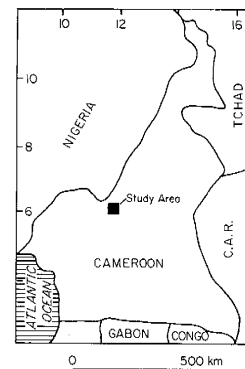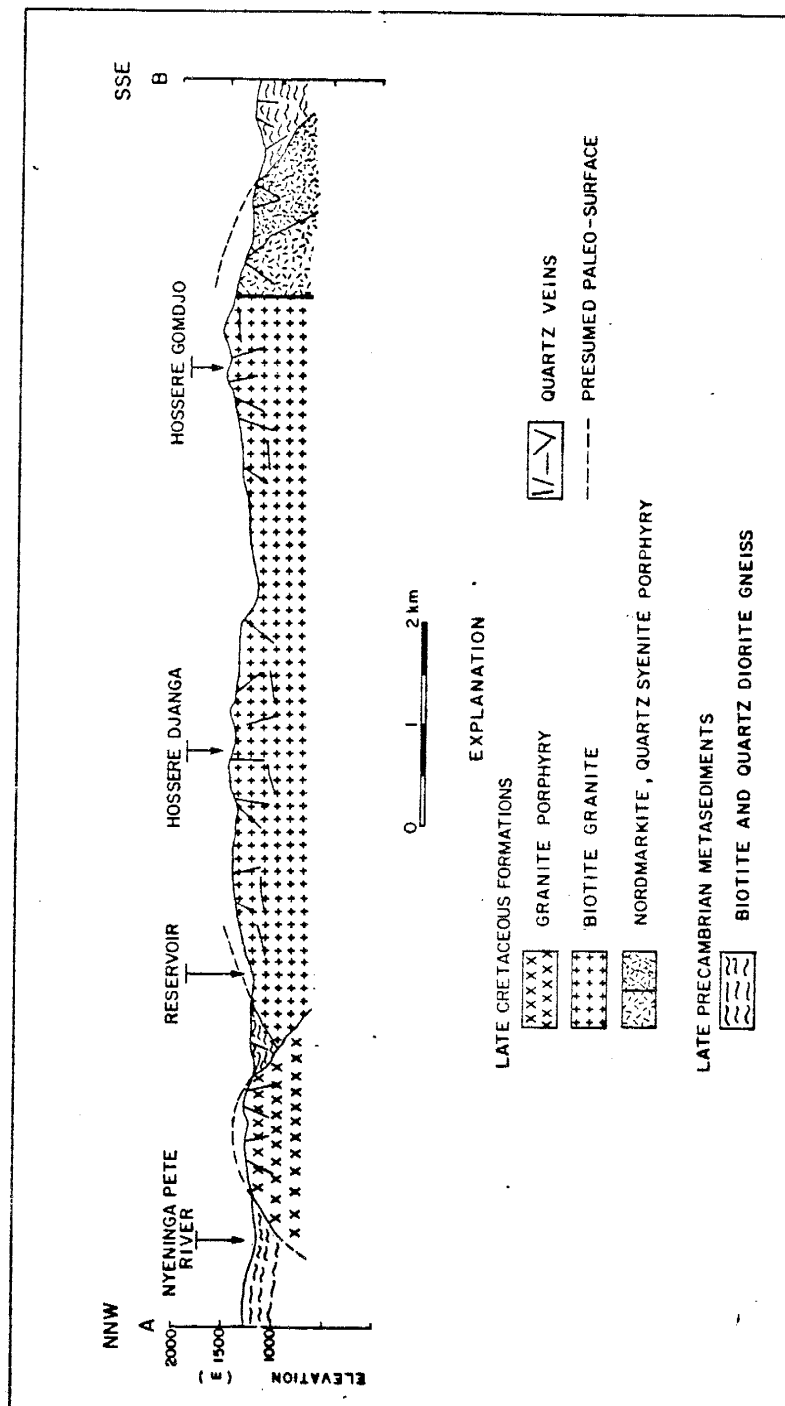
2.2.2 Late Cretaceous Igneous Series

The igneous rocks range in composition from syenite to granite and their respective porphyry equivalents (Fig. 4). The volcanic rocks are rhyolites. Granite is exposed over a nearly oval surface area of about 65 km^2, and is in faulted contact with the syenites. Rhyolite is not in contact with the granite; it overlies the biotite gneiss as a minor occurrence east of the granite stock. Granite porphyry crops out around the margins of the granite. This igneous rock suite intrudes the Late Precambrian metasediments and metavolcanics. No contact aureole was observed around the granite.

The various rock units are described in presumed order of intrusion or emplacement.

Quartz syenite and quartz syenite porphyry

The fault zone between the syenite and the granite is characterized by a silicified breccia composed of granite and syenite fragments. The transition quartz syenite and quartz syenite porphyry is not evident. Macroscopic patterns such as change of texture and relative abundance of quartz in hand specimen led to an inferred contact between the two syenite rocks. However, this contact may be gradational. Both rocks are equally rich in quartz; 5 to 15 percent. Microperthitic K-feldspar ranges from 70 to 80 percent of the rock. Plagioclase is less than 1 percent.

Hornblende, 5 percent of the rock, is the principal mafic mineral. Chlorite and magnetite are pseudomorphous after hornblende. Accessory minerals are zircon and apatite. Quartz is instertitial and forms granophyric intergrowths with feldspars. Orthoclase and microcline are present. Microcline crossed-hatched twinning is rare. Orthoclase shows Carlsbad twinning. Microperthites occur in higher density on the border of the orthoclase and microcline crystals. The center of the crystals are nearly homogeneous with but a few exsolution lamellae. Chlorite-magnetite micro-veinlets locally cut orthoclase crystals. The general texture is hypidiomorphic granular with mostly interlocked large tabular K-feldspar crystals.

Rhyolite

Rhyolite is exposed over 1 km^2 east of the granite stock. Mafic, aphanitic-appearing xenoliths are common. These xenoliths are angular in shape and vary in size from few millimeters up to 10 cm in diameter. Baked or chilled rims are developed around the xenoliths. This indicates that cold xenoliths were entrained within still hot and molten host material. Chemical analyses of these mafic inclusions suggest the xenoliths are of benmoreite composition.

Within the rhyolites, euhedral K-feldspar megacrysts occur singly through a very fine groundmass; this suggests a magmatic origin of the rock. Minute K-feldspar laths are randomly oriented within the groundmass and form a felty

texture. The felty texture of the rhyolitic rock and the baked or chilled margins around the benmoreite xenoliths suggest an extrusive nature for this formation. The size of the outcrops and the area extent of this unit do not permit one to trace the source from which these volcanics were erupted.

These rhyolites are coarsely porphyritic. Euhedral sanidine and rounded quartz phenocrysts occur in a very finedgrained microcrystalline groundmass made up of sanidine and quartz. Sanidine phenocrysts are locally associated with embayed quartz, thus forming a microgranophyric texture. Apatite and zircon are the only identified accessory minerals. Microveinlets of quartz transgressing earlier formed phenocrysts are visible under the microscope. Small amount of altered biotite and hornblende are present. Alteration products are chlorite and magnetite.

Biotite granite and biotite-riebeckite granite

Two granite types can be distinguished based on the presence of riebeckite. Biotite granite is the main variety and amounts to about 85 percent of the outcrop of the Mayo-Darlé granite (Fig. 4). The biotite-riebeckite granite crops out in the northwest corner of the igneous complex (Fig. 4). Because the contact between these two rock types was not exposed, the intrusive relationship is not clear and the contact between them was inferred. Biotite granite commonly occurs as a white-grey, medium-grained rock.

Fine-grained granites, though minor, occur sporadically around the margins of the main granite body. Coarse-grained granite is in contact with country rock along most of the granite margin.

Micropegmatitic veins are interspersed within the main body. Most outcrops consist of highly fractured rocks which gives the outcrops a blocky appearance. The directions of fracturing are NE and NW (Fig. 4). Both granite types are transgressed by quartz veins with the same orientation as the joint set. Greisen veins occur associated with tin mineralization in the northeast corner of the granite body. Greisen veins are generally restricted to the biotite granite. These veins are dealt with in more detail in the section treating tin mineralization. Modal composition of the biotite granite is 35 to 50 percent quartz, 30 to 40 percent microperthitic K-feldspar, and 5 to 10 percent biotite. Plagioclase is minor and often amount to 1 percent. Accessory minerals in both granite types are zircon, fluorite, magnetite, ilmenite, hematite, apatite, and monazite (rare). Chloritization of biotite is common. Microperthites form 20 to 30 percent of K-feldspar laths. Braid, string, and patch microperthites are observed. K-feldspar exhibits dark-grey interference colors. It was difficult to distinguish K-feldspars as either orthoclase or microcline. However, crystals showing cross-hatched twinning (albite and pericline laws) were readily identified as microcline. Based on the relative high density of such

sections, it was concluded that most K-feldspars hosting microperthites were microcline. Some microcline crystals exhibit typical albite twinning, though locally this twinning becomes gritty. K-feldspar contains small crystals of hornblende and/or biotite, resulting in a poikilitic texture.

Quartz and feldspar phenocrysts stand out in a fine to medium-grained matrix composed of interstitial quartz and feldspar. The overall texture is hypidiomorphic granular. Granophyric texture is common. Matrix quartz exhibits a slight undulatory extinction and locally forms rims around large quartz and feldspar grains. Quartz is clear and glassy; small cracks are visible under the microscope. Greenish brown biotite occurs as isolated crystals, but more commonly as aggregrates; dark pleochroic haloes are common in biotite. In the riebeckite-bearing variety, biotite is minor; riebeckite occurs as fibrous, elongated and prismatic, deep blue euhedral to subhedral crystals. Riebeckite in this variety would amount up to 15 percent in modal composition. Aegirine was mentioned in the riebeckite granite (Koch, 1959), but was not confirmed during examination of thin sections of this granite type. If present, aegirine is very rare.

Granite porphyry

Granite porphyry is characteristic of the margins of the large granite intrusion. It intrudes biotite gneiss. Two

units, located northwest and southeast of the granite, were recognized (Fig. 4). Mineralogically the granite porphyry is similar to the biotite granite. The texture is different: rounded to hexagonal quartz grains and euhedral to subhedral perthitic K-feldspar phenocrysts are present in a microcrystalline groundmass composed of quartz, K-feldspar, and hornblende. Most biotite and hornblende are altered to magnetite and chlorite. Microcline is the major K-feldspar present; it commonly exhibits cross-hatched twinning. Orthoclase phenocrysts show Carlsbad twinning. Granophyric intergrowths of feldspar and quartz are common.

2.2 STRUCTURAL GEOLOGY

The general trend of foliation within the basement gneisses at Mayo-Darlé is NE-NNE, paralleling the Cameroon line. The dip of foliations is variable (Fig. 4). Biotite gneisses cropping out on the northern part of the study area show a prevailing northwest dip averaging 35°. East of the granite intrusive, the foliation dips 30° southeast. The divergent dip directions suggest the existence of an anticline or doming of the gneiss by the intrusion.

Three major faults have been mapped in the area (Fig. 4). A faulted contact striking N 20 E separates the granite and the syenites. Evidences for faulting comprise a mylonitic zone characterized by fracturing of both rock types and subsequent cementation by silicification. A vertical

(normal) fault east of the granite strikes N 30 W. In the northeast corner of the granite, a vertical fault contact has been observed. In both instances, a change of the foliation dip from about 40° to almost vertical was observed. A NW trending zone of extensive shearing was observed within the granite (Fig. 4).

The jointing of the granite is by far the most impressive local structural feature. Most of the resulting fractures are filled with quartz, and in the mineralized areas, with quartz-cassiterite-topaz assemblages. Quartz-filled fractures intersect both igneous rocks and metasediments. This suggests that jointing and fracturing could post date granite crystallization and emplacement. The basement is also jointed similarly to the granite. This argues against cooling of the granite as a major mechanism responsible for the generation of these fractures. Tectonic forces and/or magma pressures probably caused these fractures. More recent movement is evidenced by the high density of small cracks associated with right lateral slips in the veins. This could be due to the influence of the general movement along the Cameroon line.

The directions of 168 vertical quartz and quartz-cassiterite veins were recorded. Although the rose diagram (Fig. 6) shows considerable variation, two predominant directions emerge: N 40 W and N 35 E. The two directions define a set of conjugate fractures. The two directions form a compressional acute angle of 75°. Stress orient-

ations σ_1 and σ_3 are inferred from the available data with σ_2 vertical (Fig. 7). A compression slightly west of north may have produced the two sets of shear fractures.
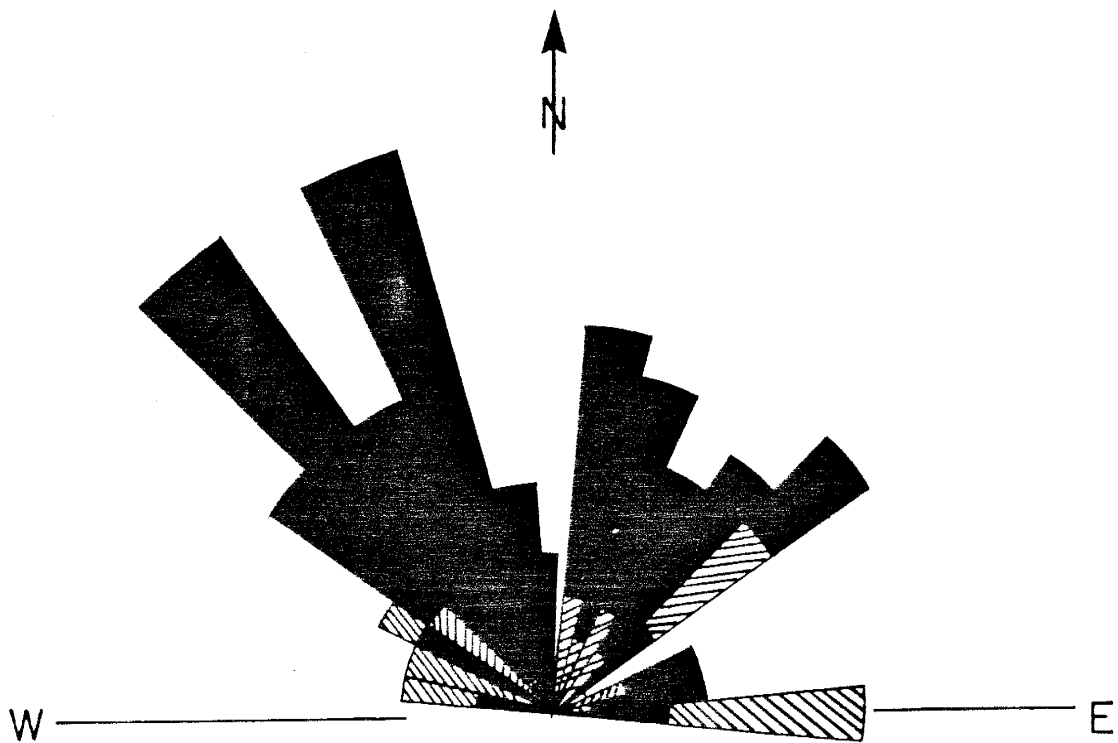
Fig. 6. Rose diagram of quartz and greisen veinlet strikes. Dark = veins and veinlets occurring within the granite. Hatched = strikes of veinlets within the metasediments.
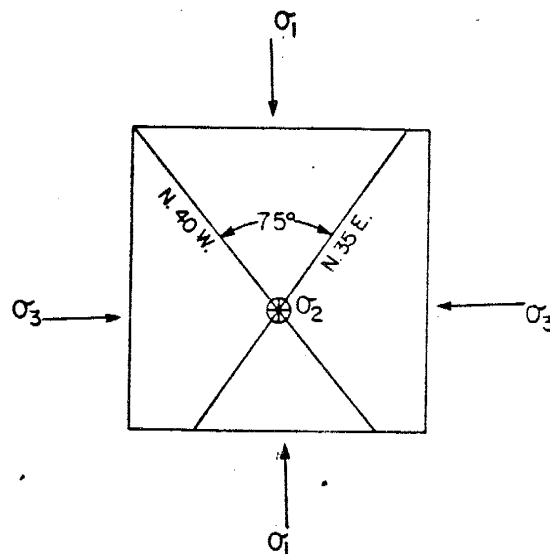
Fig. 7. Stress orientation diagram inferred from quartz veinlets within the granite.

The granite is fairly homogeneous. Since no field evidence for assimilation (presence of xenoliths) was observed, it seems likely that forceful injection was the probable mechanism of emplacement. The gentle dip (average 23°) of the granite/metasediments contacts suggests that only the uppermost part of the granitic dome is presently exposed on the erosional surface. Figure 5 shows a NNW-SSE section across the Mayo-Darlé complex.

CHAPTER 3.   PETROCHEMISTRY OF THE MAYO-DARLÉ IGNEOUS SERIES

Whole-rock major and trace element analyses of quartz syenite, rhyolite, granite, and granite porphyry are provided in Tables 1 and 2 of Appendix I. Details for techniques used are provided in the same appendix.

Modal compositions of the rocks and the major element rock chemistry were used to name the different rock types of the complex. Sorensen's (1974) classification scheme of alkali rocks and Cox, Bell, and Pankhurst (1979) rock classification based on total alkali versus SiO_2 were used. The Mayo-Darlé igneous rock suite forms an alkali complex characterized by high K_2O content (4.1 to 5.9) and K-feldspar as the predominant feldspar type. The complex based on the two previously mentioned classification schemes consists of alkali quartz syenite or nordmarkite, rhyolite with benmoreite xenoliths, alkali biotite granite, biotite-riebeckite granite which is peralkaline, and granite porphyry.

3.1 MAJOR ELEMENTS

The Mayo-Darlé igneous series is characterized by high SiO_2 content. SiO_2 values range from 68 percent in the quartz syenite to 78 percent in biotite granite. Mafic inclusions within the rhyolite have 56 percent SiO_2. The

total alkali $(Na_2O + K_2O)$ content is moderate and shows a steady decrease from 10.5 percent in the quartz syenite to 8.3 in the granite porphyry. Biotite and biotite-riebeckite granite average 8.34 total alkali content. K_2O is consistently slightly higher than Na_2O in all rock types except rhyolite (Fig. 8). K_2O/Na_2O ratios average 0.80 while mafic inclusions contained within the rhyolite average 1.06. Figures 8 through 11 illustrate the correlation between the various elements.
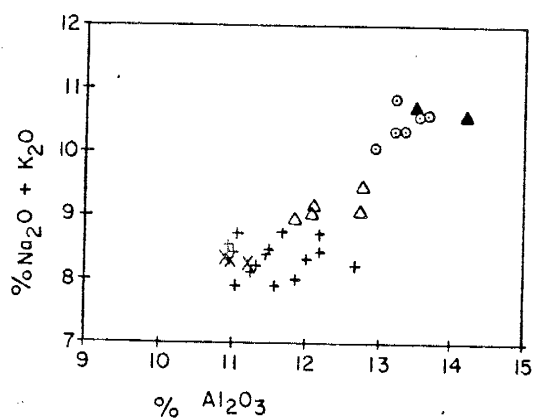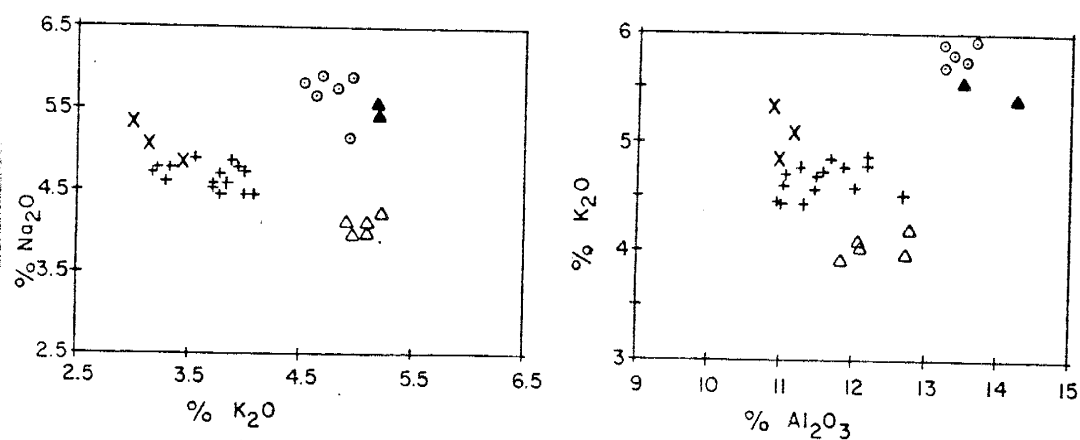
Fig. 8. Harker variation diagrams: Na_2O vs K_2O; K_2O vs Al_2O_3; $Na_2O + K_2O$ vs Al_2O_3.
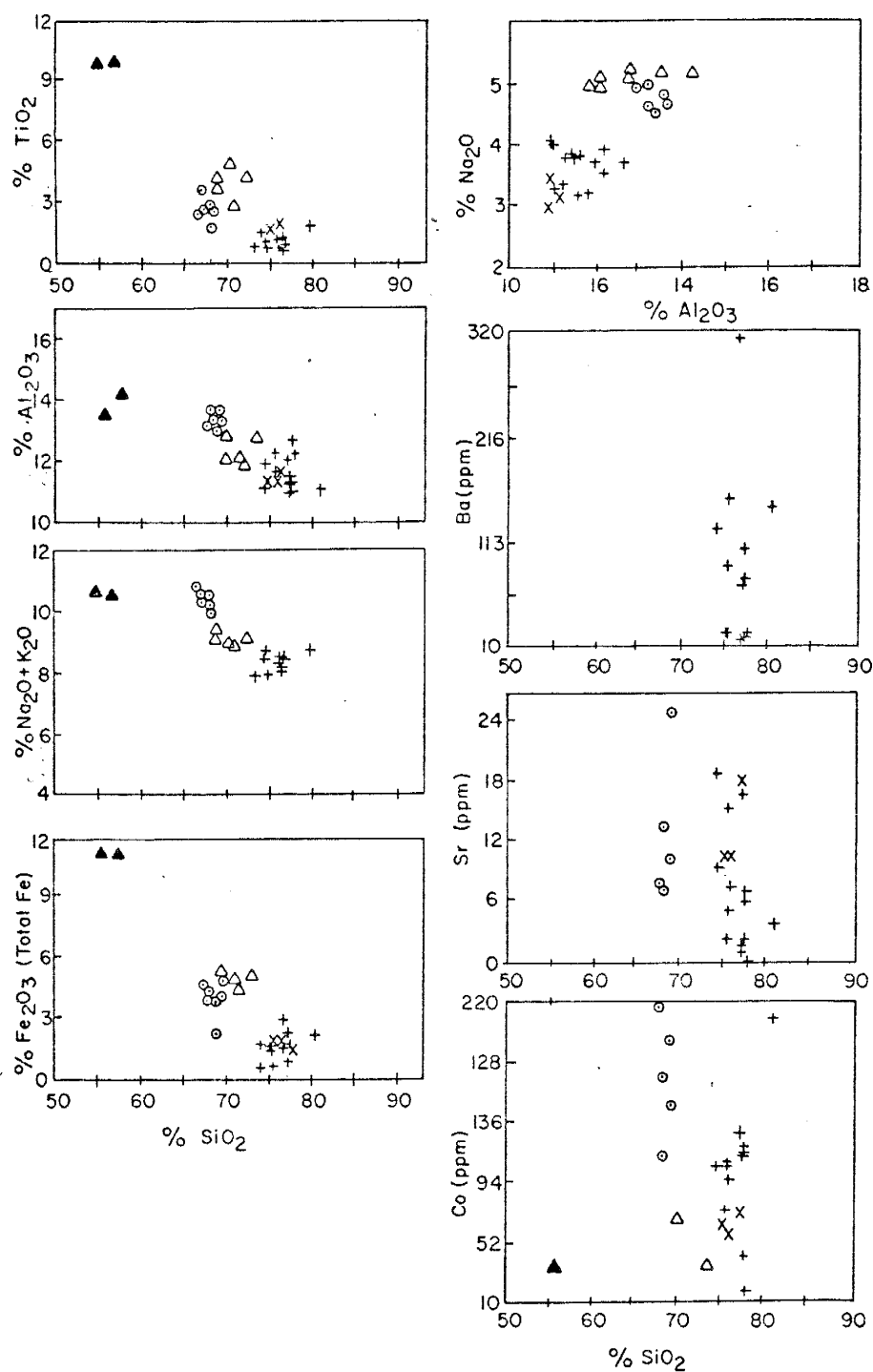
Fig. 9. Major oxide variation diagrams and Ba, Sr, and Co vs SiO$_2$ plots.

Fig. 10. Hf vs Ta; TiO_2/Ta vs Ta; Rb vs Cs; Sr vs K_2O; Rb vs K_2O.
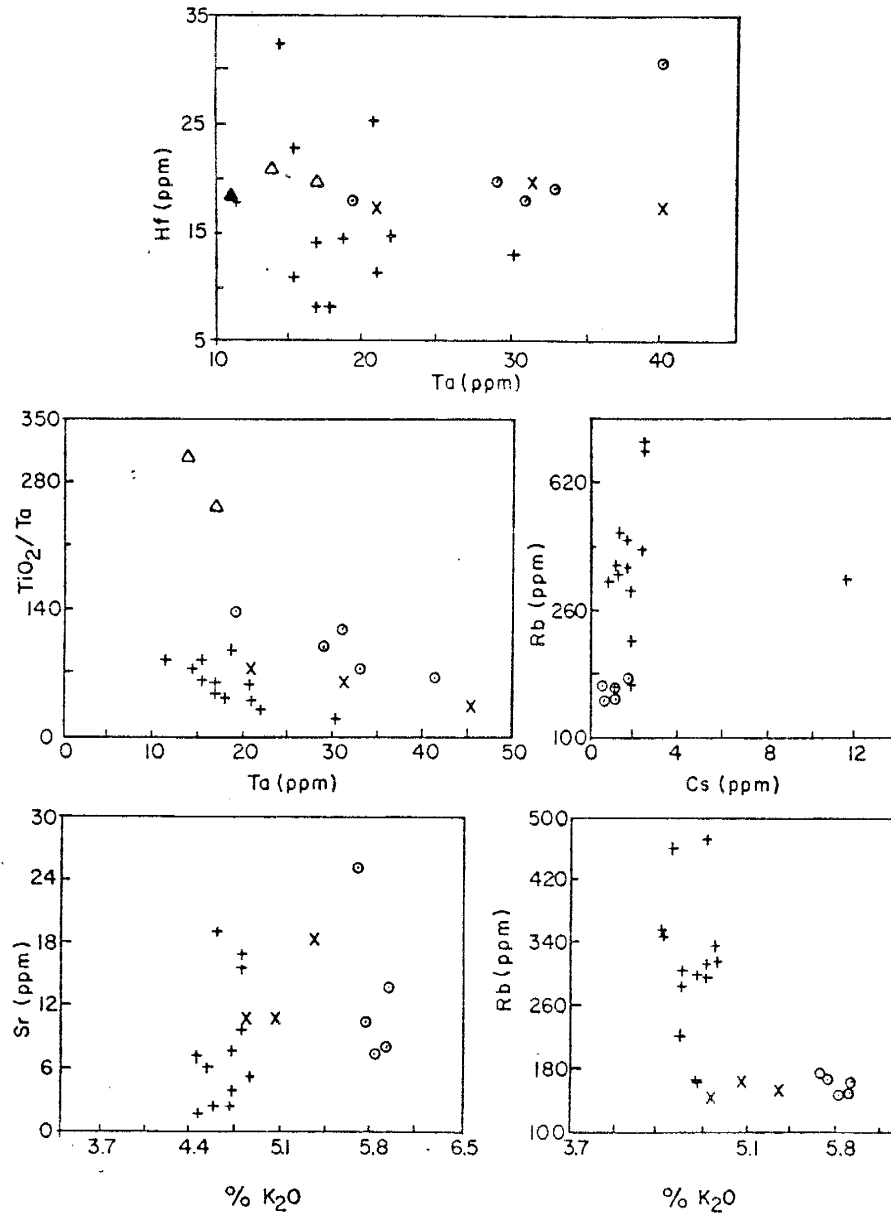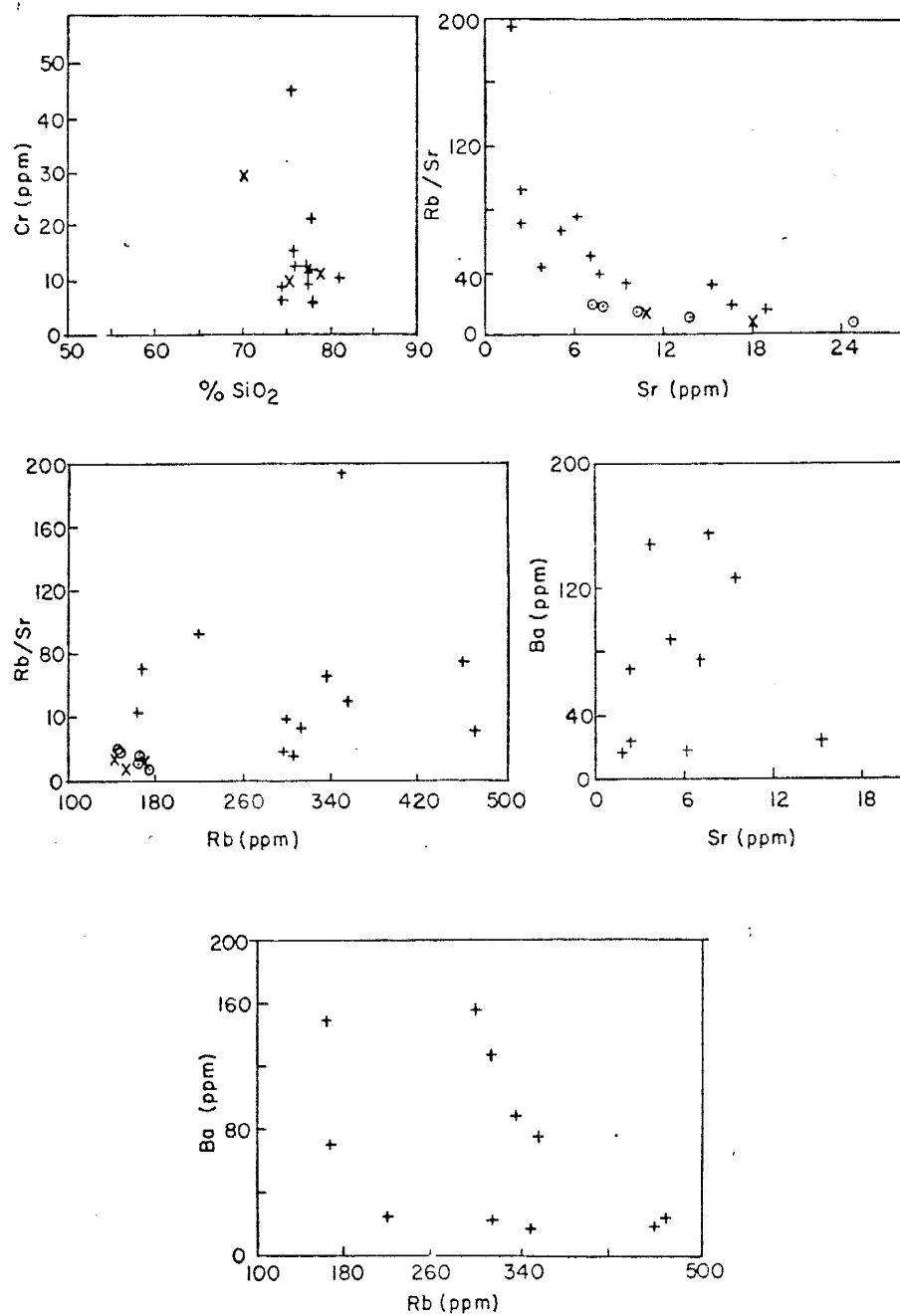
Fig. 11. Cr vs SiO$_2$; Rb/Sr vs Sr; Rb/Sr vs Rb; Ba vs Sr; Ba vs Rb.

The suite shows a decrease in Al_2O_3 with increasing SiO_2 content (Fig. 9). Total alkali content and Al_2O_3 content both decrease with increasing SiO_2 content. TiO_2 and Fe_2O_3 as total Fe show a slight decreasing trend with increasing SiO_2 content. MgO is consistently low within the entire rock suite. CaO decreases from a quartz syenite high of 0.60 weight percent to a low of 0.35 weight percent in biotite granite. Rhyolite is more abundant in CaO with an average of 1.22; mafic inclusions in K-rhyolite consist of 3.76 weight percent CaO.

MOLAR PLOT IN THE TERNARY SYSTEM
AL_2O_3, Na_2O+K_2O, CaO FOR THE
MAYO-DARLE IGNEOUS ROCKS

⊕ Biotite−riebeckite granite
+ Biotite granite
• Quartz syenite
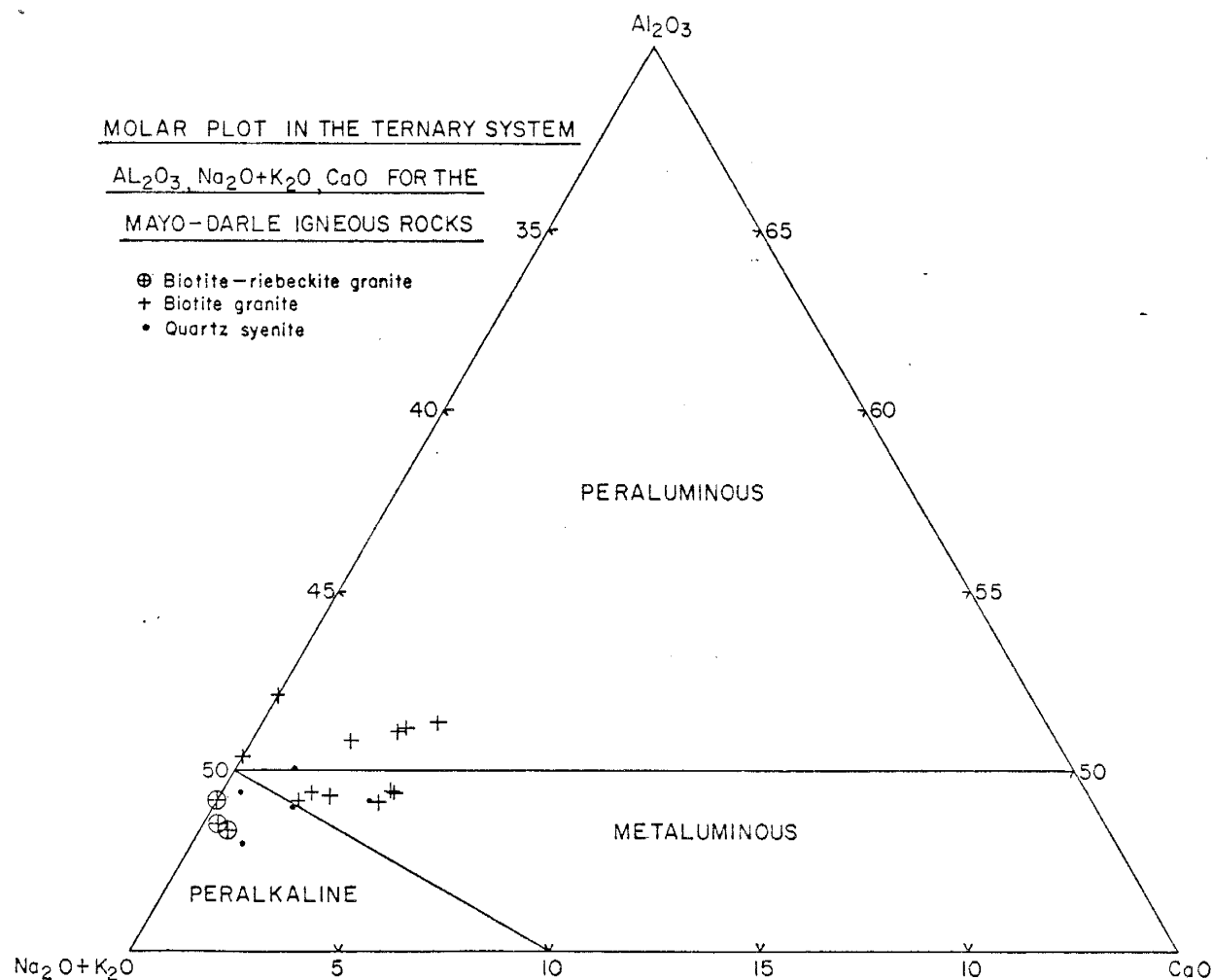
Fig. 12. Molar plot in the ternary system Al_2O_3, $Na_2O + K_2O$, CaO

The molar plot in the ternary system Al_2O_3, $Na_2O + K_2O$, and CaO indicates that all samples of biotite granite are metaluminous or slightly peraluminous (Fig. 12). Biotite-riebeckite granite samples plot on the peralkaline field (Fig. 12). Quartz-syenite samples plot in the peraluminous and metaluminous field (Fig. 12). The agpaitic index, $(Na_2O + K_2O)/Al_2O_3$, is used to differentiate between the two granite types. The agpaitic index of biotite granite ranges from 0.86 (peraluminous samples) to 0.99 (metaluminous samples). The agpaitic index of biotite-riebeckite granite ranges from 1.03 to 1.04 (peralkaline type).

TABLE 1.   TRACE ELEMENT RATIOS

	Granite Porphyry Average (n=3)	Biotite Granite Average (n=8)	Rhyolite Average (n=5)	Syenite Average (n=5)
$\dfrac{TiO_2}{Ta}$	35 – 77 (52)	20 – 95 (12)	251 – 890 (442)	66 – 139 (94)
$\dfrac{Rb}{Sr}$	8.4 – 15.4 (12)	31 – 284 (41)	0.06 – 12.6 (1.0)	7.0 – 20.3 (11)
$\dfrac{K}{Rb}$	260 – 292 (275)	82.0 – 172 (117)	212 – 313 (259)	272 – 330
$\dfrac{K}{Sr}$	2463 – 4010	2043 – 51557	264 – 2686	1917 – 6710
$\dfrac{Sr}{Ba}$		0.003 – 0.64 (0.082)		
$\dfrac{Ba}{Rb}$		0.04 – 1.11 (0.29)		
$\dfrac{Eu}{Eu*}$	0.19 – 0.39	0.16 – 0.39	0.46 – 0.69	0.22 – 0.50
$\left(\dfrac{La}{Sm}\right)_N$	1.2 – 2.2	2.0 – 3.7	2.8 – 3.3	2.9 – 4.4
$\left(\dfrac{Yb}{Lu}\right)_N$		1.0 – 1.4		
$\dfrac{La}{Yb}$	1.7 – 5.6	3.1 – 12.9	6.2 – 13.1	8.0 – 51.8

3.2 TRACE ELEMENTS

3.2.1 Rare Earth Elements

Rare earth patterns indicate constant characteristics throughout the entire igneous series (Fig. 13 through 18):

1) Relative slight enrichment of light rare earth over heavy elements.

2) Heavy rare earths are only slightly fractionated (almost flat slopes) within each rock type except the quartz syenite, which shows relatively high fractionation of heavy rare earths.

3) Well pronounced negative Eu anomaly.

4) Progressive decrease in absolute rare earth abundance with SiO_2 content within the igneous complex.

A close examination of individual envelopes of each rock type indicates that the Eu anomalies (Eu/Eu*) increase from a moderate range of 0.22 to 0.50 in the quartz syenite to a low range of 0.19 to 0.39 of the quartz porphyry (Table 1). Eu* is the extrapolated value of Eu if no anomaly was present. The sum of the seven rare earth elements which were analyzed (La, Ce, Sm, Eu, Tb, Yb, and Lu) ranges from 105 ppm in the granite porphyry to 454 ppm in the quartz syenite. The quartz syenite exhibits more fractionated rare earths patterns (La/Yb = 8 to 52) than the high SiO_2 members of the suite (La/Yb = 2 to 13) (Table 1).
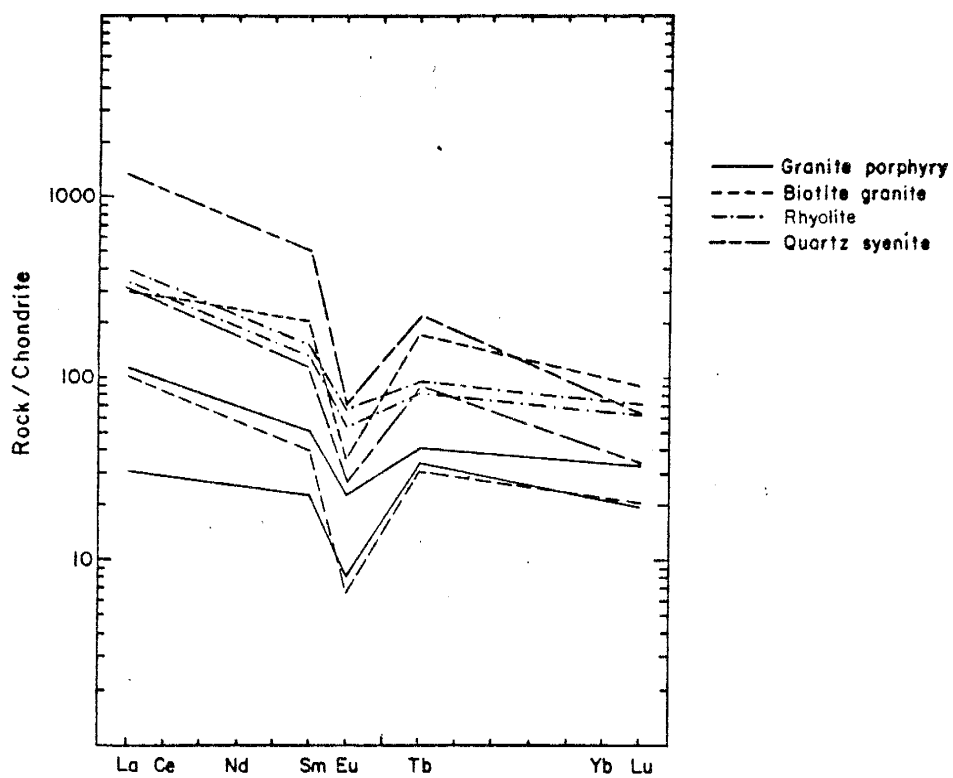
Fig. 13. Rare earth element patterns for the Mayo-Darlé complex.
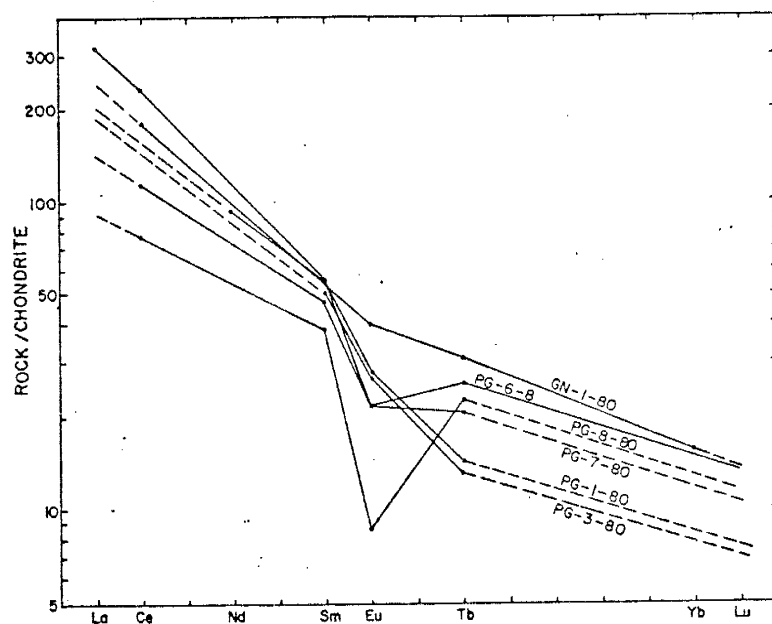
Fig. 14. Rare earth patterns of the metasediments.
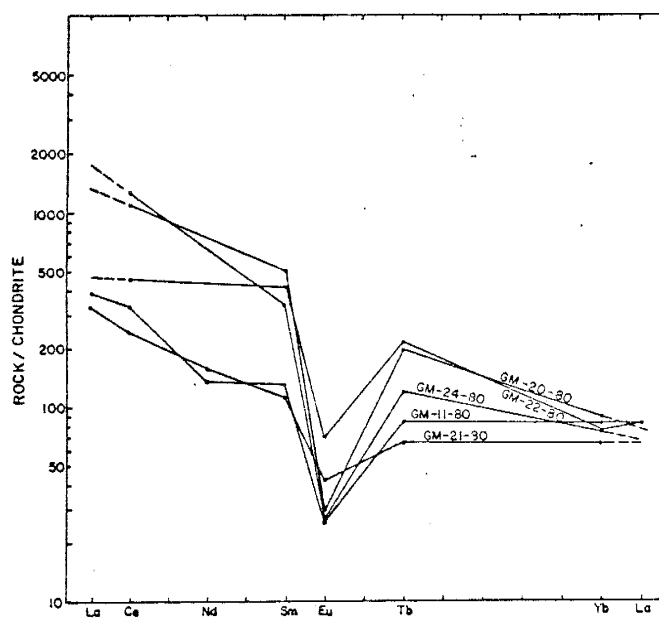
Fig. 15.   Rare earth patterns of quartz-syenite.
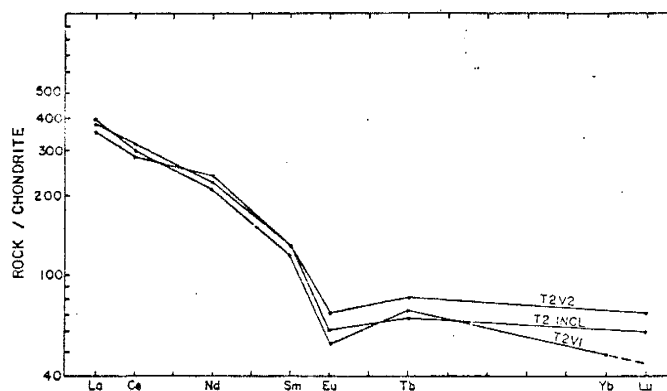
Fig. 16.   Rare earth patterns of rhyolite.
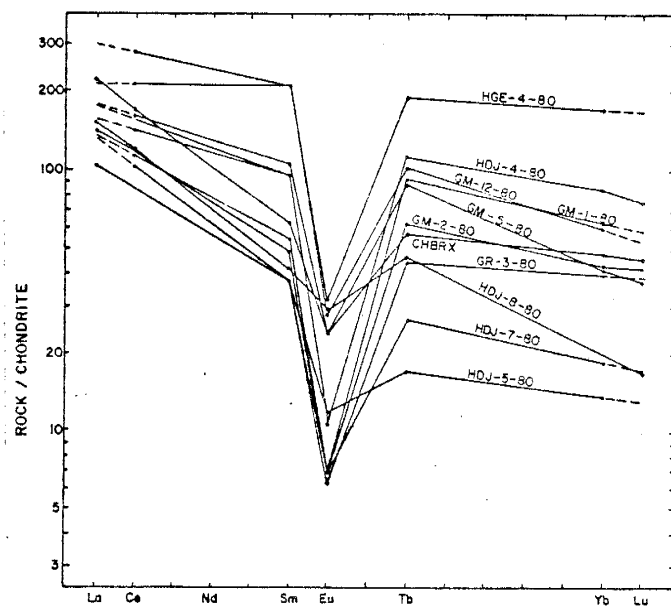
Fig. 17.   Rare earth patterns of granite.
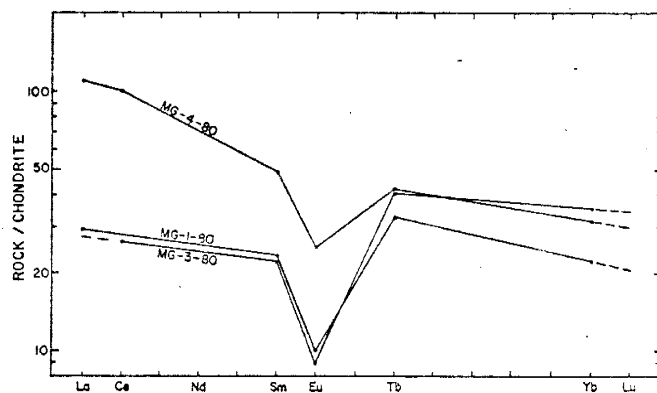
Fig. 18.   Rare earth patterns of granite porphyry.

3.2.2 Other Trace Elements

All samples were analyzed for 10 trace elements in addition to rare earths (Rb, Sr, Cs, Ba, Sc, Zr, Hf, Ta, Cr, and Co). Rubidium concentrations consistently increase within the series from a low average of 120 ppm in the quartz syenite to a an average of 310 ppm Rb in the granite. The rubidium content of the biotite granite near tin mineralization averages 340 $\pm$ 20 ppm. Biotite granite 2 km from tin mineralization averages 280 $\pm$ 20 ppm Rb, and the biotite-riebeckite granite has an average of 320 ppm Rb. Although the number of samples for each type of granite analyzed is small, the difference in their Rb content is important.

Strontium concentrations, are consistently low within the series with the exception of rhyolite, which exhibits a relatively erratic Sr distribution. In general Sr content decreases from an average of 13 ppm in quartz syenite to a low average of 7.5 ppm in the granites. Average barium concentration in the granites is 90 ppm. Barium was not detected in other rock types. Cesium concentrations do not indicate a trend within the rock sequence. Average Cs concentration within the entire complex is 1.5 ppm. One granite sample near tin mineralization has a high Cs content (11 ppm). Cobalt concentrations show a consistent decrease from quartz syenite to granite with the exception of rhyolite. Quartz syenite Co content is 164 ppm, biotite

granite Co concentration averages 100 ppm, and the quartz porphyry has an average Co content of 64 ppm. Chromium concentrations are low within the entire complex. Average Cr content is 11 ppm. Scandium concentrations are low within the entire series. Zirconium content decreases from quartz syenite (490 ppm) to granite porphyry (350 ppm). Biotite granite Zr content averages 390 ppm. Hafnium values are low compared to zirconium. Hafnium concentrations average 17 ppm within the igneous suite. Tantalum content shows no systematic behavior. Average Ta content of the complex is 23 ppm, quartz syenite averages 30 ppm Ta, rhyolite averages 14 ppm, while biotite granite and granite porphyry average 18 ppm and 32 ppm Ta respectively.

3.2.3 Interelement Relationships

Correlation diagrams of trace element and major elements are given in Figures 9 through 11 to help visualize possible trends within each rock type and within the entire complex. Rubidium content increases with SiO_2 within the complex. The highly differentiated biotite granite and biotite-riebeckite granite are very high in Rb. Rb/Sr ratios increase with increasing SiO_2 content throughout the igneous series with the exception of granite porphyry which has a lower Rb/Sr ratio compared to the biotite granite. K/Rb ratio decreases from quartz syenite to biotite granite. The decrease in K/Rb ratio is consistent with SiO_2 increase

within the complex with the exception of granite porphyry values. Rubidium and Sr show opposite trends with regard to SiO_2 increase within the complex. Strontium concentrations decrease with increasing SiO_2 content within each rock type and throughout the entire complex.

Strontium content slightly decreases with increasing K_2O content within the igneous series (Fig. 10). Cobalt concentrations decrease with increasing SiO_2 content. Chromium does not show a systematic trend with SiO_2 enrichment. Hf-Ta plot (Fig. 10) shows no correlation within the series. Ba-Sr and Ba-Rb plots of granite samples (Fig. 11) do not indicate a correlation between these elements. Plotted on a ternary diagram Ba-Rb-Sr, all granite samples fall in the strongly differentiated granite field (Fig. 19). The TiO_2/Ta ratio has been used in many studies of granites associated with tin mineralization (Boissavy-Vinau and Roger, 1980). TiO_2/Ta versus Ta plot (Fig. 10) indicates a trend of decreasing TiO_2/Ta ratios from the quartz syenite to the biotite granite.
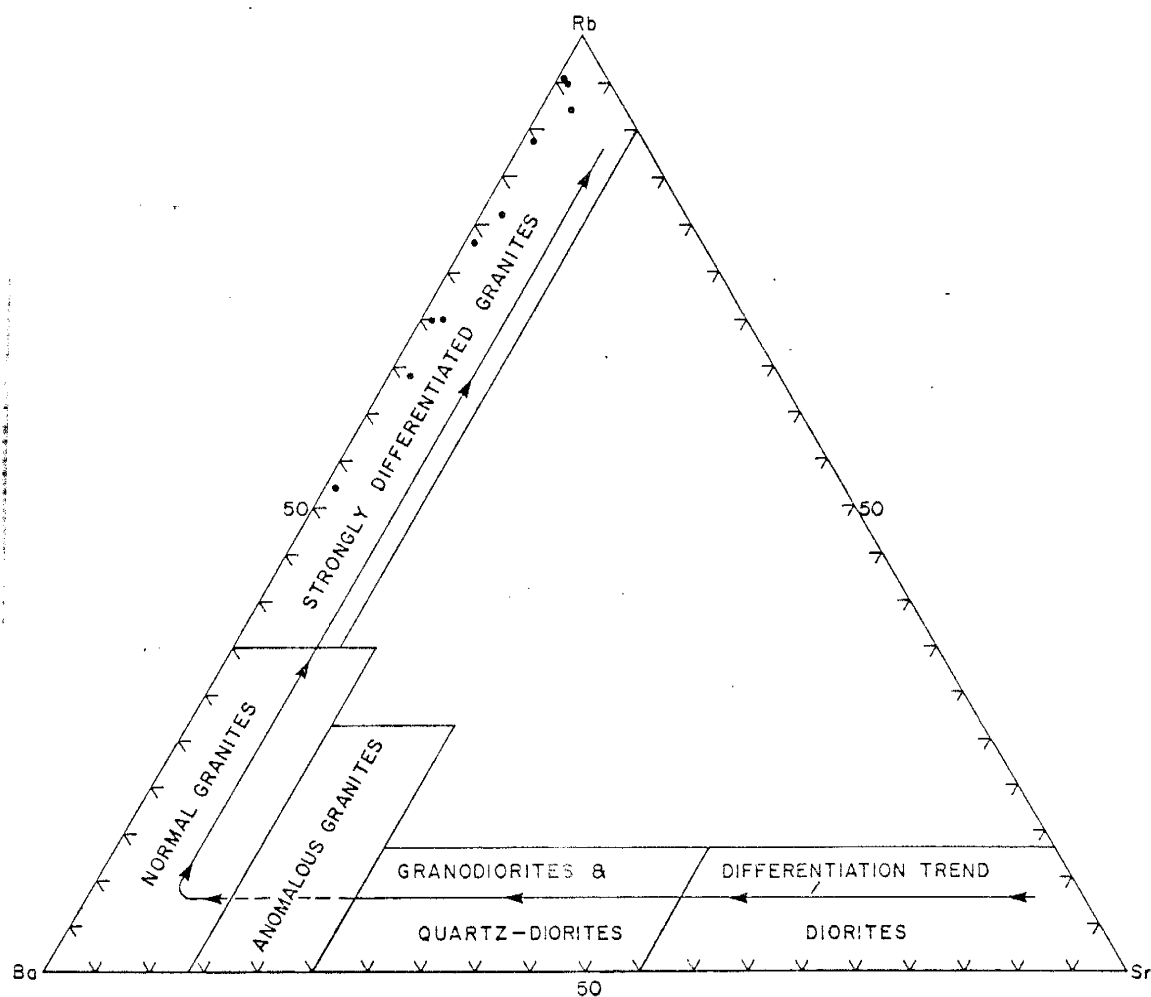
Fig. 19. Ba-Rb-Sr plot (Adapted from El Bouseily, et al., 1975).

CHAPTER 4. Rb–Sr AGE DETERMINATIONS

Rb-Sr data for all samples are given in Appendix I. Isotopic data are given in Appendix II. Details of analytical procedures are provided in Appendix II. Table 2 summarizes previous age determinations of the Mayo-Darlé granite.

TABLE 2. AGE DETERMINATION AT MAYO-DARLÉ

Method	Reference	Age (m.y.)	$(^{87}Sr/^{86}Sr)_o$
Rb-Sr	This study	73 ± 6	0.7030 ± 0.0035
Rb-Sr	Lasserre, M. (1978)	63.3 ± 1.3	0.7027 ± 0.0011
K-Ar	Cantagrel, J.M. (1978)	49.5 ± 1	---
K-Ar	Cantagrel, J.M. (1978)	48.5 ± 2	---
Rb-Sr	Gazel, et al. (1963)	65 ± 12	---

4.1 THE BASEMENT ROCKS

Five whole-rock samples of biotite gneiss and two whole-rock samples of quartz-diorite gneiss were analyzed for Rb and Sr isotopes. Figure 20 indicates that all seven analyses are co-linear within analytical error and consequently do define a least-squares cubic isochron which yields an age of 614 ± 20 m.y. (1 6) with a $^{87}Sr/^{86}Sr$

CHAPTER 4. Rb–Sr AGE DETERMINATIONS

Rb–Sr data for all samples are given in Appendix I. Isotopic data are given in Appendix II. Details of analytical procedures are provided in Appendix II. Table 2 summarizes previous age determinations of the Mayo-Darlé granite.

TABLE 2. AGE DETERMINATION AT MAYO-DARLÉ

Method	Reference	Age (m.y.)	$(^{87}Sr/^{86}Sr)_o$
Rb–Sr	This study	73 $\pm$ 6	0.7030 $\pm$ 0.0035
Rb–Sr	Lasserre, M. (1978)	63.3 $\pm$ 1.3	0.7027 $\pm$ 0.0011
K–Ar	Cantagrel, J.M. (1978)	49.5 $\pm$ 1	---
K–Ar	Cantagrel, J.M. (1978)	48.5 $\pm$ 2	---
Rb–Sr	Gazel, et al. (1963)	65 $\pm$ 12	---

4.1 THE BASEMENT ROCKS

Five whole-rock samples of biotite gneiss and two whole-rock samples of quartz-diorite gneiss were analyzed for Rb and Sr isotopes. Figure 20 indicates that all seven analyses are co-linear within analytical error and consequently do define a least-squares cubic isochron which yields an age of 614 $\pm$ 20 m.y. (1 ó) with a $^{87}Sr/^{86}Sr$

intercept value of 0.7059 ± 0.0007 (1 δ). This age corresponds to the Pan-African orogeny, an all-African event which occurred 550 ± 100 million years ago (Clifford, 1970). In Cameroon, metasediments, metavolcanics and granites from the south-central plateau to as far north as the Chad basin, have been affected by the Pan-African orogeny (Lasserre (1964); Lasserre et al. (1976, 1981)).

Fig. 20. Isochron diagrams

Metasediments: age = 614 $\pm$ 20 m.y.

$$(^{87}Sr/^{86}Sr)_O = 0.7059 \pm 0.0007$$

Quartz-sysenite: age = 73 $\pm$ 6 m.y.

$$(^{87}Sr/^{86}Sr)_O = 0.7030 \pm 0.0035$$

Rhyolite: $(^{87}Sr/^{86}Sr)_O = 0.7075 \pm 0.0020$

Granite: $(^{87}Sr/^{86}Sr)_O = 0.7094 \pm 0.0019$
(Blank triangles represent analyses taken
from Lasserre, 1978)
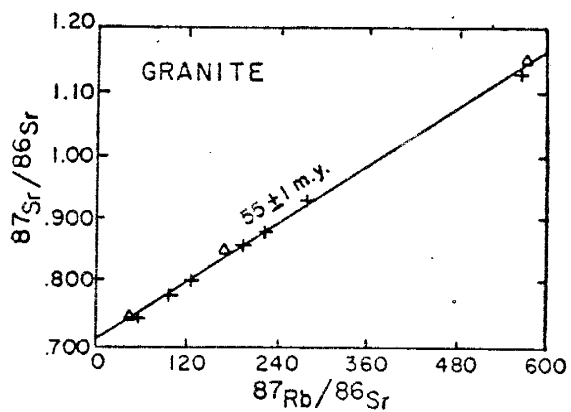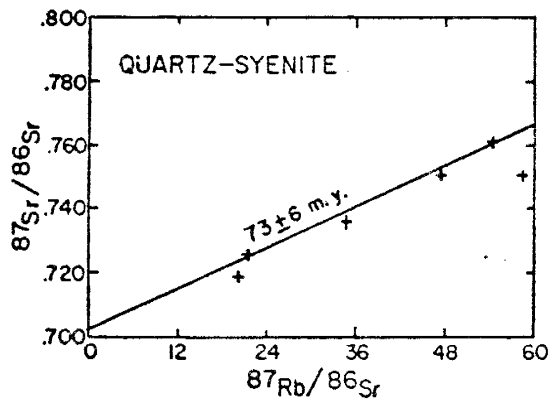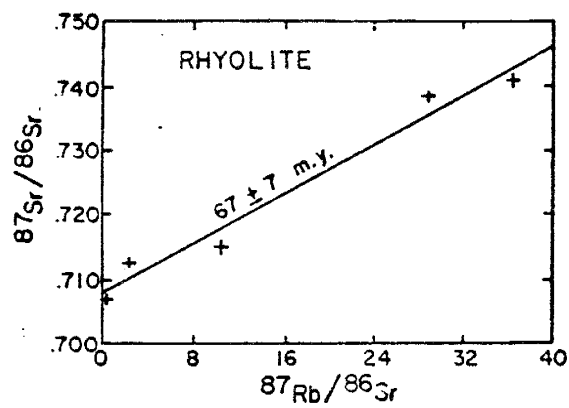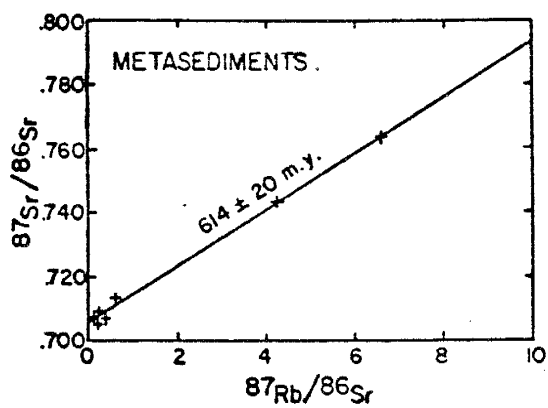
4.2 AGES OF THE IGNEOUS ROCKS

4.2.1 Quartz Syenite

The six samples of quartz-syenite analyzed are not
co-linear and consequently do not define a unique isochron.
However four of the points are co-linear within analytical
error and define a least-squares cubic isochron yielding an
age of 73 $\pm$ 6 m.y. (1 δ) with a $^{87}Sr/^{86}Sr$ initial value of
0.7030 $\pm$ 0.0035 (1 δ) (Fig. 20). The two points off the
isochron may have lost some radiogenic ^{87}Sr even though
samples analyzed for Rb and Sr isotopes were all fresh and
unaffected by weathering. The low initial $^{87}Sr/^{86}Sr$ ratio
places the parental source of the syenites within mantle
values as defined by Faure and Powell (1972). Lasserre
(1978) suggests a mantle source for the Mayo-Darlé complex.

4.2.2 Rhyolite

Four rhyolite samples and one sample of a benmoreite
xenolith defined a least-squares cubic isochron which yields
a $^{87}Sr/^{86}Sr$ initial ratio of 0.7075 $\pm$ 0.0020 (1 δ) (Fig.
20). There is a scattering of the points about the
isochron. Strontium values recorded for this unit vary
widely from 12 ppm to 404 ppm Sr, which indicates that the
volcanics are not a homogeneous rock unit. Heterogeneity
within the immediate source of rhyolite and/or contamination
from benmoreite xenoliths could could explain the scattering

of data points about the isochron.

4.2.3 Granite

Analyses of biotite granite and biotite-riebeckite granite define a least-squares cubic isochron yielding an age of 55 ± 1 m.y. (1 δ) with a $^{87}Sr/^{86}Sr$ intercept value of 0.7094 ± 0.0019 (1 δ) (Fig. 20). The four samples with Rb greater than 304 ppm define a straight line with an intercept value of 0.7207 ± 0.0074 (1 δ) and an age of 52 ± 1 m.y. (1 δ). Low Rb points (from samples collected away from the mineralized area) fall on a straight segment with an intercept value of 0.7109 ± 0.0032 (1 δ) which indicates an age of 53 ± 3 m.y. (1 δ). The bending of the granite isochron may indicate a disturbance of the strontium isotope systematics within the granite, expressed as a rotation of the isochron and a definite increase in overall $^{87}Sr/^{86}Sr$ intercept value. The rotation of the isochron is influenced by high Rb samples collected near the mineralized zone compared to low Rb samples which were collected further away from the mineralization.

Results of the Rb-Sr studies are summarized in Table 3.

TABLE 3.   SUMMARY OF Rb-Sr DATA

Rock	Rb (range) ppm	Sr (range) ppm	Rb/Sr average	$(^{87}Sr/^{86}Sr)_o$	Age (million years)
Meta-sediments	47-143	102-980	0.217	0.7059 $\pm$ 0.0007	614 $\pm$ 20
Quartz syenite	146-174	7-25	11.22	0.7030 $\pm$ 0.0035	73 $\pm$ 6
Rhyolite	23-172	12-404	1.00	0.7075 $\pm$ 0.0020	67 $\pm$ 7
Granite	220-457	2.0-19	38.10	0.7094 $\pm$ 0.0019	55 $\pm$ 1

CHAPTER 5. TIN MINERALIZATION

5.1 OCCURRENCES OF MINERALIZATION

Tin mineralization occurs almost continuously in a 4 km^2 area in the northeast part of the granite with a high grade zone associated with silicified breccia pipes. Mineralization is confined to stockwork veinlets and a main vein system. Alluvial and residual ores constitute the secondary deposit.

5.1.1 Primary Ores

Stockwork mineralization

The residual deposit grades downward into stockwork ores. Stockwork mineralization is characterized by submillimeter up to 3 cm wide, randomly oriented quartz and greisen veinlets with disseminated cassiterite cross-cutting the granite. Greisen assemblages at Mayo-Darlé consist of quartz, topaz, and zinnwaldite. The veinlet fillings occupy a set of conjugate fractures. Stockwork mineralization makes up about 3 km^2 in area. The vertical extent is not known. Large volumes of rocks have an estimated 0.1 to 0.3 percent SnO_2. Estimates of this potential low-grade tin ore are in excess of 100 million metric tons. Stockwork veinlets contain quartz, cassiterite, chlorite, hematite,

and minor fluorite, topaz, and zinnwaldite. No sulfide phase was observed.

Vein mineralization

Vertical and horizontal sets of veins occur randomly within the mineralized zone.

Vertical greisen lodes

Vertical greisen lodes occur as one to two meter-wide, quartz-rich veins, locally traceable over distances up to 50 m. These lodes radiate from barren, highly silicified breccias, irregular in shape and size. Subcircular breccias with a diameter up to 50 m at places are common. The contacts between the lodes and the host granite, where exposed, are sharp, indicating deposition by a post-crystallization event. The veins consist of 99 percent equigranular, fine to medium-grained, sugary quartz and 1 to 5 mm cassiterite grains. Cassiterite occurs as brownish-red to reddish black, strongly zoned crystals. Cassiterite locally is interstitial to quartz, but it mainly occurs as either isolated grains or as aggregates. The remaining one percent of vein material is made up of minerals recognized in thin section in decreasing order of abundance: needle-like greenish micas, identified as zinnwaldite (Koch, 1959), clear topaz grains, chlorite, fluorite, columbite, monazite, and zircon. Tourmaline, although mentioned by Koch (1959) and Morawietz (1968), has not been observed.

Morawietz (1968) reported weight percentages of 2.5 to 20% SnO_2 and locally 0.3 to 3% topaz, and 0.05 to 0.4% columbite in assays of samples from vertical quartz-cassiterite lodes.

Horizontal greisen lodes

Flat lying lodes or veins are present in Mayo-Darlé. They range from a few centimeters up to a meter in thickness. Their lateral extent is not known; the maximum traceable lateral extent in one outcrop is 50 m. The thickness is almost constant within a given vein. Dips of 5° to 10° are typical. The vertical structural relationship of horizontal veins is not clear. No connection has been observed between any two horizontal veins. In hand specimen, vein materials exhibit a sugary texture with quartz phenocrysts locally present in a fine-grained matrix of equant quartz grains. Microscopically, the texture is hypidiomorphic granular. The horizontal veins consist of 96 percent milky massive quartz and 2 percent disseminated cassiterite. Chlorite, fluorite, zinnwaldite, and topaz are more abundant (2%) than in the vertical veins. Zircon, monazite, and columbite were not observed. Cassiterite occurs as reddish brown to reddish black, strongly zoned crystals in patches within the quartz matrix. Chlorite occurs as black-green platy crystals. Zinnwaldite occurs as dispersed flakes within the matrix. Topaz is very sparse.

Locally, vugs are present within horizontal veins. These vugs contain two generations of quartz: massive with dis-

seminated cassiterite, and euhedral quartz crystals with no cassiterite, radiating from the vugs' walls.

Vein paragenesis

There is only evidence for one stage of mineralization (Fig. 21). Since no contact between horizontal and vertical veins has been observed, contemporaneity of both types of veins is assumed on the basis of their similar mineralogy and textural patterns. The sparse occurrence of minerals other than quartz and cassiterite makes it difficult to identify a clear paragenetic relationship between the various minerals. In both sets of veins, quartz is early and makes up most of the vein. In horizontal veins, euhedral quartz lines the walls and is surrounded by more massive sugary quartz accompanied by cassiterite. Topaz, when present, is associated with zinnwaldite and cassiterite. Topaz, chlorite, and zinnwaldite are relatively more abundant in horizontal veins. The horizontal veins exhibit a greenish brown color due to chlorite and zinnwaldite abundance. Tourmaline was not observed in the veins. Vertical veins contain columbite, monazite, and zircon as accessory minerals. These minerals have not been observed in horizontal veins.

Fig. 21. Generalized paragenesis of mineralized greisen veins.

PARAGENESIS

QUARTZ CASSITERITE LODES

QUARTZ
TOPAZ
MUSCOVITE-ZINNWALDITE
CASSITERITE
CHLORITE
FLUORITE
HEMATITE

HORIZONTAL GREISEN VEINS

QUARTZ
TOPAZ
MUSCOVITE-ZINNWALDITE
CASSITERITE
CHLORITE
FLUORITE
HEMATITE

5.1.2   Secondary Deposit

Alluvial deposit

The alluvial deposit occurs as conglomeratic beds unconformably overlying the intensely kaolinized granite.   These beds average 50 cm in thickness and occur in relatively narrow channels 50 m wide.   The conglomerate units consist of pebble size euhedral to subhedral quartz crystals, clayish material, and angular lithic fragments from the metasediments and rhyolitic volcanics. Cassiterite grains in the conglomerate beds vary in size from few millimeters up to 5 cm in diameter.   Panning of about 10 kg of conglomerate material yielded 0.860 kg to 1 kg of SnO_2 concentrate, or 8 to 10% SnO_2.   A thin clay layer 10 to 20 cm thick directly overlies the conglomerate beds (Fig. 22). The clay unit is covered by colluvial deposits, 20 m thick (Fig. 22). Materials from the colluvial unit were panned at 3 m intervals.   An average of 0.5 g SnO_2 per 10 kg of panned material or 0.005% SnO_2 was obtained for the entire unit. The soil cover yielded 0.09% SnO_2.   The placer deposit is interpreted as having formed from erosion of mineralized volcanics which preceded the granite.   These volcanics were probably similar in composition to remnants of rhyolitic volcanics present in the area. Angular lithic fragments within the conglomerate indicated that eroded materials were not transported over long distances before deposition.
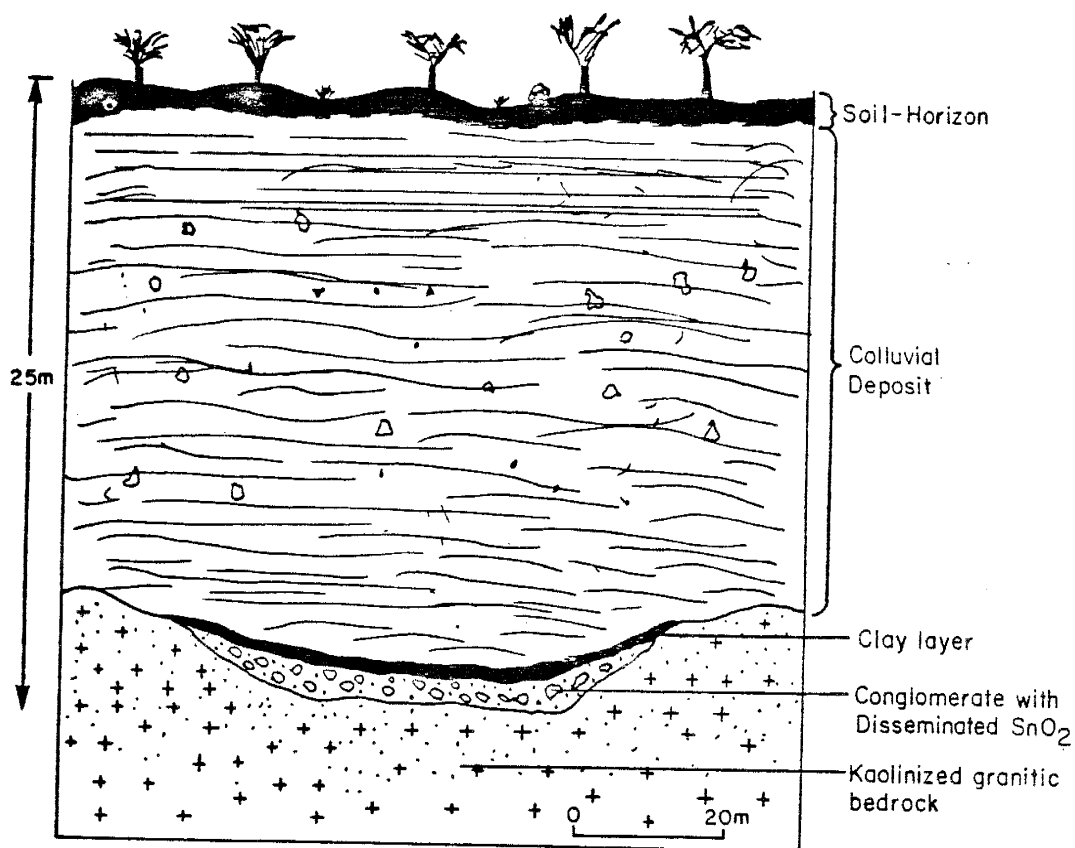
Fig. 22.   Schematic Cross-section of occurrence of
alluvial tin at Mayo-Darlé.

Residual deposit

The residual deposit is formed by in-situ weathering of the mineralized granite. The protore is characterized by a high density of quartz and greisen veinlets. Hematization of the host granite is prevailing and is a valuable criterion for finding this type of deposit in the area. The thickness of soil horizons average 3 m locally. Panning of soil materials at 50 cm intervals indicates an increase in grade from 0.01% at the surface to about 1% SnO_2 just above the granite at one locality. The average grade of the residual deposit is 0.06% SnO_2.

5.2 HYDROTHERMAL ALTERATION

Well-defined alteration zones are not present at Mayo-Darlé. Wall rock alteration is interspersed within the mineralized area. Silicification, chloritization, kaolinization, hematization, and greisenization are present.

Greisen assemblages at Mayo-Darlé consist of quartz and cassiterite as main minerals. Topaz, zinnwaldite, chlorite, and fluorite occur in minor amounts. The term quartz-cassiterite greisen is preferred because of the predominance of these two minerals over the minor occurring species. All constituents of the greisen assemblage (excepting cassiterite) are present in the granite around the mineralized area.

Silicification is evidenced by overgrowth of quartz

around early formed quartz and K-feldspar phenocrysts within the granite. Other evidence of silica enrichment includes the high density of quartz veinlets cross-cutting all igneous rocks of the complex and extending into the meta-sediments.

Chloritization is evidenced by replacement of biotite by chlorite in the granite around mineralized areas. In some greisen veinlets chlorite is a major constituent. Horizontal veins contain more chlorite than do vertical veins.

Stockwork mineralization is characterized by intense hematization of the granite stock. Hematite stain is pervasive around the veinlets and gives a pinkish red color to the granite. Zones of intense kaolinization (up to 0.2 km^2 in area) are scattered within the mineralized area. Typically, the granite is completely altered to kaolinite and quartz. Locally pervasive kaolinization may be associated with quartz-cassiterite greisen veins, though kaolinization usually occurs away from mineralized greisen veins. All alteration types, excepting kaolinization, seem related to greisenization. Temperature decrease and changes brought about by the greisenization process are believed to have initiated subsequent alteration: silicification, chloritization, and hematization. Figure 23 suggests a chronological sequence with decreasing temperatures.

```
Beginning of                    End of the      End of the
the Hydrothermal              Mineralization    Hydrothermal
event                             period           event
    |                               |                |

    DECREASING TEMPERATURES ----->


  |---- Greisenization ------------------|

    |---- Silicification ----------------------------------------|

      |---- Chloritization --------------------------------|

                        |---- Hematization -------------|

                            |-- Kaolinization -|
```
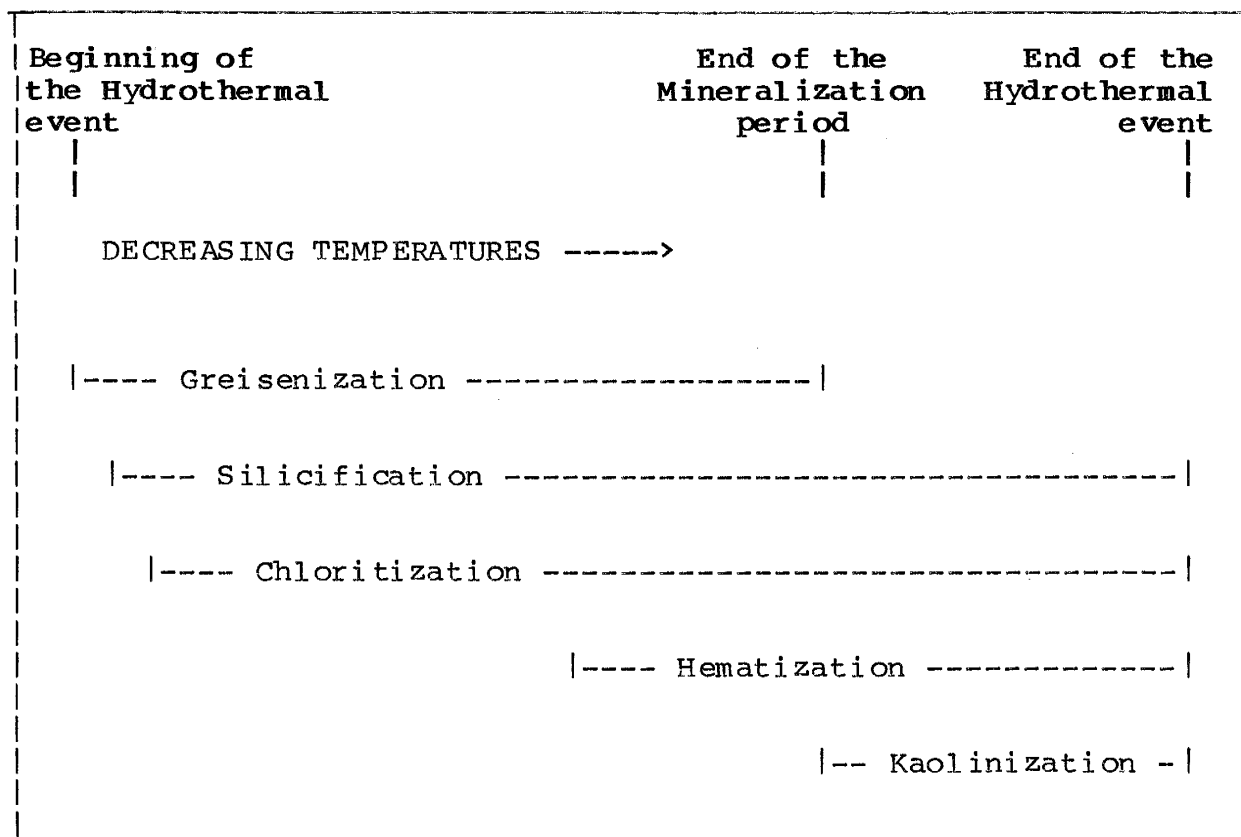
Fig. 23.   Schematic sequential order of occurrence of alteration.

5.3   FLUID INCLUSION STUDIES

The coarse crystalline veins at Mayo-Darle' provided
excellent material for fluid inclusion study. The only
drawback was the small number of suitable minerals involved
in the study.   Of all the minerals within the paragenetic
sequence, only quartz and cassiterite proved to be abundant
and suitable enough for fluid inclusion studies.   Fluid
inclusions in cassiterite were difficult to study because of
the rarity of inclusions, their small size, and the near
opacity of the mineral. Polished plates of cassiterite were
examined for qualitative information, quantitative data
having proved too poor for meaningful consideration.

A total of 36 doubly polished thick sections of vein
materials were prepared: 13 from vertical greisen veins, 13
from horizontal greisen veins, 5 from barren quartz veins,
and 5 from the granite. Optical examination indicated there
were primary, pseudosecondary, and secondary inclusions
using criteria described by Kelly and Turneaure (1970), and
Roedder (1979). Only primary and pseudosecondary inclusions
were subsequently considered.

5.3.1   Types of Inclusions

Five types of inclusions are distinguished on the basis of their gas-liquid ratios, presence of daughter minerals at room temperature, and homogenization behavior upon heating (Fig. 24A-F; Table 4).   Type A, two-phase, liquid-rich inclusions consist of at least 75 volume percent aqueous liquid, the remaining volume is occupied by a vapor phase. Type A inclusions homogenize by vapor disappearance (Fig. 24-E).   Type B inclusions are vapor-rich, averaging 80 volume percent gas.   These inclusions homogenize by liquid disappearence (Fig. 24, E and F).   Type C inclusions, the most common type, contain a variable liquid to gas ratio and a cubic halite crystal as daughter mineral (Fig. 24 C). Type C inclusions homogenize either by vapor disappearance or by halite disappearance, but rarely by liquid disappearance.   Inclusions of type D and E are multiphase inclusions with two or more daughter minerals.

Fig. 24.   Primary fluid inclusions in quartz-cassiterite
veins.

         A. and B.   Primary type D inclusions
                   (l = liquid, v = vapor, h = halite,
                   c = cryolite).

         C.   Primary halite-bearing type C inclusions
                (hm = hematite).

         D.   Primary type E inclusion
                (anh = anhydrite).

         E.   Primary liquid-rich type A inclusion.

         F.   Primary vapor-rich type B inclusion.
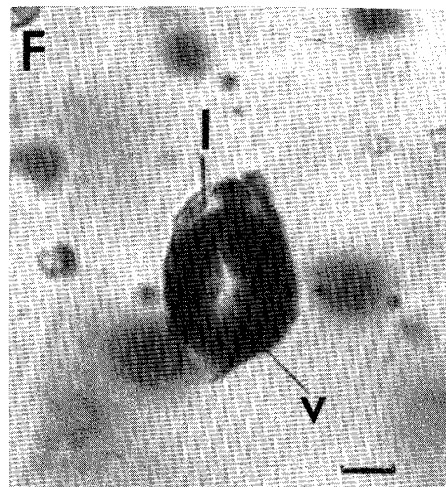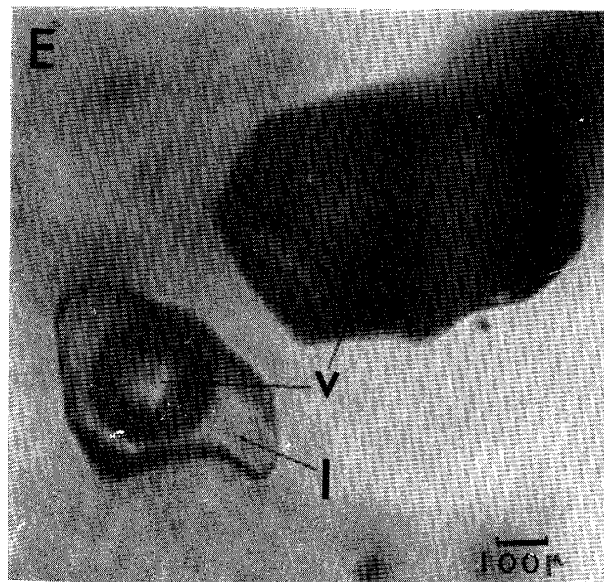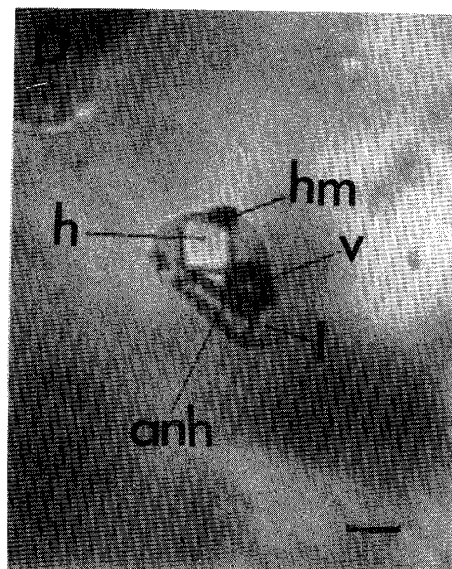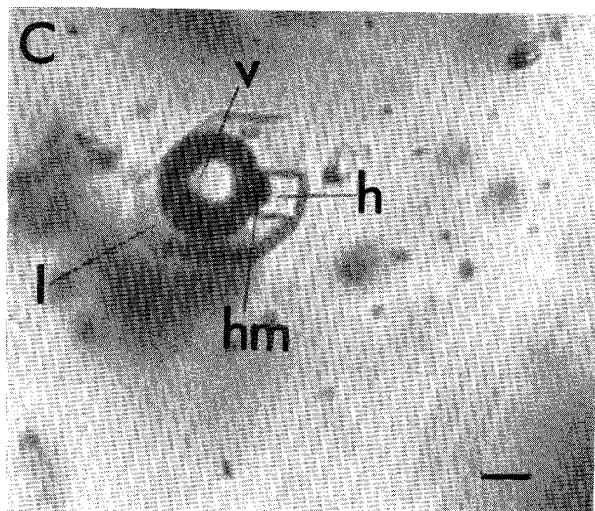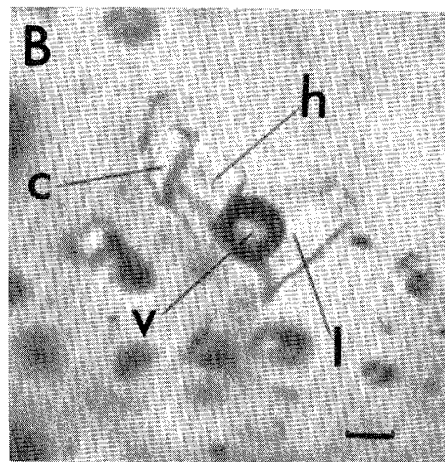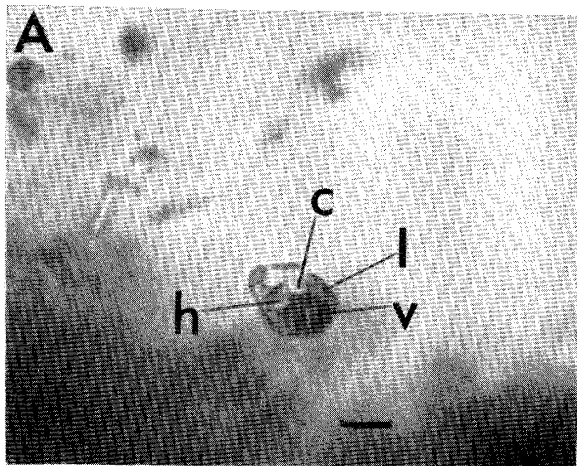
Table 4. Types of fluid inclusions.

TYPES OF FLUID INCLUSION			
TYPE	ABUNDANCE	COMPOSITION	HOMOGENIZATION
A	~20%	Liquid – rich ~21 wt. % NaCl	Vapor 300° – 599° C
B	~10 %	Vapor–rich ~21 wt % NaCl	Liquid 385° – 599° C
C	~50%	Vap + Liq +halite ~40 wt % NaCl	Halite 270° – 536°C
D	~7%	Liq + Vap + hal + Cryolite(?)	Vapor 289° – 595°C
E	~3 %	Liq + Vap + H ± Cry. ± anh ± hem ± others	
F	Secondary inclusions along healed cracks.		

5.3.2 Daughter Minerals

Halite is the only daughter mineral present in type C inclusions. In type D inclusions, clear, colorless, high birefringent, cubic to hexagonal crystals dissolving at temperatures of $300^{O}C$ and above were identified as cryolite. Type D inclusions are characterized by the presence of halite and cryolite as daughter minerals. Other recognized solid phases in addition to halite and cryolite in type E inclusions include hematite and anhydrite (Fig. 24 C and D). Hematite exhibits a distinctive reddish black color, it is platy to hexagonal in shape. Anhydrite occurs as high relief, birefrigent, rectangular or elongated needle-like crystals.

5.3.3 Cassiterite in Inclusions

A reddish brown to orange, zoned and birefingent solid phase, identified as cassiterite, was observed in inclusions from quartz-cassiterite greisen veins. Variable amounts of cassiterite occur only in some of the halite-bearing fluid inclusions. The variable phase ratios and the rarity of such inclusions suggest accidental trapping of cassiterite during the time of formation of the fluid inclusions. It is equally possible that cassiterite could have actually nucleated and crystallized out of the fluid, or that accidentally trapped cassiterite particles acted as nuclei for further

growth within the inclusions.

Cassiterite has been reported in fluid inclusions from other tin deposits (Norman and Trangcotchasan, 1982), as having been trapped as a solid phase along with inclusion waters. As such, cassiterite is considered a pseudo-daughter mineral.

5.3.4 Homogenization Data

Homogenization data were obtained using a dual purpose freezing/heating stage. For methodology and equipment, refer to Appendix III.

More than 1000 inclusions were examined, of which data was taken from 483. Forty-four percent of the inclusions were of type A, 26 percent were of type B, 27.5 percent were of type C, and 2.5 percent were type D and E inclusions. The data are summarized in Table 5.

Liquid-rich type A inclusions homogenize by vapor disappearance. Thirty-five (35%) percent of type A inclusions homogenize in the range 167 to 299°C; 59.5 percent homogenize in the range 300 - 599°C, and 5.5 percent of type A inclusions did not homogenize up to 600°C, the maximum obtainable temperature of the stage used.

Vapor-rich type B inclusions exhibited a more homogeneous group behavior (Table 5). Eighty-five percent (85%) of all type B inclusions homogenized by liquid disappearance in the range 385° to 599°C. Fifteen percent (15%) of type B

inclusions did not homogenize up to $600^{O}C$ (Fig. 25 through 28; Table 5).

Halite-bearing type C inclusions homogenized in two ways: halite homogenization and vapor homogenization. Halite homogenization is characterized by the dissolution of halite crystals after vapor disappearance. In vapor homogenization, halite crystals dissolve before vapor disappearance. Halite homogenization and vapor homogenization in type C inclusions occurred with almost equal frequency in vertical and horizontal veins. Most of the inclusions that homogenized by halite disappearance did so in the range 300° to $540^{O}C$ with a mean at $430^{O}C$ (Fig. 25 through 28; and Table 5).

Some type A inclusions exhibited unusual behavior when heated. These inclusions were heated until homogenization by vapor disappearance at approximately $200^{O}C$. Upon continuous heating a vapor reappeared around $330^{O}C$. This new vapor phase increased in size with increasing temperature. Critical point was not reached; two phases were observed up to the maximum limit of $600^{O}C$. Upon cooling, the vapor phase disappeared around $-15^{O}C$. When reheated, the vapor phase reappeared as the ice melted at $0^{O}C$; disappeared at $200^{O}C$ and a new vapor phase reappeared at approximately $330^{O}C$. The above observations were reproducible in each of 12 such inclusions. In one instance a solid pase precipitated from such an inclusion around $330^{O}C$. The solid redissolved instantly when the temperature fell below $330^{O}C$. A possible explanation of this unusual behavior is discussed in a later section.

Table 5.   Homogenization behavior of the   three   main
inclusion types.

HOMOGENIZATION BEHAVIOR OF THE THREE MAIN INCLUSION TYPES

TYPE A

HOMOGENIZATION	Quartz–Cassiterite Lodes	Horizontal Greisen Veins	Barren Quartz Veins
	Vapor Disappearance	Vapor Disappearance	Vapor Disappearance
	37 % 167°–299°C	33 % 184°–299°C	7 % 222°–299°C
	60.5 % 300°–599°C	58.5 % 300°–591°C	93 % 300°–377°C
	2.5 % ≥600°C	8.5 % ≥600°C	

TYPE B

HOMOGENIZATION	Quartz–Cassiterite Lodes	Horizontal Greisen Veins	Barren Quartz Veins
	Liquid Disappearance	Liquid Disappearance	Liquid Disappearance
	93 % 385°–599°C	78 % 397°–593°C	5 Inclusions 430°–599°C
	7 % ≥600°C	22 % ≥600°C	

TYPE C

HOMOGENIZATION	Quartz–Cassiterite Lodes		Horizontal Greisen Veins		Barren Quartz Veins	
	Halite	Vapor	Halite	Vapor	Halite	Vapor
	8 % 224°–299°C	6.5 % 289°–300°C	23 % 270°–299°C	4 % 278°–299°C	All Inclusion(s) 371°–402°C	
	92 % 300°–536°C	90.5 % 300°–595°C	77 % 300°–533°C	92 % 300°–448°C		
		3 % ≥600°C		4 % ≥600°C		

Fig. 25. Frequency diagrams of homogenization temperatures for fluid inclusions of vertical vein quartz.

VERTICAL GREISEN VEINS; HOMOGENIZATION TEMPERATURES

VERTICAL GREISEN VEINS; HOMOGENIZATION TEMPERATURES

VAPOR DISAPPEARANCE; INCLUSION TYPE C
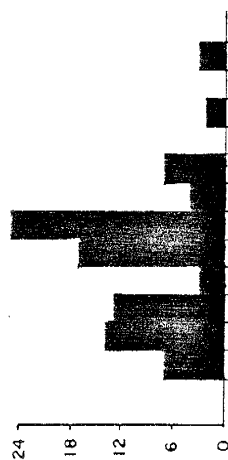
HALITE DISAPPEARANCE; INCLUSION TYPE C

NUMBER OF INCLUSIONS
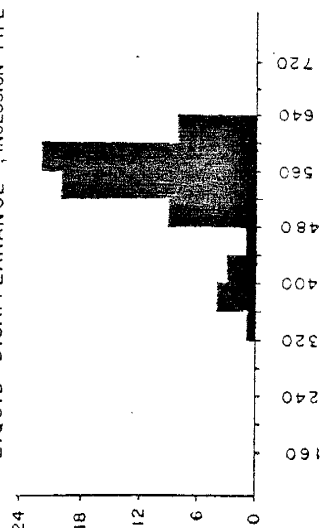
TEMPERATURE (°C)

VAPOR DISAPPEARANCE; INCLUSION TYPE A
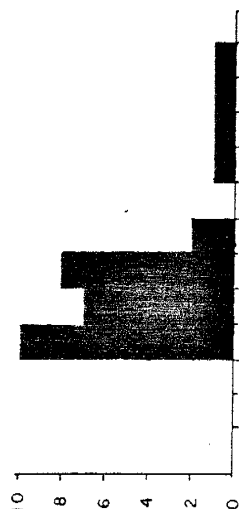
LIQUID DISAPPEARANCE; INCLUSION TYPE B

NUMBER OF INCLUSIONS
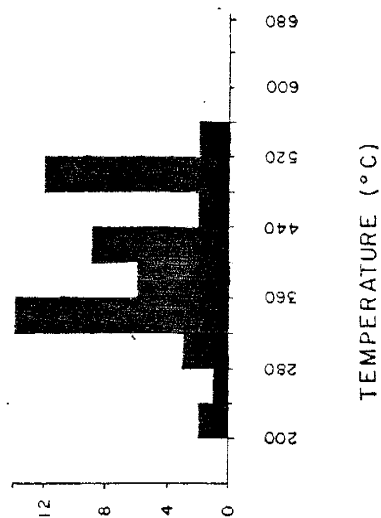
TEMPERATURE (°C)

Fig. 26. Frequency diagrams of homogenization temperatures for fluid inclusions of horizontal vein quartz.

HORIZONTAL GREISEN VEINS; HOMOGENIZATION TEMPERATURES

VAPOR DISAPPEARANCE; INCLUSION TYPE C

HALITE DISAPPEARANCE; INCLUSION TYPE C
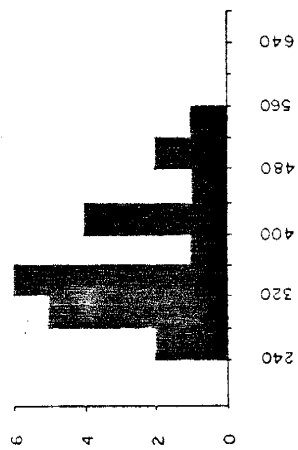
NUMBER OF INCLUSIONS

TEMPERATURE (°C)

HORIZONTAL GREISEN VEINS; HOMOGENIZATION TEMPERATURES

VAPOR DISAPPEARANCE; INCLUSION TYPE A
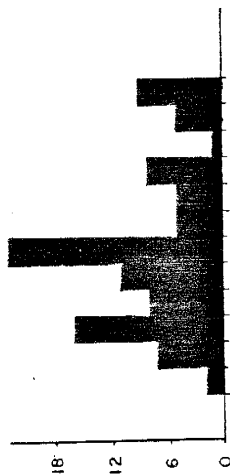
LIQUID DISAPPEARANCE; INCLUSION TYPE B
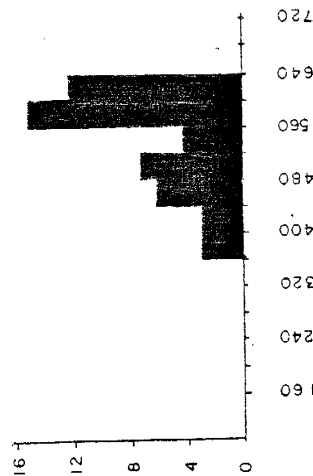
NUMBER OF INCLUSIONS

TEMPERATURE (°C)

Fig. 27. Frequency diagrams of homogenization temper-
atures and salinities vs temperature of homogenization
in inclusions of barren vein quartz.
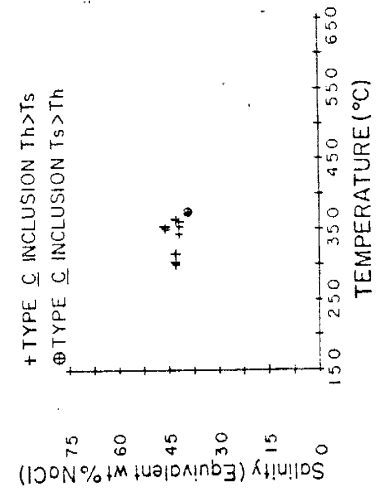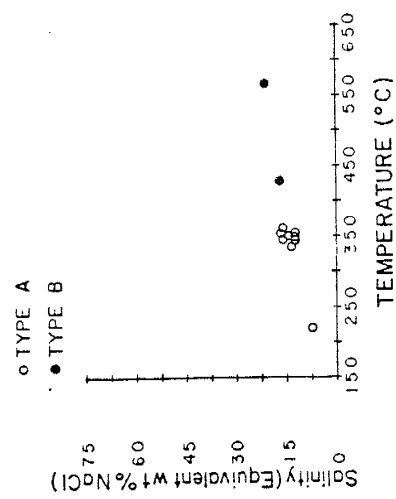
BARREN QUARTZ VEINS; HOMOGENIZATION TEMPERATURES

VAPOR DISAPPEARANCE ; INCLUSION TYPES A and B

L = Liquid Disappearance

HALITE DISAPPEARANCE; INCLUSION TYPE C

V = Vapor Disappearance

NUMBER OF INCLUSIONS

TEMPERATURE (°C)

BARREN QUARTZ VEINS

o TYPE A
• TYPE B

Salinity (Equivalent wt% NaCl)

TEMPERATURE (°C)

+ TYPE C INCLUSION Th>Ts
⊕ TYPE C INCLUSION Ts>Th

Salinity (Equivalent wt% NaCl)
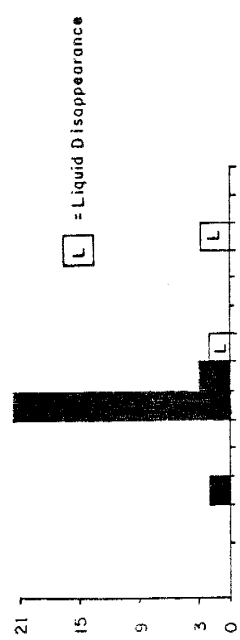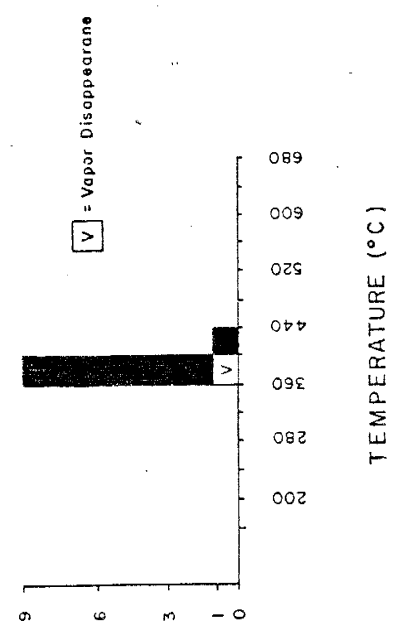
TEMPERATURE (°C)

HORIZONTAL GREISEN VEINS ; PHASE DISAPPEARANCE TEMPERATURES

VAPOR ; INCLUSION TYPE C

HALITE ; INCLUSION TYPE C

NUMBER OF INCLUSIONS
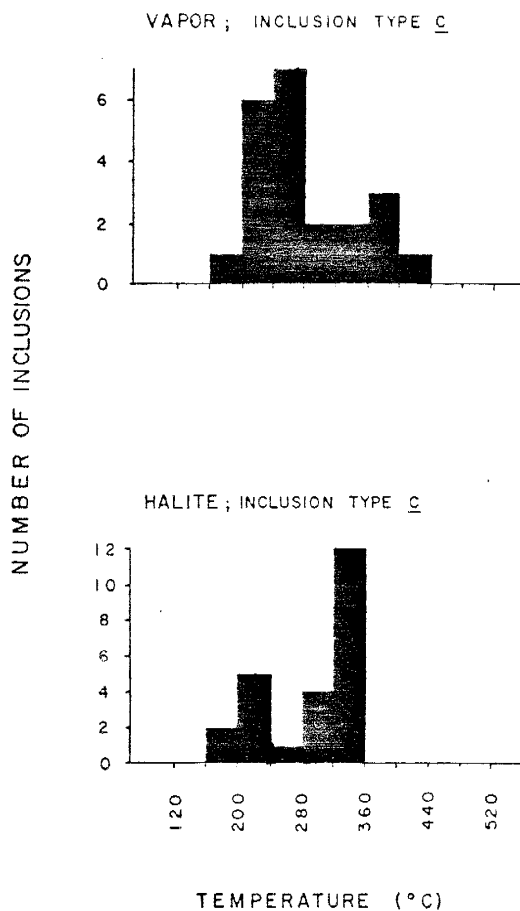
TEMPERATURE (°C)

Fig. 28A. Temperatures of phase disappearance, type C inclusions of horizontal vein quartz.

VERTICAL GREISEN VEINS; PHASE DISAPPEARANCE TEMPERTURES

VAPOR; INCLUSION TYPE C

HALITE; INCLUSION TYPE C

CRYOLITE; INCLUSION TYPE D

NUMBER OF INCLUSIONS
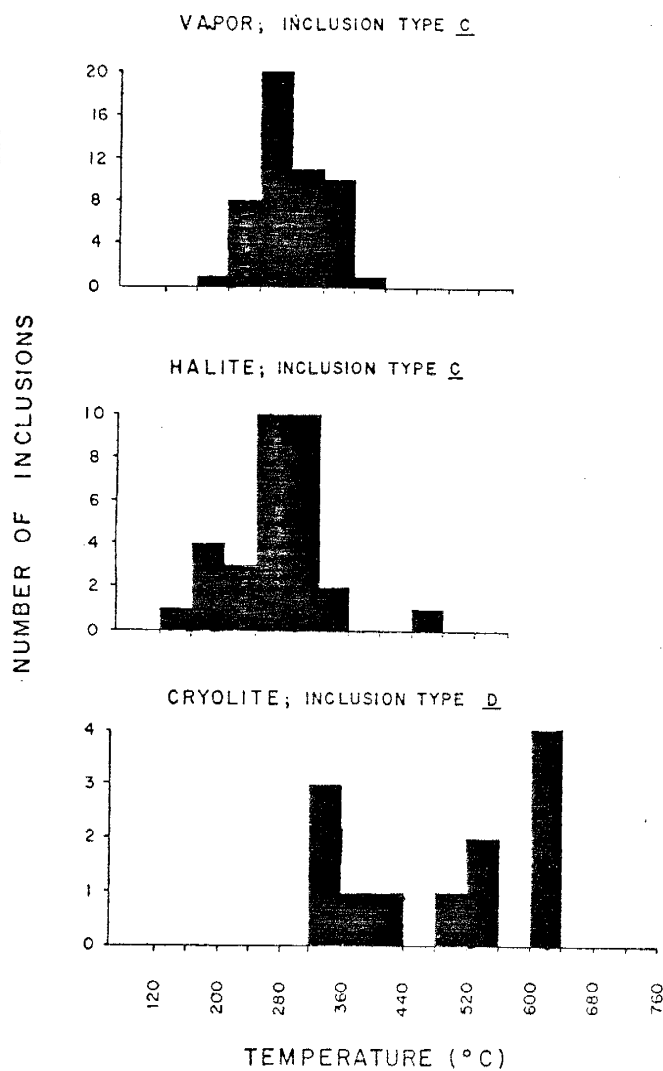
TEMPERATURE (°C)

Fig. 28B.   Temperatures of phase disappearance, type C
and D inclusions of vertical vein quartz.

Fluid salinities

Few salinity measurements were made on type A and B inclusions because these inclusions were difficult to freeze. About 30 percent of all type A and B inclusions within a given field of view froze when cooled to $-100^{\circ}C$. The few type A and B inclusions which did freeze yielded a mean salinity of 21 equivalent weight percent NaCl (Fig. 29). Halite-bearing type C inclusions indicated salinities in the range of 30 to 60 equivalent weight percent NaCl.
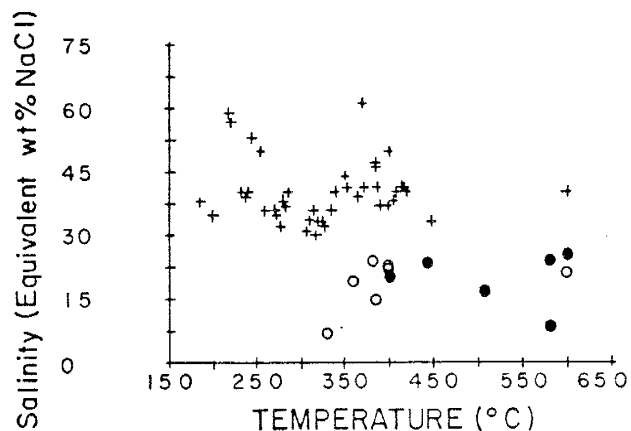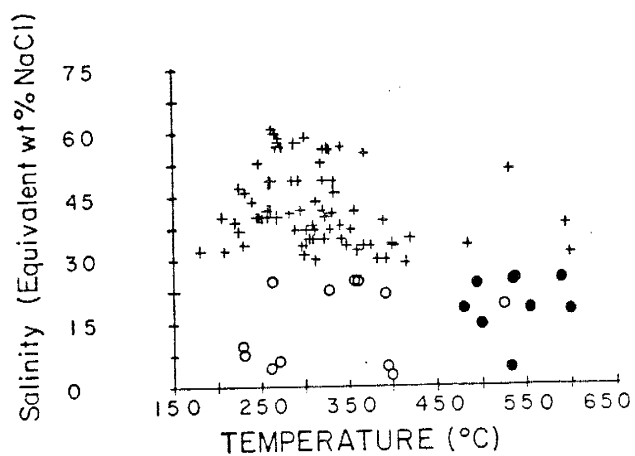
Fig. 29. Measured salinities vs homogenization temperatures for type A, B, and C inclusions in horizontal and vertical vein quartz.

Evidence of boiling

Type A, B, and C (liquid-rich, vapor-rich, and halite-bearing) inclusions occur together within a given field of view in all quartz samples examined. These inclusions occur in close proximity but remain randomly distributed with respect to each other. Type A inclusions exhibit a wide range of liquid to vapor ratios, suggesting that original fluids, from which these inclusions were derived, were actually boiling at the time of trapping.

The occurrence of the three types of inclusions (A, B, and C) is best explained by trapping from boiling, dense, saline brines. Other evidence of boiling is provided by simultaneous disappearance of vapor and halite in some halite-bearing inclusions. Within the same crystals this process was observed to occur around $320^{O}C$ and again around $520^{O}C$. Type A and B inclusions associated with such type C inclusions homogenized at the same temperature. Salinities at these temperatures were inferred from halite dissolution temperatures. Boiling conditions of $320^{O}C$ and 38 equivalent weight percent NaCl, and $520^{O}C$ and 55 equivalent weight percent NaCl were inferred (Keevil, 1942).

Halite homogenization

Halite dissolved before or after the disappearance of the vapor phase when type C inclusions were heated. Ts and Th are recorded temperatures of halite and vapor disappearance respectively in a given type C inclusion. Halite homogenization occurs when $Ts > Th$, or halite is the last phase to disappear before complete homogenization into the liquid phase (Fig. 30).

HORIZONTAL GREISEN VEINS; TYPE C INCLUSIONS
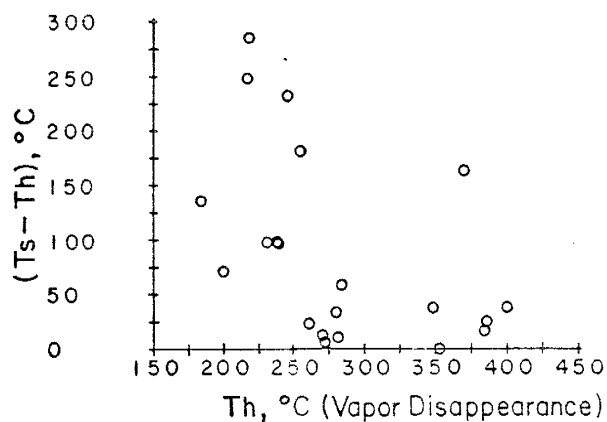
VERTICAL GREISEN VEINS; TYPE C INCLUSION
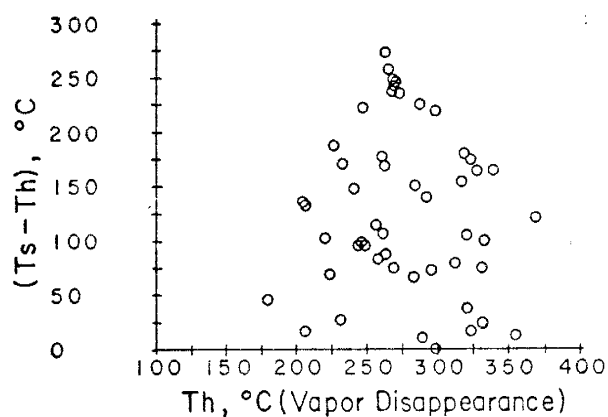
Fig. 30. (Ts - Th) vs Th diagrams of type C inclusions of horizontal and vertical vein quartz. Ts = temperature of dissolution of halite; Th = temperature of vapor disappearance.

Figure 31, adapted from Erwood, Kesler, and Cloke (1979),
illustrates probable conditions of formation of halite-
bearing inclusions. In this P-T diagram, MNQ and RST repre-
sent approximate isochors. A liquid trapped under cond-
itions at point M will follow the isochor to point N where
halite will begin to separate from the liquid. The cooling
path will then enter the halite-liquid field until point Q
on the solubility curve is reached. At point Q a vapor
phase will begin to separate, and the liquid will follow the
solubility curve to room temperature. An inclusion formed
this way will homogenize by halite disappearance.

Fig. 31. P – T diagram illustrating possible behavior of halite-bearing type C inclusions.   Isopleth at   40 equivalent wt. % NaCl in the system NaCl-H_2O (Adapted from Erwood, et al., 1979).

Fig. 32. P – T diagram illustrating the unusual behavior in some type A inclusions.
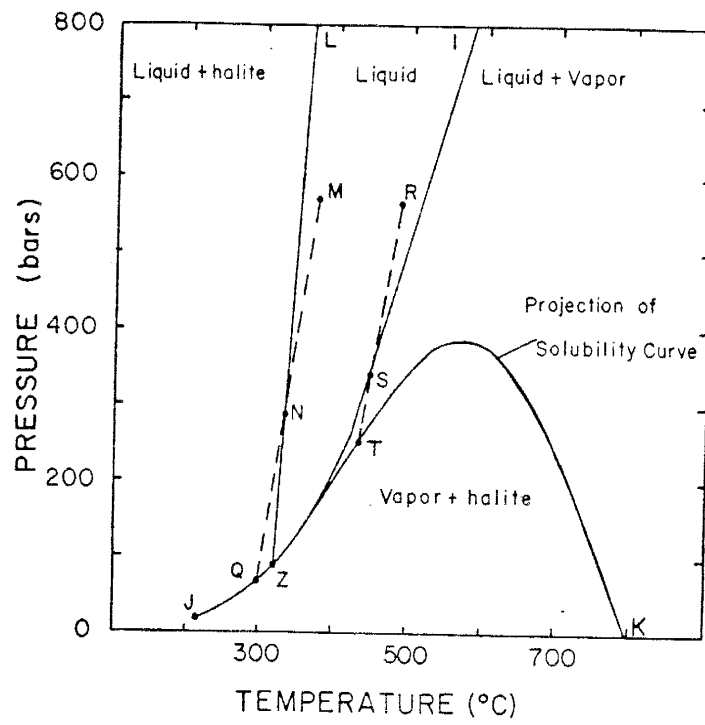
Fig. 31.
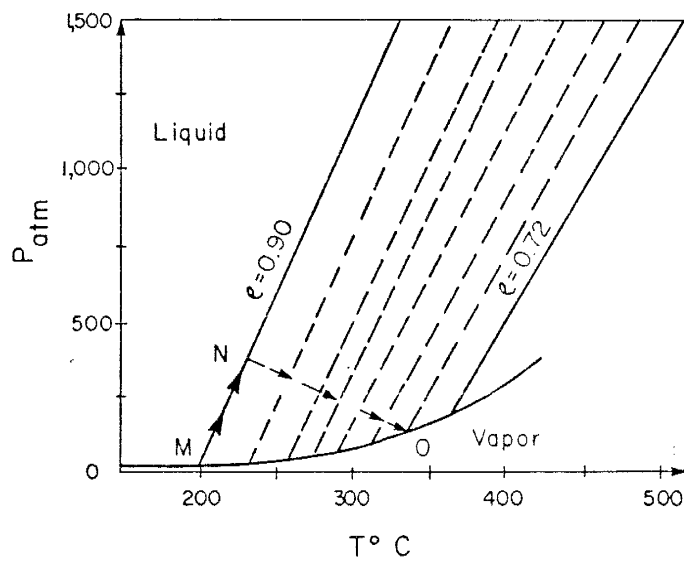
Fig. 32.

Unusual phase behavior

During the examination of inclusions showing unusual homogenization behavior as previously described, attention was given to close observation of volume or surface area of the phases present. Any change of the original size of the phases would have implied leakage of the inclusion waters, and the reproducibility of observed phase behavior would have been prevented. Observations of such inclusions during 48 hours after heating and freezing runs confirmed that leakage of inclusion waters was not involved. The unusual homogenization behavior may be best explained by change of density of the inclusion fluid.

After disappearance of the vapor bubble at $200^{O}C$, the heating path should follow a line of constant density through the liquid field. For a vapor phase to reappear at $330^{O}C$ the evolution path must intersect the phase boundary curve at that temperature. This may be achieved only by decreasing the density of the liquid as temperature increases. The P-T sketch diagram (Fig. 32) shows such inclusion behavior from point M where an isochor of density 0.90 intersects the liquid-vapor boundary. At point M (temperature: $200^{O}C$), the initial vapor phase disappears and the heating path follows the corresponding isochor into the liquid field to point N. At point N it is postulated that a steady decrease in density starts and will continue until the heating path intersects the liquid-vapor boundary at

point O (temperature: 330°C), and will remain on that
boundary until 600°C (stage upper limit).

A density change may occur when a solid phase precipit-
ates at high temperature. Such was the case in one of the
inclusions examined. It can be assumed that solid precip-
itates were also present in the remaining inclusions, but in
minute size, and easily overlooked.

5.3.5 Pressure-Depth Estimates

Estimates of pressures are obtained from type C inclus-
ions trapped along the solubility surface in the system
NaCl-H$_2$O, and from inclusion pairs trapped during boiling.
The accuracy of heating runs at temperatures around 300°C
and higher was ± 5°C (see Appendix III). Type C inclusions
with a difference of 10°C between halite dissolution and
temperature of vapor disappearance are thought to have been
trapped along the solubility surface in the system
NaCl-H$_2$O.

The best estimates of pressures were obtained from two
such groups of type C inclusions which homogenized around
320°C and 520°C. Data from Haas (1971) and Sourirajan and
Kennedy (1962) were used to obtain the pressure estimates
from these inclusions. Estimates of 75 bars and 350 bars
respectively were obtained. The estimate of 75 bars
corresponds to depth of about 300 m and 940 m under litho-
static and hydrostatic conditions, respectively. The est-

imate of 350 bars corresponds to 1300 m and 4375 m under
lithostatic and hydrostatic conditions, respectively (Table
6).

TABLE 6.   ESTIMATES OF PRESSURES AND DEPTHS

Pressures	Lithostatic Depth	Hydrostatic Depth
75 bars (320°C, 38 eq.wt. % NaCl)	300 m	940 m
350 bars (520°C, 55 eq.wt. % NaCl)	1310 m	4375 m

Assuming a geologic cover at the time of mineralization
was similar to the present volcanic cover at Mount Cameroon,
a mimimum depth of 2850 m could be estimated from the pre-
sent topography at Mayo-Darlé. Estimates of pressures (740
bars) corresponding to this depth could have prevailed as
overpressures as indicated by type C inclusions homo-
genizing by halite disappearance.

5.3.6 Composition of the ore fluids

The composition of ore-bearing fluids was estimated from fluid inclusion analyses. Type C and D inclusions constitute 50 and 7 percent, respectively, of all inclusions examined (Table 4). Halite-bearing type C inclusions indicate salinities up to 60 eq. wt. % NaCl. In most of halite- and cryolite-bearing type D inclusions, the two daughter minerals have approximated indentical phase ratios (Fig. 24). The average phase ratio of cryolite, computed as volume percent, was used to calculate the approximate F content of type D inclusions. Commonly occuring type D inclusions average 25 ppm F. The presence of type C and type D inclusions in quartz from mineralized veins indicate that the mineralizing fluids were saturated with respect to NaCl, and that these fluids were enriched in fluorine.

CHAPTER 6. DISCUSSION

6.1 PETROGENESIS OF THE IGNEOUS ROCKS

6.1.1 Introduction

Field evidences and Rb-Sr isotope studies suggest the following sequence of emplacement within the Mayo-Darlé complex: nordmarkite, rhyolite, biotite granite, and granite porphyry. Benmoreite xenoliths are thought to represent the older igneous unit of the complex on the basis of their "basicity" (low silica content). Benmoreites are considered as basic trachytes (Cox, Bell, and Pankhurst, 1979), and as such should have erupted before the crystallization of the more silica-enriched nordmarkite.

The Mayo-Darlé complex is characterized by its sharp contact with the surrounding country rocks. Xenolithic inclusions are absent within the complex, except in rhyolite. The density of pegmatitic phases within the complex is negligible. These factors are necessary for any meaningful geochemical modeling. Post-emplacement events linked to tin mineralization have affected the complex. This renders difficult the deciphering of some genetic characteristics inherited from the source rocks. However homogeneity within each rock unit prevails; this allows one to attempt to retrace the origin of the complex.

A genetic model for the igneous complex at Mayo-Darlé

must account for all types of rocks present. Possible sources of granite magmas are the upper mantle and the lower crust. Mechanisms of magma generation from these sources are fractional crystallization, partial melting, or a combination of both processes.

Field evidence, such as the presence of rock varieties reflecting various stages of possible differentiation trends or progressive melting stages, suggest either fractional crystallization or progressive melting as likely processes for the generation of the Mayo-Darlé complex. Figure 33 indicates a trend of increasing silica toward the quartz-feldspar cotectic. Most siliceous samples cluster around the thermal trough at a water vapor pressure of 1000 bars. The AFM diagram (Fig. 34) and the Alkali-Quartz-Total Fe (Fig. 35) indicate a possible differentiation lineage from benmoreite through nordmarkite and rhyolite to granite. It may be inferred from this that all igneous rocks of this complex are cogenetic and could have been derived by fractional crystallization of a basic magma to account for the entire sequence.
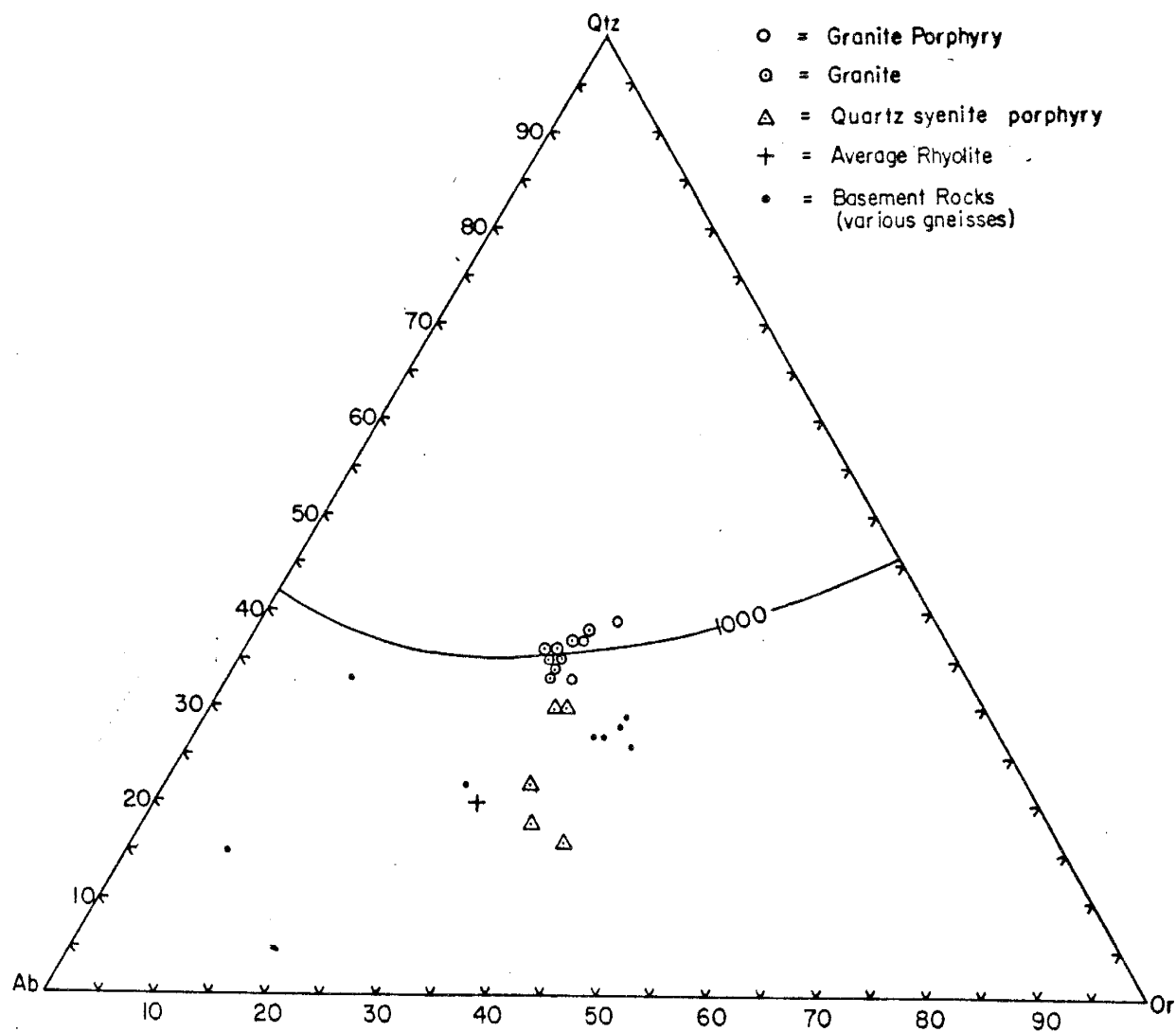
Fig. 33. Quartz-Albite-orthoclase ternary diagram showing the isobaric minumum at P_{H_2O} = 1000 bars.
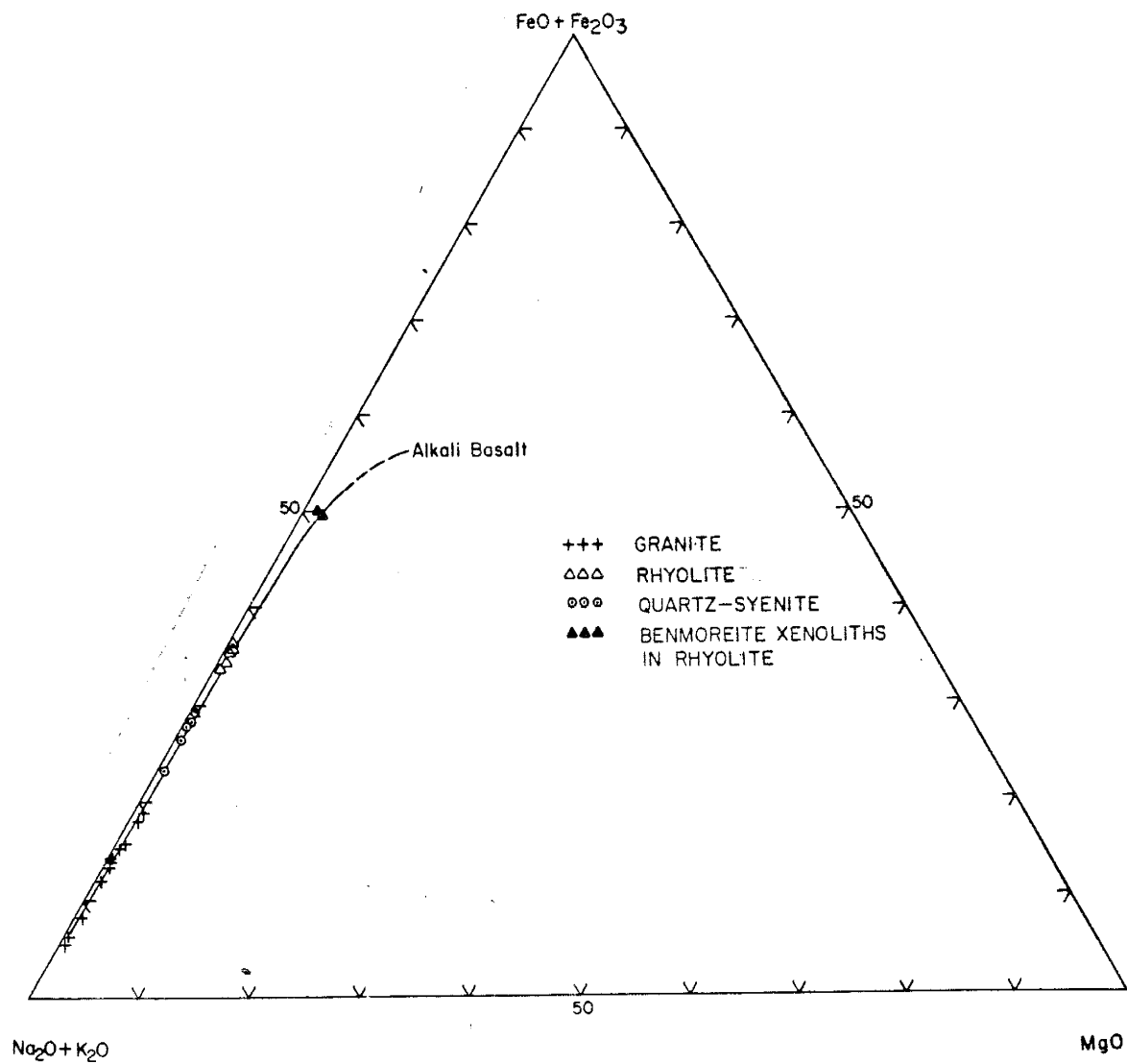
Fig. 34. AFM ternary diagram.
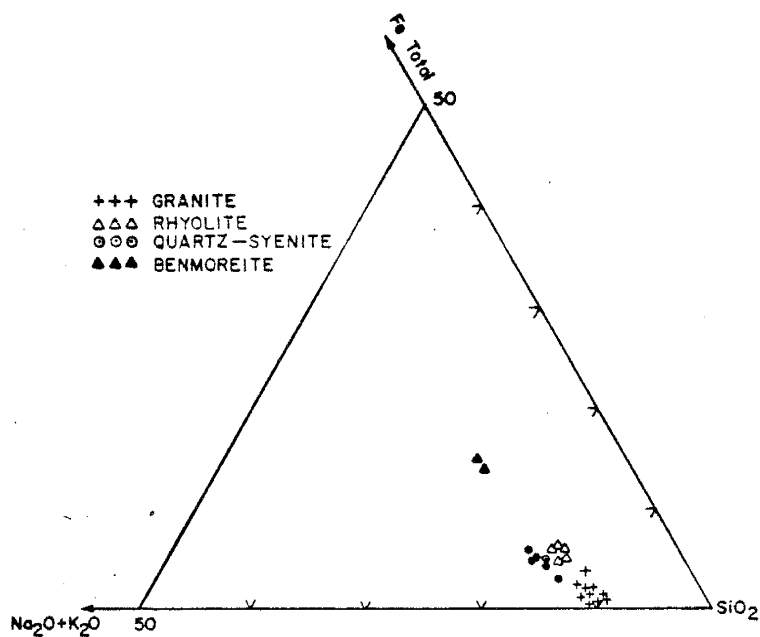
Fig. 35. Alkali-Total Fe-SiO$_2$ ternary diagram.
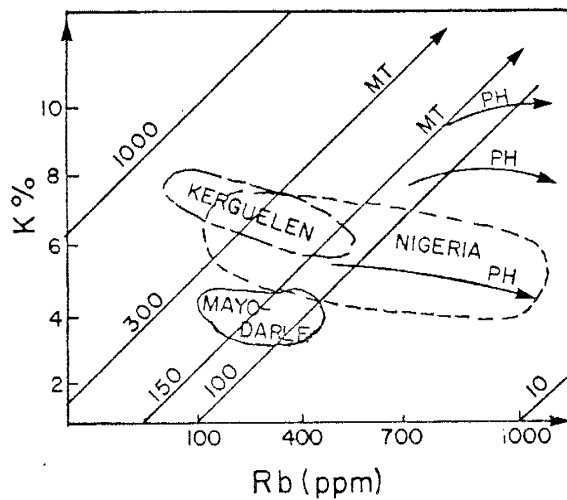
Fig. 36. K vs Rb (Adapted from Vidal, et al., 1978)
MT = Main trend; PH = Hydrothermal trend.

Different variables have been used to test the fractional crystallization hypothesis. The TiO_2/Ta ratio has been used as an indicator of the degree of differentiation in alkali syenite-granite complexes (Boissavy-Vinau and Roger, 1980). This ratio should decrease from less differentiated units to the more differentiated members of the series. Within the Mayo-Darlé complex the TiO_2/Ta ratio ranges from 890 in benmoreite to 19 in granite (Table 1). K/Rb ratios have been used to determine the crystallization sequence within the granitoid complexes of northern Nigeria (Butler, et al., 1962). K/Rb ratios decrease with increasing SiO_2 content. Within the Mayo-Darlé complex K/Rb ratios decrease from benmoreite to granite, which is consistent with the suggested lineage trend. Potassium and rubidium are very mobile elements. Hydrothermal fluids may have contributed to their concentration within the granite which was strongly affected by the mineralizing hydrothermal event. The K vs Rb plot (Fig. 36) shows the hydrothermal trends deviating from the normal behavior (Vidal, et al., 1978). The Ba-Rb-Sr plot (Fig. 19) indicates that the granites are highly differentiated.

6.1.2   Rb-Sr Evidences

The isotopic composition of Sr is a valuable indicator of the age of rocks and minerals, as well as the origin of geologic and geochemical processes which affected the

chemical composition of these rocks and minerals (Kistler, et al., 1973, Moorbath, et al., 1965, Brooks, 1966, Armstrong, 1968, and many others). Faure and Powell (1972), in their compilation of measured initial $^{87}Sr/^{86}Sr$ in granitic rocks, distinguished three categories of granites. 1) Granites with initial ratios within the basalt field (0.702-0.706) represent 50 percent of the granitic rock suites analyzed. 2) Granites with intermediate initial ratios (0.706-0.719) represent 30 percent of the analyzed granitic rock suites. 3) Granites with high initial $^{87}Sr/^{86}Sr$ ratios (> 0.719) make up 20 percent of the analyzed rocks.

The low ratios indicate that the original magma from which such granitic magmas fractionated, originated in the mantle and incorporated little or no strontium from pre-existing crustal materials (Fullagan, et al.,1971). Providing the system remained closed to Rb and Sr, granites or granitic suites are likely to be generated by fractional crystallization. The $^{87}Sr/^{86}Sr$ initial ratios within the Mayo-Darlé complex range from 0.7030 in nordmarkite to 0.7094 in biotite granite. Associated average Rb/Sr ratios range from 11.2 to 38.1 respectively.

The low initial Sr isotopic ratio indicated by nordmarkite suggests a mantle origin for the parent magma. If the rock suite composing the complex was derived by fractional crystallization processes, one would expect a much narrower range in $^{87}Sr/^{86}Sr$ initial values. It would

require ten and thirteen million years to account for the initial ratios observed within the rhyolite (0.7075) and the granite (0.7094) respectively, if both rock types were derived by fractional crystallization of a syenitic liquid with a constant Rb/Sr ratio of 11.2 and an initial $^{87}Sr/^{86}Sr$ of 0.7030. The relatively high $^{87}Sr/^{86}Sr$ initial ratios of the rhyolite and granite are in conflict with the differentiation trend suggested by field and major element evidences. Several explanations can be advanced to account for the $^{87}Sr/^{86}Sr$ data.

Nordmarkite

The initial Sr isotopic ratio yielded by the nordmarkite (0.7030 ± 0.0035) falls within the basalt field. This suggests little or no evidence of crustal involvement and favors an alkali basalt as a probable source rock. The surrounding metasediments yield a much higher initial Sr isotopic ratio (0.7059 ± 0.0007) compared to the value yielded by the nordmarkite. This implies very limited or no contamination from the surrounding country rocks during the emplacement of the syenitic intrusive.

Rhyolite and granite

The initial ratios of the rhyolites and the granites are substantially higher than the value yielded by nordmarkite (Table 3). Several hypotheses could explain the origin of these rocks.

1) Rhyolites and granites were derived from partial melting of the Pan-African metasediments.

2) Rhyolites and granites are products of different-iation of the basaltic magma from which the nordmarkites were derived. Concurrent crustal contamination from the surrounding metasediments increased the radiogenic Sr of the differentiating magmas.

3) Radiogenic Sr was added to the system after em-placement.

Major element and field evidences suggest cogeneity between all rock types within the complex. Therefore the low initial Sr isotopic ratio of nordmarkite rules out the meta-sediments as likely parental source. If the primary magma originated in the upper mantle and migrated upward through the crust, the late-crystallizing phases would be depleted in Sr. The Sr data indicate a decrease in Sr content from nordmarkite to granite. A maximum of 27% contamination from the metasediments is required if the liquids crystallizing the rhyolites and the granites were contaminated at the time of crystallization 73 million years ago. Superheating of the metasediments would be required to attain such a degree of contamination. The relatively small pluton at Mayo-Darlé could not have provided enough heat to produce this high degree of crustal contamination.

A criterion for evaluating simple mixing of mantle-derived magmas with crustal material is the hyperbolic relationship between $^{87}Sr/^{86}Sr$ and Sr (Faure, 1977). The

$^{87}Sr/^{86}Sr$ vs Sr diagram (Fig. 37) defines a relatively poor hyperbola, thus suggesting more complex processes which could have caused the pseudo-isochrons of the granites and the rhyolites.
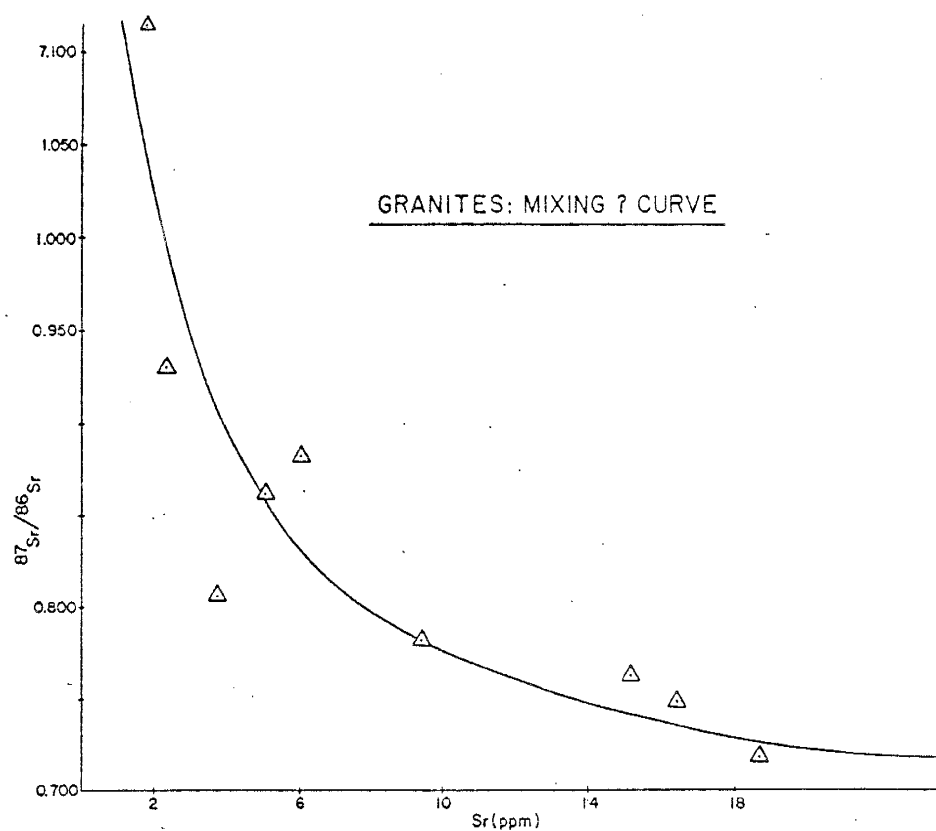
Fig. 37. $^{87}Sr/^{86}Sr$ vs Sr curve.

The volumetric paucity of xenocrysts and xenoliths within the granite is a strong indication that crustal con- tamination did not play a key role during the process of differentiation of the primary magma. Studies of young continental volcanism in southern Peru (Brooks, et al., 1976) have shown that crustal contamination was not a plausible mechanism causing the high $^{87}Sr/^{86}Sr$ initial ratios and the pseudo-isochrons observed. If the Andean crust, about 70 km thick, had little effect on upward ascending volcanics in south Peru, the presumed thinner crust along the Cameroon Line probably could not have had a greater influence on ascending magmas in the region. Crustal contamination cannot be ruled out entirely, however its influence was probably minor.

Syenite-granite associations similar to the Mayo-Darlé series have been observed in other provinces around the world. These complexes have been interpreted as having formed by fractional crystallization processes from a common parental source on the basis of Rb-Sr isotopes.

To account for all rock types of the area, Nougier and Lameyre (1974), and Lameyre, et al. (1976) have argued that the Kerguelen islands syenite-granite ring complex was derived by fractional crystallization from an alkali basalt magma. In northern Nigeria, a similar rock association in the Ririwai non-orogenic ring complex has been recently reinterpreted as a product of differentiation of a more

basic non-orogenic magma, probably of gabbroic composition (Martin and Bowden, 1981). In the Gardar alkalic province of south Greenland, Blaxland, et al. (1978) have concluded that fractional crystallization of a basic magma of alkali basalt composition could better explain the alkali syenite-granite association.

In the examples cited, strontium isotopic initial ratios of the most differentiated members are high, ranging from 0.7068 for the biotite granite of the Gardar province to 0.7110 for the Kerguelen granites, and finally up to 0.752 for the Nigerian granites (Table 7). The associated syenites, on the other hand, exhibit strontium isotopic ratios of 0.702 to 0.704 in the Gardar province, 0.7055 to 0.7059 in the Kerguelen islands, and 0.7048 in the Nigerian granites (Table 7).

Table 7. Rb-Sr EVIDENCES IN SYENITE-GRANITE COMPLEXES

	Kerguelen Islands (Lameyre, et al.,1976)	Northern Nigeria (Vidal, et al.,1978)	Gardar, S. Greenland (Blaxland, et al.,1978)	Mayo-Darle, Cameroon This Study
	$(^{87}Sr/^{86}Sr)o$			
Syenites	0.7055 – 0.7059	0.7048	0.702 – 0.706	0.7030
Granites	0.7110	0.7066 – 0.752	0.7068	0.7094
Calcu-lated Crystal-lization time	Rb/Sr=130 ~1 m.y.	Rb/Sr=30.8 ~1.4 m.y. (18-36 m.y.)	Rb/Sr=11.6 ~9.4 m.y.	Rb/Sr=11.2 ~13 m.y. Rb/Sr=38.1 ~4 m.y.
Post-crystal-lization Event		Mineral-ization	Mineral-ization	Mineral-ization

The low strontium isotopic ratios in each province also restricts the original parental magma of each rock series to the basalt field as defined by Faure and Powell (1972). The high $^{87}Sr/^{86}Sr$ initial ratios of the more differentiated members are interpreted as resulting from either in situ decay of ^{87}Rb to ^{87}Sr during the crystallization period, or as resulting from a combination of in situ decay of ^{87}Rb to ^{87}Sr and crustal contamination during the crystallization period. The calculated crystallization time for these complexes using Rb/Sr ratios of the syenites indicate anomalously long periods of crystallization (Table 7). These values are considerably reduced when high Rb/Sr ratios of the granites are used. It is suggested that processes other than simple decay of ^{87}Rb to ^{87}Sr and/or crustal contamination were involved in the enrichment of radiogenic strontium within these complexes. In northern Nigeria and southern Greenland mineralization has been reported in association with the granites. It is postulated that hydrothermal mineralizing fluids could have played an important role in the disturbance of the Rb-Sr systematics within these complexes.

Brooks and Compston (1965) suggested hydrothermal con-tamination as the likely mechanism for altering the Rb-Sr system within the Heemskirk granite. Bickford and Mose (1975) have suggested that a hydrothermal event associated with mineralization probably lowered the Sr content and

caused the high initial $^{87}Sr/^{86}Sr$ ratios of the plutonic and volcanic rocks of the St-François Mountains in southeast Missouri. Significant Sr loss and high initial $^{87}Sr/^{86}Sr$ ratios of the volcanics and granites at Mayo-Darlé probably occurred during the hydrothermal event which caused the mineralizing fluids to permeate the rocks and deposit cassiterite in veins.

Strontium isotopic analyses of fluid inclusion waters in quartz and cassiterite from mineralized greisen veins indicate Rb/Sr of 0.41 to 14.7 and calculated $^{87}Sr/^{86}Sr$ ratios ranging from 0.7074 to 0.7159 at the time of mineralization (Table 8).

TABLE 8. Rb-Sr DATA OF FLUID INCLUSION WATERS
FROM QUARTZ AND CASSITERITE

Sample	Rb (ppm)	Sr (ppm)	$^{87}Sr/^{86}Sr$ present	$^{87}Sr/^{86}Sr$ present	$^{87}Sr/^{86}Sr$ 70 m.y.
Qtz-phenocryst (granite)	50.4	6.6	22.2	0.7295	0.7074
HGE-2N-80 (tin-floor qtz)	78.6	16.7	19.2	0.7350	0.7159
SnO_2 (cassiterite)	13.7	33.2	1.2	0.7158	0.7146
Euhedral-Qtz	73.4	8.4	25.4	0.7330	0.7077
Ore-Qtz (Greisen lode)	225.8	15.3	42.9	2.2304	2.1877

This suggests that mineralizing fluids, if evolved at the time of granite crystallization, were heterogeneous and not in isotopic equilibrium with the granite. Since mineralization at Mayo-Darlé post-dates the emplacement of granite,the strontium isotopic content of the mineralizing hydrothermal fluids must have played a key role in the disturbance of the Rb-Sr system of the complex.

In summary the preceding discussion suggests that the true age of the entire complex is indicated by the syenite isochron which yielded an age of 73 $\pm$ 6 m.y. with the true initial $^{87}Sr/^{86}Sr$ value of 0.7030 $\pm$ 0.0035. The Mayo-Darlé complex could have derived by progressive fractional crystallization from alkali basaltic magma . Soon after the emplacement of the major rock units, hydrothermal fluids permeated the area, and deposited Sn in veins within the granite ,and in the process they disturbed the Rb-Sr system of the complex.

6.1.3 Major and Trace Element Modeling

Fractional crystallization and partial melting models for the generation of the Mayo-Darlé igneous rock suite were tested using statistical mixing programs (Wright and Doherty, 1970) and well established geochemical modeling methods (Allègre and Minster, 1978). Major-element data and residual phases shown in Table 3, Appendix I, were used in

this evaluation.

Parental sources around the area and sources likely to generate the observed rock suite were tested. Prime candidates are biotite gneiss and quartz diorite gneiss of the Pan-African metasediments. On the basis of major-element chemistry, partial melting of the sediments from these two sources proved unlikely to generate the observed igneous series. Partial melting of a lower crust granulite (Condie and Hunter, 1976), a high Ca-granite (Condie, 1978), followed by fractional crystallization were not able to generate all observed rock units. Partial melting of these sources can neither account for benmoreite as a daughter or as a residual rock.

A model which best explains the observed rock sequence involves fractional crystallization from an alkali basaltic parent. The observed rock suite: benmoreite, quartz-syenite, rhyolite, alkali biotite granite is similar to rock series reported in the Central Rift Valley in Kenya, East-Africa (McCall and Hornung, 1972). The sequence of intermediate to acidic rocks in the Central Rift Valley has been interpreted in terms of differentiation process affecting a mantle-derived basalt parent based on the spatial and temporal relationship between hawaiites, mugearites, and trachytes (McCall and Hornung, 1972). Strontium isotopic data within the Mayo-Darlé complex restrict a likely parent within the basalt field. The rarity of pegmatitic phases within the complex suggests a parental source with low H_2O, less than

1.2% H_2O (Maaløe and Wyllie, 1975). The parental magma could have been produced in the upper mantle-lower crust region (15-35 km); subsequent magma derivatives migrated through the crust and were later emplaced at shallow depths (about 8 km).

The most basic member of the Mayo-Darlé complex, benmoreite, could not be derived directly from an alkali olivine basalt. A liquid with mugearite composition is most likely to have preceded benmoreite. A mugearite of the Silali Volcanics in Jebunbun, Kenya was thus selected as a starting composition (McCall and Hornung, 1972). Fifty-one percent (51%) fractional crystallization (F = 0.49) of the mugearite liquid composition produced in the upper mantle or lower crustal region is required to produce benmoreite with olivine (6.6%), plagioclase (29%), clinopyroxene (9.6%), and ilmenite (4%) as residual phases. Subsequently, 44 percent fractional crystallization (F = 0.56) of benmoreite is required to generate nordmarkite with plagioclase (25%), clinopyroxene (22%), magnetite (5%), and ilmenite (4%) forming the residual rock. To account for the actual composition of nordmarkite, the benmoreite liquid should be slightly enriched in most major oxides compared to the composition of benmoreite xenoliths found in rhyolites. Rhyolites could be generated by 62 percent fractional crystallization (F = 0.38) of a liquid with nordmarkite composition with plagioclase (18%) and K-feldspar (19%) in the residue. Biotite granite could be derived from a

rhyolitic liquid by 78 percent fractional crystallization (F = 0.22)with plagioclase (9.4%), clinopyroxene (12 %), and hornblende (0.6%) as residual phases. Iron and manganese were in excess in the immediate source of granite. A residual phase of Fe-Mn oxides could take up the excess Fe and Mn. The observed granite is low in Ca, Mg, and Na compared to the model values.

Rare earth elements within the observed rock suite decrease from nordmarkite to granite (Fig. 13). The decrease in rare earth content is in contradiction with the preferential partitioning of these elements into remaining liquids during fractional crystallization. Recent studies indicate that rare earth patterns show a steady decrease in light rare earth concentration with increasing degree of differentiation (Miller and Mittlefehldt, 1979, Condie, 1978, Fourcade and Allègre, 1981). These authors have suggested that accessory minerals such as allanite, monazite, zircon, and to lesser extent, apatite, could be entrained with early and subsequent crystallizing phases, thus causing the depletion of light rare earth and an overall decrease in rare earth elements within a given comagmatic felsic rock sequence. This argument lends the best explanation to the observed decrease in rare earth elements within the Mayo-Darlé complex.

Apatite and zircon have been observed consistently throughout the entire sequence. These two minerals preferentially concentrate heavy rare earths. Allanite and

monazite though not observed, could be present. The abundance of the accessory minerals decreases with increasing degree of differentiation within the series which is consistent with the hypothesis of formation of accessory minerals in early crystallizing phases.

The heavy rare earth elements show only slight fractionation within the series. Other trace element behavior as described in the petrochemistry section are consistent with a fractional crystallization model. The low Ba values within the granite could be accounted for by continuous removal of K-feldspar. Removal of magnetite could explain the low concentrations of Co and Cr in benmoreite and rhyolite. Strontium values decrease within the series from nordmarkite to granite. The removal of plagioclase as indicated by the fractional crystallization model cannot solely account for the lowering of Sr values within the rock suite. Hydrothermal processes which affected this complex during the mineralization period could have influenced the removal of Sr and enrichment of Rb by late, differentiated members of the series (Bickford and Mose, 1975). The rare earth elements also could have been disturbed during the hydrothermal event. Rare earth mobility by hydrothermal solutions is plausible (Kosterin, 1959, McLennan and Taylor, 1979).

The Mayo-Darlé complex is not unique along the Cameroon Line. Similar small complexes line up along this tectonic structure (Gouhier and Nougier, J. and D., 1974; Tchoua,

1974; Gouhier and Rollet, 1978). Rock units at Mount Cameroon located on the coast, SW of Mayo-Darlé, range from alkali olivine basalt to rhyolitic volcanics (Dumort,1968). Differentiated series may be characteristic of the Cameroon Line.

6.2 GENESIS OF MINERALIZATION

6.2.1 Mineralizing Fluids and Source of Tin

The high temperatures of homogenization of the inclusions and the close association of the mineralization with the granite intrusive suggest that the mineralizing brines were of magmatic hydrothermal origin. Could these fluids have directly evolved from the granite? Examination of quartz phenocrysts from the granite reveals a high density of inclusions within the phenocrysts. These inclusions are similar in composition to inclusions found in vein quartz. The two trapped fluids differ in that type D inclusions present in some vein quartz, are noticeably absent in quartz samples from the granite.

Analyses of Rb, Sr, and Sr isotopes in fluid inclusion waters of quartz samples from mineralized veins indicate that the mineralizing fluids were enriched in radiogenic Sr compared to the host granite at the time of mineralization. In addition, the calculated $^{87}Sr/^{86}Sr$ initial ratios of fluid inclusion waters at the time of mineralization reveal

that the source of the mineralizing fluids was not homogeneous with respect to Sr (Table 8). These differences point toward a source of mineralizing fluids other than the host granite.

The host granite and surrounding rocks were analyzed for Sn by x-ray fluorescence methods. None of these rock units yielded values above the limit of detectability (10 ppm). This indicates that the granite at Mayo-Darlé has a Sn content lower than the average Sn content of granites associated with tin deposits, 30 ± 15 ppm (Hosking, 1979). Tischendorf (1973) has suggested that the most important criterion in the formation of tin deposits related to granitoid intrusions is the high fluorine content of the mineralizing fluids and not the high Sn content within the host granite. Then, how was Sn concentration achieved to form this deposit?

Tischendorf (1977) indicates that within the granite tin is mainly concentrated in biotites, amphiboles, and sphene, and other minerals as listed in table 9. Hosking (1979) suggests that tin can be leached from the biotites by a two-stage process, which first converts the biotite to muscovites without loss of tin, and which then destroys the muscovites, liberating Sn along with other elements, and silicifies the rock. Barsukov (1967) succeeded in leaching 30 to 60 percent of the total rock tin from granite and 50 to 90 percent from diorite using solutions containing Na, K, Cl, F, and sodium silicates.

The mineralized area extends over 4 km^2. Stockwork mineralization estimates range from 100 to 500 million tons with grades averaging 0.15% SnO_2 or 0.15 to 0.75 million tons SnO_2. If the leached volume of rock extended to 5 km at depth and comprised a surface area of about 50 km^2, one hundred percent leaching of 250 km^3 of granitic material (density 2.6, 5-8 ppm Sn) could provide 3.2 to 5.2 million tons SnO_2. Thirty to fifty percent effective leaching could yield 0.96 to 2.6 million tons SnO_2; still enough to make the Mayo-Darlé deposit. The possibility that the source of the mineralizing fluid was enriched in Sn is not ruled out. The metasediments could have also contributed in Sn enrichment of the mineralizing fluids.

TABLE 9. Tin Concentrations in Minerals Within Granites (Tischendorf, 1977).

Mineral	Sn (ppm)
Biotite.	400
Amphibole	150
Pyroxene	15
Feldspars	10-50
Sphene	3000
Ilmenite	120-1500
Allanite	70
Magnetite	50
Zircon	75
Protolithionite	500
Tourmaline.	1500

6.2.2 Deposition of Ore

The factors that control the deposition of tin at Mayo-Darlé are the structural framework at the time of deposition, the temperature and pressure, and changes in the chemistry of the mineralizing fluids.

Structural controls

Mineralization at Mayo-Darlé is restricted to stockwork veinlets, vertical, and horizontal greisen veins. Silicified breccias are barren.

Near vertical cross-cutting stockwork veinlets are confined to sets of conjugate fractures with average compressional acute angle of 75°. Vertical greisen veins commonly occur randomly within the mineralized area. Locally, vertical veins radiate from the breccia pipes. The breccia pipes are completely silicified. Major clues in the recognition of these breccias are their lack of jointing and their apparent blocky texture.

Mineralized, flat-lying or sub-horizontal quartz-cassiterite veins constitute about 50 percent of major vein mineralization. Mineralized horizontal veins have commonly been reported in tin deposits, despite the predominance of steeply dipping or vertical veins (Hosking, 1979, Jackson, 1979, Kelly and Rye, 1979).

Structural features within the granite, reflect the stress environment which prevailed at the time of emplace-

ment. It is postulated that the granite intrusion provided a central pressure responsible for the fracturing of the granite. The fact that the density of all described structural features is higher within the granite than within surrounding country rocks, supports this hypothesis. However, the presence of quartz veins within the country rocks indicates that other forces in addition to the pressure of the crystallizing intrusive could have contributed in the development of the fracture system. Knapp and Norton (1981) have suggested that regional tectonic forces, gravitational and thermal forces may have contributed in the evolution of the tensile stresses and strains in hydrothermal systems in addition to magma pressures.

Fractures are formed along planes of weakness within the intrusive. Fractures with conjugate patterns, vertical fractures and breccias could form during the late-crystallizing stage of the instrusive. These structural patterns are common within porphyry copper deposits (Lowell and Guilbert, 1970, Burnham, 1979). Forceful hydrothermal events are commonly advanced to explain the formation of these structures (Petersen, et al., 1977, Haynes and Titley, 1980, Titley, 1975, Rehrig and Heindrick, 1972). When the internal pressure (P_{fluid}) of the crystallizing intrusive exceeds the confining pressure (pressure of the solidified granite plus overburden), superjacent roof rocks are placed under great tensile stresses which result in the fracturing

of the apical part of the crystallizing instrusive and the surrounding rocks.

The stress orientation diagram (Fig. 7) indicates that the sets of fractures in conjugate patterns form when σ_2 is vertical. The plane of weakness along which these fractures developed could have been the result of regional tectonic stresses prevailing before fracturing. Vertical fractures are formed by the same mechanism, while brecciation will occur through the same mechanism but only in areas of high density fracturing. Horizontal or subhorizontal fracturing occurs when σ_3 becomes vertical.

The age relationship between horizontal and vertical veins is unknown. The hydrothermal pressure required for the formation of horizontal tin-bearing veins should be greater than the hydrothermal pressure involved in the filling of vertical fractures. Thus at any given time, subhorizontal fractures are likely to precede the vertical fractures (Budding, personal communication, 1982). Consequently it is postulated that horizontal veins probably precede the emplacement of vertical veins.

Most horizontal veins follow the topographic surface of the intrusive. Therefore, horizontal fractures which were precursors to vein filling could also be interpreted as cooling surfaces which were later dilated by overpressured fluids.

Fluid inclusions provide evidence of overpressure fluctuations. Hence, repeated activation of the fracture system

within the granite could have played an important role in the mechanical ground preparation preceding the concentration and deposition of ores. It is interesting to notice that the breccia pipes are void of mineralization, while vertical veins radiating from the pipes carry high grade ore. The breccia pipes could have acted as main locci of fluid migration while the veins were more important in the concentration and deposition of tin.

Regional features such as the Cameroon Line, a NNE trending strike-slip shear zone, and the Benue Trough north of Mayo-Darlé, had a significant (though not clearly evident) influence on the local tectonics. The granite ridges at Mayo-Darlé trend in the general direction of the Cameroon Line. Most of the mineralized veinlets follow the long axis of the granite intrusion.

The fractures which provided the loci for vein mineralization at Mayo-Darlé, could have formed by tectonic and residual stresses due to events that occurred long before the tectonic activity, the contraction resulting from the cooling of the intrusive, and the magmatic forces. The preceding discussion emphasizes the fact that hydrothermal magma pressures, more than any other force, played a central role in the formation of all types of structural features at Mayo-Darlé.

Temperature and pressure controls

It is impossible to establish any age relationship among

the different types of inclusions because all inclusion types commonly occur together randomly in a single quartz crystal. However, the fluid inclusion data were only obtained from horizontal and vertical veins. Stockwork veinlets could exhibit a different pattern.

Fluid inclusion temperatures in a given sample range from 220° to 550°C. Fluid salinities in contrast, remain high in liquid-rich, and halite-bearing inclusions. This suggests that temperatures were fluctuating during mineralization. Temperature fluctuation could be interpreted as evidence of episodic boiling of the mineralizing fluids. However Buchanan (1981) suggests that episodic pressure release, more than temperature fluctuations, will cause episodic boiling of the mineralizing fluids. The presence of horizontal veins and silicified breccia indicates periods of high pressure.

Episodic boiling of mineralizing fluids results in the rise of pH of these fluids (Buchanan, 1981). Changes in the chemistry of the fluids, changes in oxygen fugacity of the system, and decrease in temperature occur during boiling. During the process of greisenization, these changes will favor the precipitation of ore and gangue minerals.

Fluid inclusions suggest a period of episodic boiling and thus mineralization between 520° and 320°C. Pressures fluctuate between 350 bars and 75 bars. The last evidence of boiling was recorded at 320°C at pressure of 75 bars implying a shallow depth of 940 m (Table 6).

Lateral and vertical extent
of primary mineralization

Extensive mineralization is confined to an area of 4 km^2. Lateral and vertical extent of primary mineralization within the granite cannot be estimated with the present data. During the course of mining, some veins were traced laterally to the granite ridges for about 100 m.

The gently dipping (23°) contacts of the granite with the metasediments suggest that only the uppermost part of the doming intrusive has been exposed. Tin commonly occurs in the apical part of the associated granitic intrusion (Taylor, 1979, Hosking, 1979). The Mayo-Darlé granite has not yet been deeply eroded. Volcanic clasts, probably from the rhyolitic volcanics which erupted before the emplacement of the intrusive, can still be recognized in paleovalleys filled by colluvium. Moreover, the conglomeratic SnO_2-rich placer directly overlying the granite consists of angular to subrounded clasts, syggesting transport from short distances.

It may thus be postulated that mineralization extends to considerable depths. Porphyry tin deposits in Bolivia have commonly been mined to depths of 300 m to 600 m (Rivas, 1979). Similar vertical extensions are possible for the Mayo-Darlé deposit.

6.3 ALTERATION

Ore deposition and alteration processes at Mayo-Darlé are interdependent. Alteration is located around highly mineralized areas, except kaolinization which occurs in isolated spots in the vicinity of the mineralized zone.

Greisenization

Wall rock alteration was initiated before the formation of mineralized features. This is suggested by greisenization of the granite around the mineralized veins cross-cutting the granite. Greisen around stockwork veinlets grades into unaltered biotite granite 1 cm from the veinlets. Greisenization occurs in the early stage of hydrothermal process (Shcherba, 1970). It is characterized by acid leaching of primary constituents of the granites by F-rich mineralizing solutions. During this process biotites are altered to chlorite and magnetite, and later to muscovite and quartz. K-feldspar is decomposed to muscovite and quartz. Quartz recrystallization is indicated by overgrowth of quartz around early phenocrysts in the granite. Precipitation of solutes during the late stage of greisenization results in the formation of the observed greisen assemblage: quartz-topaz-zinnwaldite. The range of pH required for greisenization is 8 to 4 (Tischendorf, 1973). Temperatures recorded by fluids inclusions indicate

550° to 300°C. This temperature range agrees with the range observed for quartz-cassiterite greisen veins in the Kazakhstan (Shcherba, 1970).

It is suggested that Sn was leached from the granite during early greisenization periods; Sr content was lowered, and Rb content was increased. The resulting solution enriched in Sn might have migrated through channelways provided by the fractures. Boiling occurred as temperature and pressure fluctuated. Deposition of cassiterite occurred within the veins following the formation of the greisen assemblage. Cassiterite in greisen lodes is interstitial to quartz, zinnwaldite, and topaz, which is consistent with the suggested sequence of deposition.

Silicification

Silicification is related to the process of greisenization. Quartz precipitation is mainly controlled by temperature decrease as indicated by fluid inclusions during the process of greisenization (Shcherba, 1970). The result is the formation of veins with 96 to 99 percent quartz, and enrichment of silica within the affected granite (SiO_2 up to 80%). Silica caps as reported in Panasqueira, Portugal (Kelly and Rye, 1979) are not present at Mayo-Darlé.

Chloritization

During the greisenization process, leaching of potassium

from biotites result in the formation of chlorite. The leaching process is caused by hydrogen metasomatism. Quartz-chlorite veinlets are common within the granite. These veinlets are barren of cassiterite.

Hematization

Hematization is strong around the stockwork veinlets. Chlorite plus hematite are commonly pseudomorphous after biotite within the granite; hematization was simultaneous with or slightly later than chloritization of biotites. Hematization may be associated with late hydrothermal processes after the main period of deposition of cassiterite, which suggests continued oxidizing conditions in the late stage of the mineralizing event.

Kaolinization

Large volumes of granite are intensely kaolinized. Kaolinite occurs mostly in isolated areas within the granite away from vein mineralization. In most tin deposits of SW England, kaolinite occurs in association with the phase of vein mineralization (Exley, 1957, Sheppard, 1977, Jackson, 1979). Kaolinite is spacially associated with mineralized fissures or sheeted joint systems in the Cornubian tin field (Jackson, 1979). At Mayo-Darlé such occurrences are rare.

The genesis of kaolinite related to granites associated with tin mineralization remains a source of controversy. In

SW England both a low temperature supergene origin and a hydrothermal origin have been reported (Exley, 1957, Sheppard, 1977). Exley (1957,1976) suggests that acid hydrothermal solutions of low temperatures (350° to 200°C, Hemsley and Jones, 1964), were responsible of kaolinization processes in the waning stages of mineralization within the St-Austell granite. D/H and $^{18}O/^{16}O$ analyses in kaolinite of the Cornubian batholith indicate that kaolinite resulted from weathering (Sheppard, 1977). Kaolinite in the Cornubian batholith is isotopically consistent with having formed in a tropical to warm temperate climate during the Cretaceous-Tertiary.

The genesis of the Mayo-Darlé kaolinite must be inferred from field association because of the lack of isotopic evidences. The occurrence of kaolinite away from main mineralization loci and the upper temperature limit for formation of kaolinite (350° to 200°C) indicate that kaolinization might have occured during late stage hydrothermal activity. Hypogene acid hydrothermal solutions permeating through the granite reacted with alkali feldspars to form K-rich micas which in turn were converted to kaolinite (Hemsley and Jones, 1964). Amidst this hypothesis, it cannot be ruled out that kaolinization might also have occurred as a result of tropical weathering after completion of the main mineralization period. D/H and $^{18}O/^{16}O$ studies may put further constraints on the origin of kaolinite at Mayo-Darlé.

6.4   CLASSIFICATION

6.4.1   Mayo-Darlé, a Tin Porphyry Deposit

Comparison of the Mayo-Darlé tin deposit with a   model
porphyry copper deposit (Lowell and Guilbert, 1970), and
Bolivian porphyry tin deposits (Sillitoe, Halls, and Grant,
1975) reveals that the Mayo-Darlé deposit shows most major
characteristics of porphyry deposits (Table 10). The stock
is subvolcanic in character and in sharp contact with wall
rocks. Coeval volcanics, rhyolites are preserved in the
area. Stockwork mineralization is restricted to about 4 km^2
with grade up 0.30% SnO_2. Mineralization estimates are up
to 500 million tons.   Silicified hydrothermal breccias are
widespread. Vertical veins radiating from these breccias
carry high grade ores (2 - 20% SnO_2).   The granite stock
associated with mineralization has undergone hydrothermal
alteration. Intense kaolinization is present.   Fluid
inclusion studies indicate that hydrothermal fluids with
temperatures ranging from 300° to 550°C, and salinities of
20 to 60 equivalent wt. percent NaCl were responsible for
ore deposition.

Some differences emerge between the Bolivian tin porphyr-
ies and the Mayo-Darlé tin porphyry. Most Bolivian deposits
are associated with intrusives and/or subvolcanics of inter-
mediate composition. At Mayo-Darlé the intrusion is an
alkali biotite granite. Sulfides are present in Bolivia,

and tin occurs as cassiterite and stannite; cassitierite is the only ore mineral present at Mayo-Darlé, and sulfides are absent. Mineralized horizontal veins (tin-floors) common at Mayo-Darlé, are absent in Bolivian deposits.

The Mayo-Darlé tin deposit could thus be classified as a porphyry tin deposit, exhibiting some particular character-istics which probably result from a tectonic setting diff-erent from that of the Bolivian tin porphyries.

TABLE 9. Comparison: Porphyry Cu and Porphyry Sn Deposits

CHARACTERISTICS FEATURES		MODEL PORPHYRY COPPER DEPOSIT (Lowell and Guilbert, 1970)	BOLIVIAN PORPHYRY TIN DEPOSITS (Sillitoe, Halls, & Grant, 1975)	MAYO-DARLE TIN DEPOSIT
PREORE HOST ROCKS		Precambrian – Late Cretaceous sediments and metasediments.	Ordovician – Devonian sediments: shales, siltstones, sandstones.	Late Precambrian – Early Cambrian metasediments: biotite hornblende gneisses.
IGNEOUS HOST ROCKS	– Composition	Quartz monzonite, dacite, granite porphyry.	Quartz latite porphyry, dacite.	Alkali biotite granite, granite porphyry.
	– Age	Paleocene – Eocene	Tertiary – Late Tertiary	Late Cretaceous – Early Paleocene
	– Size/Shape	1.2 x 1.8 km, elongate irregular. Controlled by NE and NW faults.	1.7 x 1.2 km, funnel-shaped to conical. Controlled by NE, ± NW faults.	4 x 8 km, ellipsoidal. Controlled by NE trending shear zone.
	– Emplacement	Plutonic to subvolcanic, passively emplaced, ± active.	Plutonic to subvolcanic, passively emplaced, ± active.	Plutonic to subvolcanic, actively emplaced.
	– Dimensions	1.1 x 1.8 km, oval pipe-like.	1.7 x 1.2 km funnel shaped to conical.	2 x 2 km, shape unknown.
ORE DEPOSIT	– Tonnage/Grade	100 – 500 million tons with 0.45 – 0.80% Cu	100 – 500 million tons with 0.1 – 0.60% Sn.	100 – 500 million tons with 0.01 – 0.30% Sn.
	– Stockwork	Cu mineralized veinlets, chalco-pyrite, pyrite, (galena, sphalerite, silver, gold)	Mineralized multidirectional veinlets, pyrite, cassiterite.	Mineralized multidirectional veinlets, quartz, cassiterite, topaz, chlorite, zinnwaldite.
	– Vein Mineralization	Steeply dipping and branching pyrite, chalcopyrite, molybdenite.	Branching steeply dipping veins, NE and NW; quartz, pyrite, cassiterite, ± silver stage.	Extensive horizontal and vertical veins; 2 – 20% Sn, quartz, cassiterite, topaz, zinnwaldite.
	– Sulfides	Disseminated, microveinlets.	± sulfides in microveinlets: stannite, chalcopyrite, tetrahedrite, sphalerite.	Sulfides absent within the stock, present in veinlets cross-cutting metasediments.
	– Breccias	Hydrothermal breccias with disseminated sulfide.	Hydrothermal breccias (pipes, lenses, dikes), with tourmaline, cassiterite, ± pyrite.	Completely silicified hydro-thermal breccias.
	– Placers	Placers absent.	Placers are common.	Paleofluvial or lacustrine placers present.
ALTERATION		Well defined zoning, from center outward: potassic, phyllic, argillic, propylitic.	Pervasive alteration, no definite zoning. Pervasive sericitic at depth, silicification upward greisen, ± chlorite	Greisenization (quartz, topaz zinnwaldite, + fluorite), silicification, chloritization, hematization. No zoning, intense kaolinization.
ORE FLUIDS		High temperature (640 – 725°C), high saline brines (up to 60 eq. wt.% NaCl). Intermittently boiling, CO_2 present. Pressures of 80 – 1000 bars (Roedder,1971)	Temperature of 350 to 530°C, high saline brines (up to 46 eq.wt.% NaCl). Intermittently boiling. Minor CO_2 present. Depth of deposition: 250 to 1000 m, possibly up to 2000 – 4000 m.	High temperature, high saline Na-Cl-F brines, 300 – 520°C with 20 to 60 eq.wt.% NaCl. Eposod-ically boiling. Pressure 75 to 350 bars corresponding to depth of 300 – 940 m and 1300 – 4375 m under lithostatic and hydro-static conditions, respectively.

6.4.2 Tin Deposits In Plate Tectonic Setting

The Mayo-Darlé tin deposit occurs along the Cameroon Line, a strike-slip shear zone interpreted as a zone of incipient rifting (Burke, et al., 1971). Most intrusive complexes along the Cameroon Line are subvolcanic and are characterized by caldera complexes (Cantagrel, et al., 1978, Lasserre, 1978). The "Younger intrusive" complexes of Cameroon reveal many similarities with the Nigerian "Younger granites" (Tempier and Lasserre, 1980). The "Younger granites" of Nigeria are associated with tin mineralization. These granites are related to the Benue trough which has been interpreted as a failed arm, or an aulacogen, of the three arm rift developed as a triple junction between South America and West-Africa (Burke, et al., 1971). This type of tin mineralization has been described as rift-related tin deposits (Mitchell, 1979). Rift-related tin mineralizations have been found in Rondonia, Brazil, and in the St-François Mountains, Missouri, U.S.A.

Other tin deposits have been classified according to their tectontic setting (Mitchell, 1979). Tin mineralization is recognized within subduction-related magmatic arcs, outer arc granites and back arc magmatic belts. The Alaska-Aleutian deposits, the tin deposits of eastern Malaysia, and those of the Massif Central of France are examples of magmatic arc deposits. Tin deposits of southwest Japan occur in outer arc granites. Bolivian tin

deposits and tin deposits of the western Belt of Southeast Asia occur in back-arc magmatic belts. Collision-related tin mineralization occurs in the Himalayas and in the Main Range of Malaysia.

6.5 SUGGESTED GENETIC MODEL FOR THE MAYO-DARLÉ TIN DEPOSIT

A genetic model to explain the tin mineralization at Mayo-Darlé should be consistent with the following observations:

1. The hydrothermal fluids responsible for transport and deposition of ores were high-temperature, up to $550^{\circ}C$, and high-salinity, up to 60 eq. wt. % NaCl fluids.

2. The mineralizing fluids were episodically boiling due to periods of pressure changes.

3. Mineralization is confined to specific structural features: veinlets, vertical and horizontal greisen veins.

4. The Rb-Sr data of the fluid inclusion waters from the mineralized vein quartz indicated a source for the mineralizing fluids more radiogenic in Sr than the associated host granite.

The following sequence of events is postulated (Fig.

37). During the late stage of crystallization of the host rock, hydrothermal magma pressures caused the fracturing of the uppermost part of the granite and probably the surrounding country rocks. This explosive event provided the necessary ground preparation preceding mineralization. Conjugate sets of fractures, vertical fractures, breccias, and horizontal fractures were formed as a result of the hydraulic forces induced by the magma pressures. These structural features were restricted to zones of weakness within the solidified part of the granite. Zones of weakness within the granite were probably caused by the influence of regional tectonics (Cameroon Line, Benue Trough).

Fig. 38. Sketch: genetic model for tin deposition of the Mayo-Darlé complex.

Suggested Genetic Model for Sn Deposition at Mayo–Darle
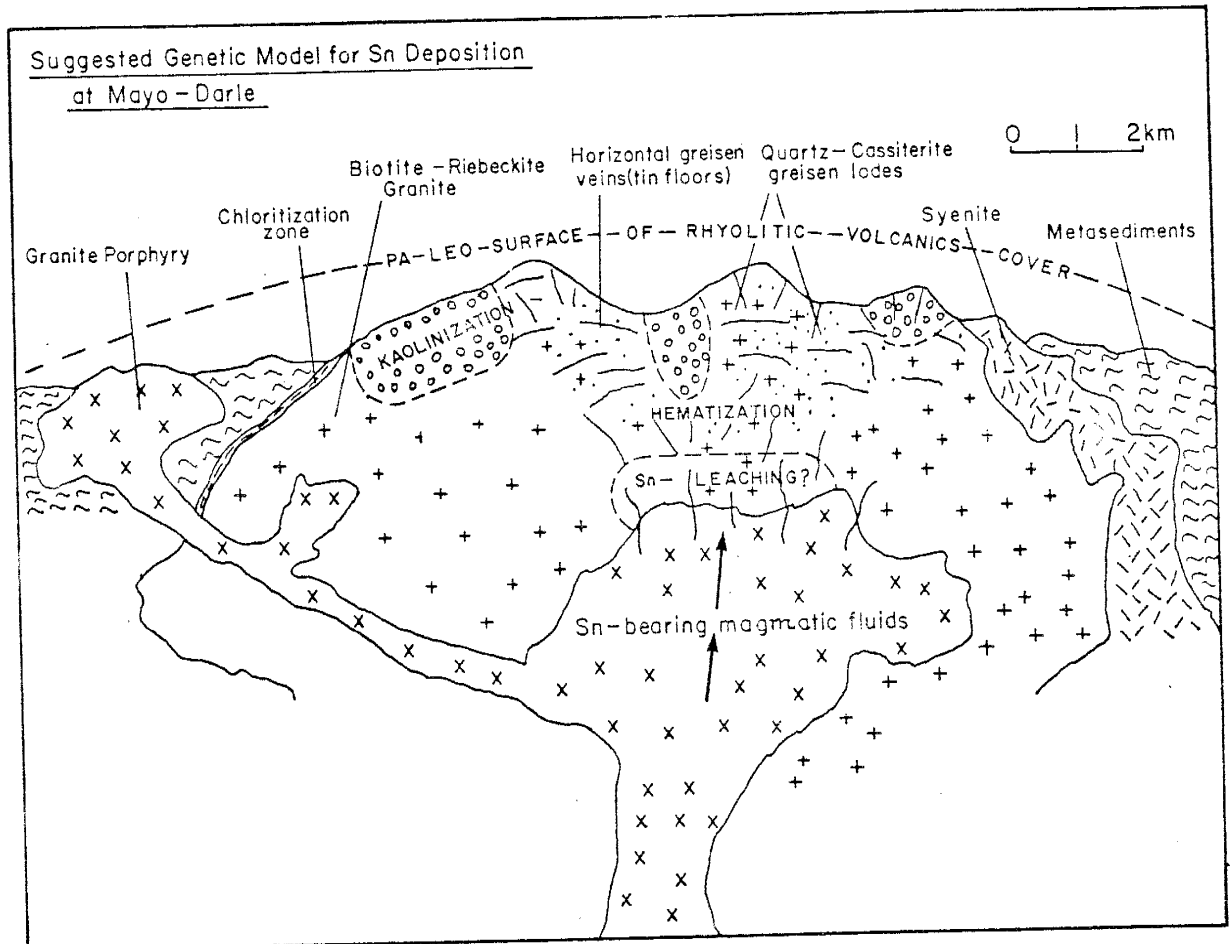
Strontium isotopic data suggest a mineralizing fluid different from the fluids evolved from the host granite. A later intrusive at depth could have reactivated the fracture system and evolved the fluids with the observed characteristics. These fluids, rich in Na, Cl, F, and radiogenic Sr, migrated upward through the host granite. These magmatic fluids may have contained little Sn initially. However during their upward migration, they scavenged tin from biotite and other tin-bearing minerals within the granite (Table 9). Tin was probably transported in solution as fluorine complexes (Tischendorf, 1973).

During periods of overpressures, the mineralizing solutions invaded the open channelways, and as pressures and/or temperatures decreased, quartz and cassiterite were deposited. Interaction of the mineralizing fluids with the wall rocks caused greisenization. Subsequent temperature decrease resulted in continuous precipitation of quartz within the veins. Chloritization followed as biotite were altered to chlorite and magnetite. Hematization of biotite and chlorite occurred in the late of the mineralizing event. Koalinization probably results by interaction of late hydrothermal solutions with the host granite after the main period of mineralization. The interaction between the granite and the mineralizing fluids is believed to have

created the special characteristics of the host granite, including initial $^{87}Sr/^{86}Sr$, high Rb, and high silica content.

SUMMARY

1. The Mayo-Darlé complex intrudes Pan-African metasediments and metavolcanics. This complex is composed of a differentiated alkalic suite of rocks consisting of quartz syenite (nordmarkite), rhyolite with benmoreite xenoliths, alkali biotite granite, biotite-riebeckite granite, and granite porphyry. This suite of rocks was derived by fractional crystallization processes from a magma of basaltic composition in the upper mantle or lower crust.

2. The age of the complex as indicated by the quartz-syenite isochron is 73 + 6 m.y. with an initial $^{87}Sr/^{86}Sr$ value of 0.7030 + 0.0035. The immediate source of the granite was probably enriched in radiogenic Sr. However, rubidium and strontium systematics were further disturbed by hydrothermal fluids involved responsible for tin mineralization. The mineralizing fluids were enriched in radiogenic Sr compared to the host granite.

3. Magmatic hydrothermal fluids, probably evolved from a late intrusive at depth, were responsible for tin mineralization. Fluid inclusion studies indicate Na-Cl-F brines of 65 - 20 eq. wt. % NaCl over a temperature range of 520 to 300°C. Boiling occurred over a temperature range 520° to 320°C. Mineralizing fluids were enriched in Sn by leaching of the Sn-enriched minerals within the host granite.

4. Pressure estimates of 350 - 75 bars indicate depths of mineralization from about 4000 m to as shallow as 940 m.

5. The Mayo-Darlé tin deposit, similar in many respects to known porphyry tin deposits of the Bolivian tin province, can be classified as a rift-related porphyry tin deposit.

APPENDIX I. MAJOR AND TRACE ELEMENTS DATA

SAMPLES

Few samples were collected during the reconnaissance
survey of the area to help in the preliminary identification
of the various rock units. The bulk of the samples used in
this study were collected during field mapping. After all
the units were recognized, a grid pattern with 1 km x 1 km
cell units was laid over the entire study area.   Systematic
sampling was carried out. Samples one to five kilograms in
weight were collected.

GEOCHEMICAL ANALYSES

Chemical analyses of all samples were carried out by
standard geochemical methods.   Fifty samples were analyzed
for Si, Al, Fe, Ca, K, and Ti using   x-ray fluorescence
techniques as described by Norrish and Hutton (1968) and
modified by Harvey et al. (1973).   Concentrations of Na,
Mg, and Mn were obtained by atomic absorption
spectrophotometry methods described in Brandvold (1974). Rb
and Sr isotopic data were determined by isotope dilution and
mass spectrometry techniques as described in Vera and Van
Schmus (1974), Van Schmus (1971).   Rare earths and other
trace elements were determined by instrumental neutron
activation using procedures described by Gordon et al.

(1968) and Condie and Lo (1971). Major elements and Rb-Sr isotopic analyses were carried out in the Isotope Geochemistry Laboratory of the University of Kansas. All other analyses were conducted at the New Mexico Institute of Mining and Technology.

TABLE Ia. COMPOSITION and NORMATIVE MINERALS OF GRANITE AND GRANITE PORPHYRY

Samples	GRANITE					
	HDJ-4-80	HDJ-5-80	HDJ-6-80	HDJ-7-80	HDJ-8-80	HGE-2-80
SiO_2	75.86	78.09	77.57	77.72	80.95	77.84
TiO_2	0.0	0.09	0.09	0.13	0.18	0.06
Al_2O_3	11.67	12.18	11.49	11.00	11.05	12.67
Fe_2O_3	1.38	1.67	1.49	2.29	2.19	0.85
MnO	0.08	0.08	0.09	0.09	0.10	0.08
MgO	0.006	0.006	0.007	0.01	0.01	0.02
CaO	0.25	N.D.	N.D.	N.D.	0.04	0.57
Na_2O	3.88	3.55	3.78	3.99	3.99	3.71
K_2O	4.86	4.88	4.69	4.44	4.71	4.52
L.O.I.	0.74	1.96	1.23	2.65	1.23	1.57
K_2O/Na_2O	1.25	1.37	1.24	1.11	1.18	1.22
Agpaitic Index: $\dfrac{Na_2O+K_2O}{Al_2O_3}$	0.99	0.91	0.98	1.03	1.05	0.87
Differentiation Index	97.4	96.4	97.6	92.6	95.5	95.0
Q	32.9	36.3	35.6	36.7	38.2	35.1
Or	28.7	28.1	27.3	25.2	26.0	26.5
Ab	35.8	32.1	34.6	34.4	31.9	33.4
An						2.4
Hbd						1.0
Bio	1.5	1.8	1.7	2.4	2.3	0.5
Mt	0.5	0.7	0.6	0.9	0.8	0.3
Wo	0.5				0.1	
Cor		0.6	0.1			0.4

TABLE Ia.   (con't)

Samples	GRANITE					
	HGE-4-80	GR-3-80	GR-4-80	CHBRX	CHLV	GM-12-80
SiO_2	77.27	74.52	77.40	74.43	76.11	77.33
TiO_2	0.09	0.08	0.07	0.08	0.08	0.11
Al_2O_3	10.94	11.04	11.25	11.84	11.59	11.99
Fe_2O_3	2.85	1.67	1.68	0.49	0.62	1.53
MnO	0.10	0.06	0.02	N.D.	N.D.	0.09
MgO	0.008	0.03	0.03	0.01	0.02	0.01
CaO	0.07	0.51	0.49	0.45	0.42	0.31
Na_2O	4.07	3.29	3.34	3.22	3.18	3.72
K_2O	4.45	4.60	4.78	4.78	4.72	4.59
L.O.I.	2.20	1.73	1.80	1.84	1.91	2.62
K_2O/Na_2O	1.09	1.40	1.43	1.48	1.48	1.23
Agpaitic Index: $\dfrac{Na_2O+K_2O}{Al_2O_3}$	1.05	0.94	0.95	0.88	0.89	0.92
Differ-entiation Index	91.1	95.3	95.6	96.2	96.3	95.6
Q	36.4	36.2	36.9	35.9	37.6	35.1
Or	25.0	27.7	27.9	29.6	28.8	26.9
Ab	33.9	31.3	30.7	30.7	29.9	33.7
An		1.8	1.6	2.4	2.2	0.8
Hbd						1.6
Bio	2.8	1.9	1.7	0.6	0.8	0.9
Mt	1.1	0.7	0.7	0.2	0.3	0.6
Wo	0.1	0.3	0.4			
Cor				0.3	0.3	0.3

TABLE Ia. (con't)

Samples	GRANITE			GRANITE PORPHYRY		
	GM-1-80	GM-2-80	GM-5-80	MG-3-80	MG-4-80	MG-1-80
SiO_2	75.65	77.74	75.43	76.04	77.26	75.34
TiO_2	0.10	0.08	0.10	0.16	0.18	0.16
Al_2O_3	12.19	11.30	11.44	10.97	10.88	11.17
Fe_2O_3	1.65	1.49	1.58	1.90	1.89	1.78
MnO	0.10	0.09	0.09	0.005	0.003	0.007
MgO	0.02	0.01	0.01	0.009	0.006	N.D.
CaO	0.53	0.32	0.27	0.45	0.42	0.31
Na_2O	4.07	3.29	3.34	N.D.	N.D.	N.D.
K_2O	4.79	4.44	4.57	4.83	5.34	5.06
L.O.I.	2.12	1.84	2.07	1.03	1.15	1.78
K_2O/Na_2O	1.21	1.18	1.19	1.40	1.78	1.61
Agpaitic Index: $\frac{Na_2O+K_2O}{Al_2O_3}$	0.95	0.97	0.98	0.99	0.98	0.95
Differentiation Index	95.5	96.6	96.7	97.2	97.0	96.8
Q	31.7	36.3	34.0	36.3	37.9	36.8
Or	27.8	25.8	27.0	28.6	31.4	30.4
Ab	36.1	34.5	35.7	32.3	27.8	29.6
An	1.4	0.8	0.5			
Hbd						
Bio	1.9	1.6	1.8	2.0	2.0	1.9
Mt	0.6	0.6	0.6	0.8	0.8	0.7
Wo	0.5	0.3	0.4			
Cor					0.1	0.3

TABLE Ib.   COMPOSITIONS   AND NORMATIVE MINERALS
OF THE K-RHYOLITE AND ITS INCLUSIONS

Samples	K-RHYOLITE					MAFIC INCLUSIONS	
	T2V1	T2V2	T2V3	T2V4	T2V5	T2IN1	T2IN2
SiO_2	69.98	73.48	70.10	71.60	72.08	55.64	57.70
TiO_2	0.42	0.41	0.38	0.48	0.28	0.98	0.99
Al_2O_3	12.09	12.74	12.80	12.10	11.85	13.48	14.22
Fe_2O_3	4.98	5.01	5.10	4.88	4.53	11.03	11.04
MnO	0.09	0.09	0.07	0.10	0.12	0.24	0.23
MgO	0.08	0.07	0.06	0.09	0.10	0.38	0.36
CaO	1.14	1.27	1.30	1.32	1.09	3.86	3.81
Na_2O	5.09	5.09	5.24	4.92	4.98	5.20	5.17
K_2O	4.07	3.98	4.21	4.10	3.34	5.56	5.41
L.O.I.	1.55	1.43	1.02	1.32	1.27	2.71	2.61
K_2O/Na_2O	0.80	0.78	0.80	0.83	0.67	1.07	1.05
Agpaitic Index: $\frac{Na_2O+K_2O}{Al_2O_3}$	1.06	0.99	1.03	1.04	0.99	1.08	1.01
Differentiation Index	85.0	92.0	89.5	89.0	89.3	71.7	75.3
Q	17.1	23.5	22.4	26.0	27.4	2.8	5.1
Or	24.8	23.3	24.8	24.0	23.2	34.7	32.8
Ab	43.1	45.2	42.3	39.1	38.7	21.4	23.3
An	21.5	0.1				21.4	23.3
Mt	0.7	1.8	4.45	4.16	3.49	0.4	1.9
Wo		2.5	2.25	2.18	2.04		
Fs	3.7	2.8					
En	0.2	0.2	0.15	0.22	0.25		
Ol						10.3	9.8
Ne						12.8	14.0
Ac	3.2		1.70	1.94	2.97	4.9	0.7
Il	0.6	0.6	0.15	0.21	0.25	1.4	1.4

TABLE Ic.   COMPOSITIONS   AND NORMATIVE MINERALS OF SYENITE

Samples	SYENITE					
	GM-11-80	GM-14-80	GM-20-80	GM-21-80	GM-22-80	GM-24-80
SiO_2	69.22	69.22	68.32	68.92	68.21	67.82
TiO_2	0.27	0.22	0.36	0.29	0.26	0.24
Al_2O_3	13.22	12.93	13.34	13.55	13.66	13.21
Fe_2O_3	3.92	2.30	4.35	3.87	4.12	4.57
MnO	0.10	0.10	0.15	0.13	0.09	0.22
MgO	0.006	0.003	0.008	0.001	0.001	0.007
CaO	0.55	0.17	0.85	0.67	0.77	0.58
Na_2O	4.64	4.94	4.53	4.82	4.68	4.95
K_2O	5.68	5.14	5.82	5.74	5.93	5.90
L.O.I.	1.73	2.44	2.01	2.11	2.22	2.49
K_2O/Na_2O	1.22	1.04	1.28	1.19	1.27	1.19
Agpaitic Index: $\frac{Na_2O+K_2O}{Al_2O_3}$	1.04	1.06	1.03	1.04	1.03	1.09
Differentiation Index	91.0	92.0	89.9	90.3	87.0	87.3
Q	26.7	22.1	19.3	18.9	19.4	17.3
Or	33.8	31.2	34.5	33.9	35.4	34.9
Ab	36.5	38.7	36.1	37.5	32.1	35.0
An						
Ac	2.6	3.6	2.0	2.9	6.9	6.0
Wo	0.9	0.2	1.5	1.2	1.4	1.2
En	0.02		0.02	0.02	0.02	0.6
Hm	3.0	1.1	3.6	2.8	1.7	2.5
Il	0.2	0.2	0.3	0.3	0.2	0.4
Mt						0.02

TABLE IIa.   TRACE ELEMENTS FOR GRANITES and GRANITE PORPHYRY
(Concentrations of all elements are in ppm)

Samples	GRANITE					
	HDJ-4-80	HDJ-5-80	HDJ-6-80	HDJ-7-80	HDJ-8-80	GM-2-80
La	113.4	84.8	21.5	35.5	50.6	57.0
Ce	126.1	92.4	26.5	0.78	107.7	103.8
Sm	17.3	6.9	3.4	6.9	7.7	10.0
Eu	0.73	0.81	0.22	0.48	2.0	0.48
Tb	5.3	0.79	0.43	1.3	2.2	2.9
Yb	17.0	2.6	2.5	3.7	3.9	8.7
Lu	2.6		0.35		0.57	1.5
Ba	88.8	23.2	70.5	107.6	148.3	75.8
Cr	15.6	5.7	11.2	21.4	10.5	12.1
Hf	14.5	17.8	10.8	22.7	14.3	11.3
Cs	2.4	1.2	1.9		1.2	1.4
Sc	0.47	0.08	0.22	0.26	0.08	0.22
Ta	21.7	11.3	15.3	15.3	18.6	20.8
Co	106.3	17.7	110.6	117.2	205.6	111.9
Zr	129.9	105.8	376.6	529.4	632.4	285.4
U	3.3	7.3	10.9	6.1	3.5	9.7
Th	28.2	16.6	16.1	20.7	18.1	22.9
Rb	334.8	314*	167*		163.5	353*
Sr	5.1	0.2*	2.4*		3.8	7.0*

*Rb-Sr values determined by XRF; all other Rb-Sr values
were obtained by isotope dilution and mass spectrometry.

TABLE IIa. (con´t)

Samples	GRANITE					
	GM-5-80	GM-1-80	GM-12-80	CHBRX	CHLV	HGE-2-80
La	72.9	72.9	152.1	74.4	751.3	138.1
Ce	138.9	140.6	251.6	149.98	673.5	136.5
Sm	19.7	17.2	38.1	11.6	54.0	20.6
Eu	1.7	0.48	1.9	1.7	2.6	0.49
Tb	4.2	4.4	4.9	2.7	5.9	9.3
Yb	9.2	12.6	12.0	9.6	22.2	44.6
Lu	1.3	1.6	1.4	1.5	2.6	7.4
Ba	23.7	23.6	315.3	126.8	156.1	18.2
Cr	45.2		12.7	6.4	12.7	
Hf	13.9	32.3	25.2	8.2	8.2	13.0
Cs	1.9	2.5	1.9	1.7	11.6	2.5
Sc	0.07	0.26	0.61	0.34	0.61	0.54
Ta	16.8	14.2	20.5	17.7	16.7	29.9
Co	72.5	102.7	125.1	102.7	94.6	42.2
Zr	384.2	642.3	413.7	258.9	539	
U	4.7	4.8	5.3	7.2	6.6	10.0
Th	26.2		15.0	38.5	43.2	54.8
Rb	220.8	468.6	284*	311.9	298*	457.6
Sr	2.4	15.2*	1.0*	9.4	7.6*	6.1

*Rb-Sr values determined by XRF; all other Rb-Sr values were obtained by isotope dilution and mass spectrometry.

TABLE IIa. (con't)

Samples	GRANITE			GRANITE PORPHYRY		
	HGE-4-80	GR-3-80	GR-4-80	MG-1-80	MG-3-80	MG-4-80
La	165.2	56.4	48.0	9.8	12.6	36.6
Ce	201.4		105.5		23.2	88.9
Sm	40.6	9.9	9.0	4.3	4.2	8.9
Eu	2.2		0.44	0.69	0.62	1.8
Tb	9.0	2.8	2.1	1.5	1.9	2.0
Yb	34.1	30.4	8.0	4.5	7.2	6.5
Lu	4.1	4.2				
Ba	16.7					
Cr		8.7	9.3	9.9		3.8
Hf	21.6	7.4	6.7	17.1	17.3	19.3
Cs	1.7	1.3	0.88	1.1	1.0	0.69
Sc			0.37	0.11	0.19	0.29
Ta				45.1	20.7	31.1
Co				61.8	57.9	71.1
Zr				209.3	420.1	370.7
U	7.0	5.8	5.6	6.6	3.2	4.5
Th	14.5	43.5	41.8	19.5	20.9	16.9
Rb	347.0	303.9	295.6	162.0*	145.0*	152*
Sr	1.8	18.7	16.5	10.5*	10.6*	18.0*

*Rb-Sr values determined by XRF;   all other Rb-Sr values
were obtained by isotope dilution and mass spectrometry.

TABLE IIb. TRACE ELEMENTS FOR SYENITES and RHYOLITES
(Concentrations of all elements are in ppm)

Samples	SYENITE					K-RHYOLITE		
	GM-11-80	GM-20-80	GM-21-80	GM-22-80	GM-24-80	T2IN1	T2IN1	T2IN1
La	127.4	734.9	110.0	412.5	808.6	116.8	124.4	127.7
Ce	293.9	980.4	217.4	411.7	904.7	252.3	277.1	263.7
Sm	23.9	91.6	20.6	74.2	60.7	22.4	23.2	21.2
Eu	1.8	2.0	3.1	4.9	1.9	4.1	4.9	3.7
Tb	3.9	9.4	3.2	10.3	5.8	3.2	3.8	3.4
Yb	16.9	19.5	13.7	15.5	15.6	15.4	20.2	9.7
Lu	4.9	3.5	3.4	2.8		2.0	2.4	2.2
Ba	325.2				223.8	117.0	96.6	371.9
Cr	20.9	15.8				10.4		
Hf	30.5	18.0	19.6	17.9	18.9	18.3	19.8	20.9
Cs	1.8	0.71	0.62	1.2	1.2	1.1		
Sc	0.65			0.19	0.58	11.3	3.0	3.1
Ta	41.0	30.7	28.7	19.1	32.7	11.0	16.7	13.7
Co	144.6	109.8	190.2	164.8	212.9	33.6	67.5	36.0
Zr	418.6	638.8	610.3	296.8				
U	13.5	4.2	3.7	4.8	5.1	3.1	1.7	
Th	30.1	26.0	24.1	26.8	23.9	11.8	22.5	23.5
Rb	173.5	146.2	166.8	163.5	148.3	172.3	107.9	108.5
Sr	24.6	7.2	10.2	13.6	7.9	47.3	127.8	127.4

TABLE IIc.   TRACE ELEMENTS FOR THE BASEMENT ROCKS
(Concentrations of all elements are in ppm)

Samples	BIOTITE GNEISS				
	GN-1-80	GN-2-80	GN-3-80	GN-4-80	MDJ-8-80
La	62.4	43.5	31.6	47.4	19.5
Ce	159.9	112.5	86.9	104.9	19.9
Sm	9.4	7.7	6.4	8.0	1.4
Eu	2.7	3.0	2.1	2.7	1.1
Tb	1.5	0.72	0.56	0.55	0.22
Yb	3.1	2.7	1.8	1.7	0.63
Lu	0.93	0.18	0.42	0.48	
Ba	1691	1506	1400	934	523.8
Cr	43.3	83.0	151.5	233.2	15.9
Hf	11.2	7.2	4.3	4.8	3.3
Cs	1.4	5.2		1.5	
Sc	12.3	18.6	14.7	16.7	5.4
Ta	5.6	2.7	4.1	2.2	9.9
Co	38.6	28.4	33.8	36.2	40.5
Zr	763.0				
U	1.2				1.1
Th	16.1	2.5	0.61	3.2	1.7
Rb	142.6	70.2	74.3	68.6	47.0
Sr	672.6	979.3	795.9	979.7	382.9

TABLE IIc.   (con't)

Samples	QUARTZ-DIORITE GNEISS					
	PG-1-80	PG-3-80	PG-5-80	PG-6-80	PG-7-80	PG-8-80
La	96.8	103.9	81.2	82.9	54.2	41.7
Ce	178.4	207.1	163.6	172.8	102.2	67.4
Sm	9.1	10.1	10.0	9.8	8.4	6.9
Eu	1.8	1.9	0.98	1.5	1.5	0.59
Tb	0.66	0.62	0.55	1.2	0.97	1.1
Yb	0.72		0.31	0.71	0.23	1.7
Lu	1.0				0.95	1.3
Ba	751.5	806.6	17.6	537.5	389.5	216.4
Cr						
Hf	6.1	6.2	6.1	5.7	3.0	2.9
Cs	1.9	1.3	0.52	0.76	0.53	0.97
Sc	2.4	2.0	2.9	3.2	2.3	2.4
Ta	14.7	9.7	13.4	8.8	16.5	11.3
Co	35.1	28.5	49.9	45.7	49.1	38.3
Zr	166.2		294.7			32.1
U	4.8	4.7	5.8	3.7	4.6	6.7
Th	47.6	47.1	44.4	42.2	38.6	24.3
Rb	243*	267*	250.4	254*	245*	232.1
Sr	174*	158*	170.2	167*	145*	102.2

*Rb-Sr values determined by XRF; all other Rb-Sr values were obtained by isotope dilution and mass spectrometry.

TABLE III.   MAJOR ELEMENT MODELING

	P1* Mugearite	R1 1-F=0.51	D1 = P2 Benmoreite	R2 1-F=0.44	D2 = P3 Qtz-syen.
SiO_2	51.10	45.17	56.70	47.21	68.60
TiO_2	2.67	4.09	0.98	3.79	0.27
Al_2O_3	16.10	18.51	13.80	12.02	13.30
Fe_2O_3	5.11	0.00	11.00	6.18	3.85
FeO	5.38	11.34	0.00	11.52	0.00
MnO	0.25	0.12	0.23	0.15	0.15
MgO	3.26	6.30	0.36	5.87	0.01
CaO	6.48	10.93	3.76	9.54	0.60
Na_2O	4.31	2.39	5.17	3.57	4.76
K_2O	2.62	0.13	5.48	0.12	5.70
			Mode		Mode
Quartz			10		10
Plagioclase			50(An40)		
K-feldspar			10		30
Biotite			1		1
Amphibole			15		5
Orthopyroxene			8		
Clinopyroxene					
Apatite					
Ilmenite					
Magnetite			3		2
Olivine					

* P1 = Mugearite, Jebunbun, Silali Volcanic, Kenya

TABLE III. (con´t)

	R3 1-F=0.62	D3 = P4 Rhyol.	R4 1-f=0.78	D4 Biot-gran
SiO_2	59.55	71.40	54.40	76.60
TiO_2	0.00	0.39	0.46	0.09
Al_2O_3	24.35	12.30	12.68	11.60
Fe_2O_3	0.41	4.90	17.13	1.71
FeO	0.00	0.00	0.87	0.00
MnO	0.00	0.09	0.01	0.09
MgO	0.00	0.08	0.33	0.01
CaO	6.23	1.22	3.73	0.35
Na_2O	4.69	5.06	9.74	3.68
K_2O	4.76	4.06	0.59	4.65
		Mode		Mode
Quartz		35		45
Plagioclase				1(An25)
K-feldspar		60		40
Biotite		2		8
Amphibole				
Orthopyroxene				
Clinopyroxene				
Apatite				1
Ilmenite				
Magnetite				1
Olivine				

TABLE IV. DIRECTIONS OF VERTICAL QUARTZ AND
GREISEN VEINS IN THE MAYO-DARLÉ AREA

METASEDIMENTS				
N 85 E	N 18 E	N 10 E	N 85 E	N 55 E
N 87 E	N 20 E	N 70 W	N 90 E	N 62 W
N 10 W	N 90 E	N 65 W	N 28 E	N 43 W
N 65 E	N 90 E	N 70 W	N 50 E	N 65 W
N 40 E	N 72 E	N 80 E	N 75 W	N 80 W
N 30 E	N 46 E	N 78 W	N 80 W	N 63 W
N 20 E	N 50 E	N 48 W	N 85 E	N 40 E
N 50 E	N 55 W	N 70 W	N 55 W	N 85 E
N 25 E	N 56 W	N 45 E	N 82 W	
N 45 E	N 5 E	N 50 E	N 50 W	

IGNEOUS ROCKS				
N 85 W	N 65 E	N 52 E	N 5 W	N 23 W
N 65 W	N 20 E	N 7 E	N 15 E	N 25 W
N 23 W	N 5 E	N 15 E	N 23 W	N 5 W
N 14 E	N 18 W	N 10 E	N 65 W	N 18 W
N 70 E	N 80 E	N 8 E	N 32 W	N 35 W
N 80 E	N 38 W	N 42 E	N 26 W	N 26 W
N 34 E	N 20 W	N 42 W	N 35 W	N 18 W
N 27 E	N 18 W	N 40 W	N 25 W	N 65 E
N 80 E	N 38 W	N 42 W	N 40 W	N 65 W
N 35 E	N 15 W	N 48 W	N 50 W	N 32 E
N 13 E	N 38 W	N 48 W	N 45 W	N 15 E
N 80 E	N 25 W	N 36 E	N 34 W	N 10 E
N 85 E	N 42 E	N 38 E	N 43 W	N 90 E
N 45 E	N 50 E	N 22 E	N 5 W	N 60 W
N 52 E	N 50 E	N 30 E	N 20 E	N 20 W
N 78 E	N 38 W	N 18 W	N 44 W	N 42 W
N 25 E	N 49 W	N 25 E	N 20 E	N 10 W
N 40 W	N 14 W	N 12 E	N 48 W	N 40 W
N 8 W	N 42 W	N 50 E	N 45 E	N 35 W
N 25 W	N 75 W	N 33 E	N 35 W	N 12 W
N 85 W	N 10 E	N 10 W	N 48 W	N 22 E
N 48 W	N 5 E	N 35 W	N 25 W	N 45 E
N 5 W	N 45 E	N 40 W	N 85 E	N 50 W
N 35 E	N 52 E	N 20 E	N 35 E	N 36 E

Fig. 39. Sample Location Map
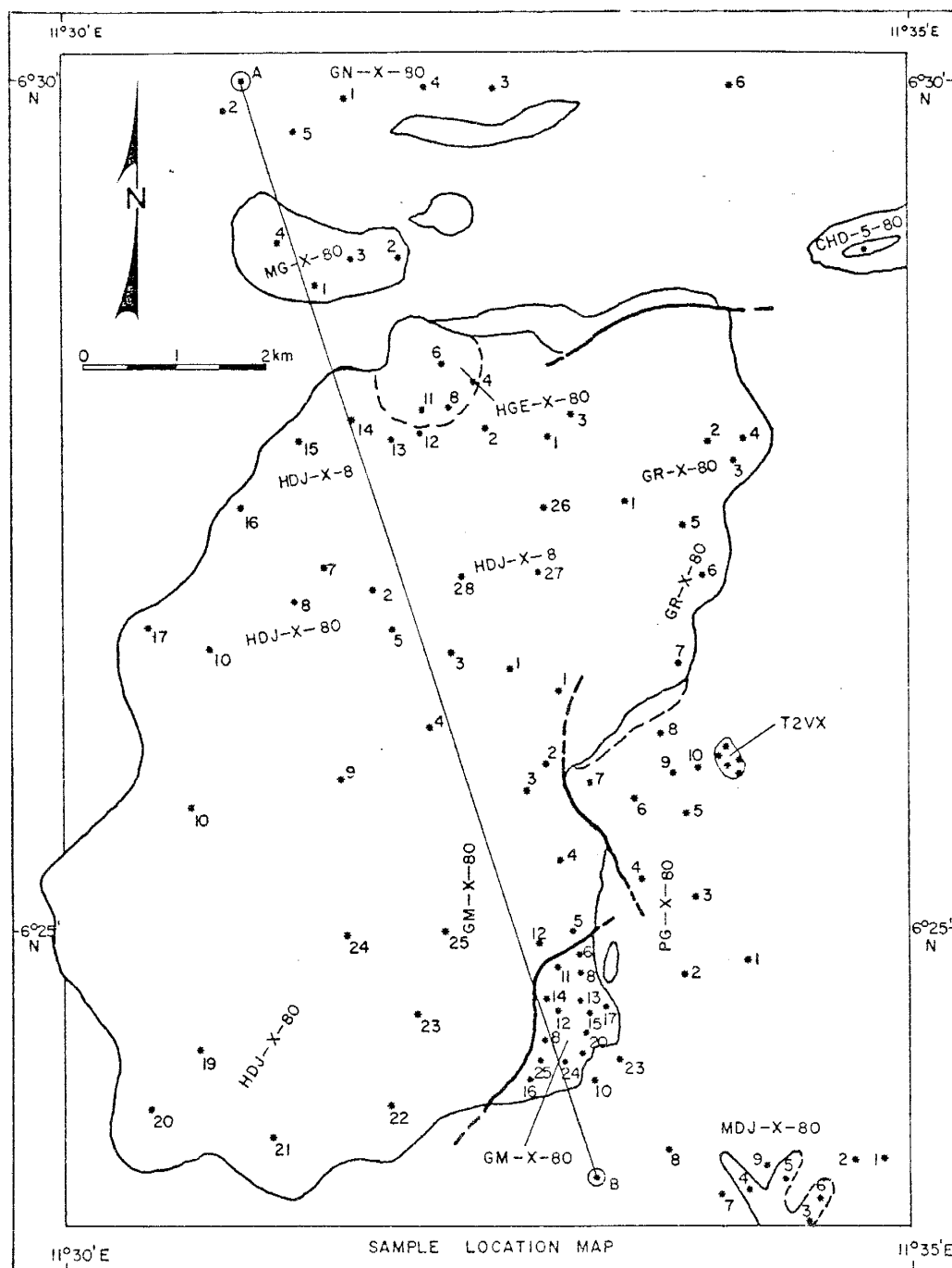
Fig. 39.   Sample Location Map

APPENDIX II. Rb-Sr DATA

Rb-Sr analyses reported here were carried out in the Isotope Geochemistry Laboratory at the University of Kansas. Data were obtained using standard isotope dilution techniques and a 60°-sector, 9 in.-radius, single-filament mass spectrometer. Summaries of the applied techniques are reported in Van Schmus (1971) and Vera and Van Schmus (1974). The constants used in this study are λ (^{87}Rb) = 1.42 x 10^{-11} yr^{-1}; $^{86}Sr/^{88}Sr$ (atomic) = 0.1194 (all Sr data were normalized to this value); $^{84}Sr/^{86}Sr$ = 0.0570; and $^{85}Rb/^{87}Rb$ = 2.5927. Recorded estimates of analytical errors for individual analyses in the Isoptope Geochemistry Laboratory are $\pm$ 2 percent for $^{87}Rb/^{86}Sr$ values and $\pm$ 0.2 percent for $^{87}Sr/^{86}Sr$ values at the 95 percent confidence level. The least-squares cubic regression method (York, 1966) was used to obtain isochron ages. Rb-Sr isochron errors are reported at the 95 percent confidence level. Analyses of fluid inclusion waters were carried out in the laboratories of the Mineralogisk-Geologisk Museum, Oslo, Norway using techniques developed by Norman, et al. (1979).

Rb-Sr ANALYTICAL DATA

Sample	Rock type	Rb (ppm)	Sr (ppm)	$^{87}Rb/^{86}Sr$ (atomic)	$^{87}Sr/^{86}Sr$ (atomic)
GRANITES					
GM-5-80	Biotite granite	220.8	2.4	275.3	0.9315
HDJ-4-80	Biotite granite	334.8	5.1	192.3	0.8621
HDJ-8-80	Biotite granite	163.5	3.8	126.6	0.8072
HGE-2-80	Biot.-Riebeckite granite	457.6	6.1	221.0	0.8831
HGE-4-80	Biot.-Riebeckite granite	346.9	1.9	560.1	1.1312
CHBRX	Biotite granite	311.9	9.4	96.3	0.7825
GR-3-80	Biotite granite	303.9	18.7	47.2	0.7486
GR-4-80	Biotite granite	295.6	16.5	52.1	0.7481
SYENITES					
GM-11-80	Syenite	173.5	24.6	20.4	0.7183
GM-14-80	Syenite	154.2	21.3	21.2	0.7262
GM-20-80	Syenite	146.2	7.3	58.4	0.7510
GM-21-80	Syenite	166.8	10.2	47.4	0.7514
GM-22-80	Syenite	163.5	13.6	34.9	0.7367
GM-24-80	Syenite	148.3	7.9	54.4	0.7611
RHYOLITES					
T2V1	Rhyolite	107.9	127.8	2.4	0.7124
T2V2	Rhyolite	155.4	12.3	36.5	0.7405
T2V3	Rhyolite	148.7	14.9	28.9	0.7385
T2V4	Rhyolite	23.4	404.1	0.167	0.7068
T2IN1	Benmoreite xenolith	172.3	47.3	10.5	0.7145

Rb-Sr ANALYTICAL DATA

Sample	Rock type	Rb (ppm)	Sr (ppm)	$^{87}Rb/^{86}Sr$ (atomic)	$^{87}Sr/^{86}Sr$ (atomic)
BASEMENT ROCKS					
GN-1-80	Biotite gneiss	142.6	672.6	0.61	0.7133
GN-2-80	Biotite gneiss	70.2	979.3	0.21	0.7059
GN-3-80	Biotite gneiss	74.3	795.9	0.27	0.7094
GN-4-80	Biotite gneiss	68.6	979.7	0.20	0.7080
PG-5-80	Quartz-diorite gneiss	250.4	170.2	4.27	0.7435
PG-8-80	Quartz-diorite gneiss	232.1	102.2	6.60	0.7635
MDJ-8-80	Biotite gneiss	47.0	382.9	0.35	0.7076
FLUID INCLUSIONS					
Qtz-pheno	Granite (pit)	50.44	6.57	22.2	0.7295
HGE-2N-80	Tin-floor quartz	78.59	11.66	19.5	0.7350
SnO_2	Cassiterite	13.68	33.21	1.2	0.7158
Euh.-Qtz.	Euhedral quartz	73.37	8.37	25.4	0.7330
Ore-Qtz.	Greisen lode quartz	225.8	15.34	42.9	2.2304

APPENDIX III. FLUID INCLUSION DATA

Fluid inclusion analyses were carried out using standard heating/freezing techniques (Roedder, 1962). Doubly polished "thick" sections with average thickness of 0.3 mm were examined using the TH600 LINKAM heating/freezing stage mounted on a Leitz microscope. The stage was calibrated using both organic and inorganic compounds. Daily calibration checks were carried out using compounds with known melting points within the range of 0° to 500^OC. Precision of the homogenization measurements, based on daily measurements of standards and repeated measurements of inclusions is $\pm 5^O$C at the 95 percent confidence level. The primary nature of the inclusions studied was based on Roedder´s (1967) criteria. Only inclusions of primary nature were examined.

The homogenization nomenclature used in this study is based on phase disappearance. Homogenization is characterized by the disappearance of the last phase (Wilson, Kesler, Clark and Kelly, 1980). Thus the following terms will be used: homogenization by vapor disappearance, meaning the vapor is the last phase to disappear before complete homogeneity is obtained. Similarly, liquid disappearance, halite disappearance, and cryolite disappearance will be used. In a multi-phase inclusion, the last phase to disappear will characterize the homogenization of that inclusion.

The following abbreviations are used within the tables:

Temp.   = temperature,
P   = primary inclusion,
Ps   = pseudosecondary inclusion,
Eq. wt. %   = Equivalent weight percent.

TABLE I.   FREEZING-HEATING DATA: TWO-PHASE INCLUSIONS

Sample	Host Mineral	Type of Inclusion	Freezing Point Temp. (°C)	Salinity NaCl Eq.wt%	Molality (m)	Homogenization Disappearance of Vapor (°C)	Liquid (°C)
			VERTICAL GREISEN VEINS				
1A	Quartz	P.	-18.80	21.79	4.78	361	
1A	Quartz	P.	-20.90	23.29	5.20	327	
1A	Quartz	P.	-23.60	25.09	5.70		534
1A	Quartz	P.	-13.60	17.55	3.65		599
1B	Quartz	P.	-4.30	6.87	1.27		
1B	Quartz	P.	-12.00	16.04	3.27		
1B	Quartz	P.	-21.90	23.97	5.39		
1B	Quartz	P.	-23.00	24.70	5.59		
1B	Quartz	P.	-22.50	24.37	5.50		
N2A	Quartz	P.	-6.50	9.86	1.87	227	
N2A	Quartz	P.	-12.70	16.72	3.44		
N2A	Quartz	P.	-5.20	8.13	1.52	230	
N2A	Quartz	P.	-7.30	10.86	2.09		
N2B	Quartz	P.	-23.50	25.03	5.68		538
N2B	Quartz	P.	-23.30	24.90	5.65		534
N2B	Quartz	P.	-23.70	25.16	5.72	263	
N2B	Quartz	P.	-23.40	24.96	5.67	355	
N2B	Quartz	P.	-23.50	25.03	5.68	358	
N2B	Quartz	P.	-23.60	25.09	5.70	360	
N2B	Quartz	P.	-15.40	19.13	4.06	524	
5A	Quartz	P.	-10.80	14.83	2.98		
5A	Quartz	P.	-4.70	7.44	1.38		
5A	Quartz	P.	-4.50	7.15	1.32		
5A	Quartz	P.	-5.20	8.13	1.52		
5A	Quartz	Ps.	-2.90	4.79	0.86	259	
5A	Quartz	P.	-4.10	6.58	1.21	270	
5A	Quartz	P.	-23.40	24.96	5.67		591
5A	Quartz	P.	-14.30	18.18	3.81		481
5A	Quartz	Ps.	-2.50	4.17	0.75		533
5B	Quartz	P.	-17.90	21.12	4.60		
5B	Quartz	P.	-7.70	11.35	2.19		
5B	Quartz	Ps.	-1.50	2.56	0.45	398	
5B	Quartz	Ps.	-2.80	4.63	0.84	392	
5B	Quartz	P.	-10.70	14.73	2.96		499
5B	Quartz	P.	-14.30	18.18	3.81		554
5B	Quartz	P.	-22.30	24.24	5.46		494
8B	Quartz	P.	-7.00	10.49	2.01		
8B	Quartz	P.	-18.00	21.20	4.62		
8B	Quartz	P.	-16.60	20.11	4.32		
8B	Quartz	P.	-4.30	6.87	1.27		

TABLE I.   (con't)

Sample	Host Mineral	Type of Inclusion	Freezing Point Temp. ($^{\circ}$C)	Salinity NaCl Eq.wt%	Molality (m)	Homogenization Disappearance of Vapor ($^{\circ}$C)	Liquid ($^{\circ}$C)
HORIZONTAL GREISEN VEINS
11A	Quartz	P.	−22.50	24.37	5.50		
11A	Quartz	P.	−23.00	24.70	5.59		
4A	Quartz	P.	−10.90	14.94	3.01		
4A	Quartz	P.	−22.40	24.30	5.48	382	
4A	Quartz	P.	−15.80	19.46	4.15	361	
4A	Quartz	P.	−20.90	23.29	5.20	399	
4A	Quartz	P.	−19.20	22.09	4.86	400	
4A	Quartz	P.	−4.50	7.15	1.32	329	
4A	Quartz	P.	−10.90	14.94	3.01	384	
4A	Quartz	P.	−13.00	17.00	3.51		507
4A	Quartz	P.	−17.00	20.43	4.41		401
12B	Quartz	P.	−23.40	24.96	5.67		
12B	Quartz	P.	−24.60	25.75	5.88		
12B	Quartz	P.	−23.30	24.90	5.65		
12B	Quartz	P.	−24.40	25.61	5.84		>600
12B	Quartz	P.	−22.30	24.24	5.46		581
12B	Quartz	P.	−5.40	8.40	1.57		580
12B	Quartz	P.	−21.00	23.36	5.22		442
6A	Quartz	P.	−18.60	21.65	4.74		>600
BARREN QUARTZ VEINS
14A	Quartz	P.	−9.00	12.88	2.53	350	
14A	Quartz	P.	−9.30	13.22	2.61	334	
14A	Quartz	P.	−4.70	7.44	1.38	221	
14A	Quartz	P.	−12.70	16.72	3.44	355	
14A	Quartz	P.	−8.70	12.53	2.45	354	
14A	Quartz	P.	−12.10	16.14	3.30	344	
14A	Quartz	P.	−12.40	16.43	3.37		
14A	Quartz	P.	−10.70	14.73	2.96	349	
14A	Quartz	P.	−12.20	16.24	3.32	362	
14A	Quartz	P.	−11.00	15.04	3.03		429
14A	Quartz	P.	−14.40	18.27	3.83		562
14B	Quartz	P.	−9.00	12.88	2.53	348	
14B	Quartz	P.	−8.50	12.30	2.40	345	

TABLE II.   HOMOGENIZATION DATA: TWO-PHASE INCLUSIONS

Sample	Host Mineral	Type of Inclusion	Homogenization	
			Disappearance of	
			Vapor (^{o}C)	Liquid (^{o}C)
VERTICAL GREISEN VEINS				
2A	Quartz	P	166	
2A	Quartz	P	167	
2A	Quartz	P	169	
2A	Quartz	P	170	
2A	Quartz	P	171	
2A	Quartz	P	175	
2A	Quartz	P	184	
2A	Quartz	P	216	
2A	Quartz	P	221	
2A	Quartz	P	221	
2A	Quartz	P	224	
2A	Quartz	P	229	
2A	Quartz	P	235	
2A	Quartz	P	240	
2A	Quartz	P	262	
2A	Quartz	P	264	
2A	Quartz	P	268	
2A	Quartz	P	270	
2A	Quartz	P	270	
2A	Quartz	P	346	
2A	Quartz	P	356	
2A	Quartz	P	359	
2A	Quartz	P	370	
2A	Quartz	P		399
2A	Quartz	P		497
2A	Quartz	P		501
2A	Quartz	P		519
2A	Quartz	P		521
2A	Quartz	P		528
2A	Quartz	P		531
2A	Quartz	P		537
2A	Quartz	P		569
2A	Quartz	P		547
2A	Quartz	P		591
2B	Quartz	P	380	
2B	Quartz	P	324	
2B	Quartz	P	284	
2B	Quartz	P	285	
2B	Quartz	P	389	
2B	Quartz	P	385	

TABLE II. (con´t)

Sample	Host Mineral	Type of Inclusion	Homogenization	
			Disappearance of	
			Vapor (^{o}C)	Liquid (^{o}C)
VERTICAL GREISEN VEINS				
2B	Quartz	P	>600	
2B	Quartz	P	>600	
2B	Quartz	P		389
2B	Quartz	P		385
2B	Quartz	P		>600
2B	Quartz	P		>600
3A	Quartz	P	360	
3A	Quartz	P	377	
3A	Quartz	P	270	
3A	Quartz	P	411	
3A	Quartz	P		582
3A	Quartz	P		464
3A	Quartz	P		553
3A	Quartz	P		553
3B	Quartz	P	206	
3B	Quartz	P	323	
3B	Quartz	P	299	
3B	Quartz	P	344	
3B	Quartz	P	399	
3B	Quartz	P	358	
3B	Quartz	P	356	
3B	Quartz	P	372	
3B	Quartz	P	>600	
3B	Quartz	P	372	
3B	Quartz	P		594
3B	Quartz	P		573
3B	Quartz	P		561
3B	Quartz	P		597
1A	Quartz	P	450	
1A	Quartz	P	447	
1A	Quartz	P	449	
1A	Quartz	P	451	
1A	Quartz	P	459	
1A	Quartz	P	324	
1A	Quartz	P	391	
1A	Quartz	P	327	
1A	Quartz	P		572
1A	Quartz	P		584
1A	Quartz	P		>600
1A	Quartz	P		>600

TABLE II. (con't)

Sample	Host Mineral	Type of Inclusion	Homogenization	
			Disappearance of	
			Vapor (°C)	Liquid (°C)

VERTICAL GREISEN VEINS

Sample	Host Mineral	Type of Inclusion	Vapor (°C)	Liquid (°C)
1B	Quartz	P	207	
1B	Quartz	P	342	
1B	Quartz	P		332
1B	Quartz	P		582
1B	Quartz	P		584
1B	Quartz	P		562
1B	Quartz	P		571
1B	Quartz	P		559
1B	Quartz	P		394
1B	Quartz	P		595
1B	Quartz	P		409
1B	Quartz	P		411
1B	Quartz	P		417
1B	Quartz	P		534
1B	Quartz	P		599
9B	Quartz	P	401	
9B	Quartz	P	393	
9B	Quartz	P		>600
9B	Quartz	P		>600
9B	Quartz	P		542
N2A	Quartz	P	442	
N2A	Quartz	P	506	
N2A	Quartz	P	399	
N2A	Quartz	P	394	
N2A	Quartz	P	441	
N2A	Quartz	P	205	
N2A	Quartz	P	227	
N2A	Quartz	P	230	
N2B	Quartz	P	376	
N2B	Quartz	P	371	
N2B	Quartz	P	367	
N2B	Quartz	P	399	
N2B	Quartz	P	263	
N2B	Quartz	P	355	
N2B	Quartz	P	358	
N2B	Quartz	P	360	
N2B	Quartz	P	524	
N2B	Quartz	P		563
N2B	Quartz	P		>600
N2B	Quartz	P		592

TABLE II. (con't)

Sample	Host Mineral	Type of Inclusion	Homogenization	
			Disappearance of	
			Vapor (^{o}C)	Liquid (^{o}C)
VERTICAL GREISEN VEINS				
N2B	Quartz	P		538
N2B	Quartz	P		534
N2B	Quartz	P		529
5A	Quartz	P	423	
5A	Quartz	P	395	
5A	Quartz	P	259	
5A	Quartz	P	270	
5A	Quartz	P		599
5A	Quartz	P		589
5A	Quartz	P		591
5A	Quartz	P		481
5A	Quartz	P		533
5B	Quartz	P	404	
5B	Quartz	P	390	
5B	Quartz	P	398	
5B	Quartz	P	392	
5B	Quartz	P		499
5B	Quartz	P		554
5B	Quartz	P		494
2A	Quartz	P	218	
HORIZONTAL GREISEN VEINS				
18A	Quartz	P	312	
18A	Quartz	P	323	
18A	Quartz	P	349	
18A	Quartz	P	>600	
18A	Quartz	P	>600	
18A	Quartz	P	>600	
18A	Quartz	P	>600	
18A	Quartz	P	>600	
18A	Quartz	P		>600
18A	Quartz	P		>600
18B	Quartz	P	244	
18B	Quartz	P	248	
18B	Quartz	P	264	
18B	Quartz	P	245	
18B	Quartz	P	183	
18B	Quartz	P		591
18B	Quartz	P		>600
18B	Quartz	P		575

TABLE II. (con't)

Sample	Host Mineral	Type of Inclusion	Homogenization	
			Disappearance of	
			Vapor (^{o}C)	Liquid (^{o}C)
HORIZONTAL GREISEN VEINS				
18B	Quartz	P		>600
18B	Quartz	P		571
18B	Quartz	P		549
18B	Quartz	P		448
11A	Quartz	P	578	
11A	Quartz	P	337	
11A	Quartz	P	>600	
11A	Quartz	P	221	
11A	Quartz	P		595
11A	Quartz	P		>600
11A	Quartz	P		396
11A	Quartz	P		527
11A	Quartz	P		528
11A	Quartz	P		572
11A	Quartz	P		580
11A	Quartz	P		569
11A	Quartz	P		591
11A	Quartz	P		>600
11A	Quartz	P		>600
11A	Quartz	P		>600
10A	Quartz	P	256	
10A	Quartz	P	232	
10A	Quartz	P	238	
10A	Quartz	P	484	
10A	Quartz	P	457	
10A	Quartz	P	287	
10A	Quartz	P	299	
10A	Quartz	P	472	
10A	Quartz	P	437	
10A	Quartz	P		597
10A	Quartz	P		414
10A	Quartz	P		397
10A	Quartz	P		512
10B	Quartz	P	484	
10B	Quartz	P	398	
10B	Quartz	P	328	
10B	Quartz	P	367	
10B	Quartz	P	280	
10B	Quartz	P	286	
10B	Quartz	P	291	

TABLE II. (con't)

| Sample | Host Mineral | Type of Inclusion | Homogenization | |
| | | | Disappearance of | |
			Vapor (^{o}C)	Liquid (^{o}C)
HORIZONTAL GREISEN VEINS				
10B	Quartz	P		449
10B	Quartz	P		397
10B	Quartz	P		400
10B	Quartz	P		519
10B	Quartz	P		573
10B	Quartz	P		592
10B	Quartz	P		>600
10B	Quartz	P		>600
12A	Quartz	P	234	
12A	Quartz	P	254	
12A	Quartz	P	274	
12A	Quartz	P	259	
12A	Quartz	P	266	
12A	Quartz	P	362	
12A	Quartz	P	295	
12A	Quartz	P	244	
12A	Quartz	P	554	
12A	Quartz	P	237	
12A	Quartz	P	275	
12A	Quartz	P	481	
12A	Quartz	P	250	
12A	Quartz	P	278	
12A	Quartz	P	251	
12A	Quartz	P	246	
12A	Quartz	P	229	
12B	Quartz	P	323	
12B	Quartz	P	326	
12B	Quartz	P	296	
12B	Quartz	P	474	
12B	Quartz	P	499	
12B	Quartz	P	514	
12B	Quartz	P	436	
12B	Quartz	P		499
12B	Quartz	P		501
12B	Quartz	P		522
12B	Quartz	P		442
12B	Quartz	P		>600
12B	Quartz	P		581
12B	Quartz	P		580
4A	Quartz	P	246	

TABLE II.   (con´t)

Sample	Host Mineral	Type of Inclusion	Homogenization	
			Disappearance of	
			Vapor ($^{\circ}$C)	Liquid ($^{\circ}$C)
		HORIZONTAL GREISEN VEINS		
4A	Quartz	P	401	
4A	Quartz	P	370	
4A	Quartz	P	369	
4A	Quartz	P	371	
4A	Quartz	P	372	
4A	Quartz	P	369	
4A	Quartz	P	371	
4A	Quartz	P	366	
4A	Quartz	P	345	
4A	Quartz	P	343	
4A	Quartz	P	382	
4A	Quartz	P	361	
4A	Quartz	P	399	
4A	Quartz	P	400	
4A	Quartz	P	329	
4A	Quartz	P	384	
4A	Quartz	P		459
4A	Quartz	P		464
4A	Quartz	P		518
4A	Quartz	P		517
4A	Quartz	P		507
4A	Quartz	P		401
4B	Quartz	P	357	
4B	Quartz	P	379	
4B	Quartz	P	186	
4B	Quartz	P	368	
4B	Quartz	P	359	
4B	Quartz	P	399	
4B	Quartz	P	364	
4B	Quartz	P	362	
6A	Quartz	P	488	
6A	Quartz	P	587	
6A	Quartz	P	591	
6A	Quartz	P	571	
6A	Quartz	P	488	
6A	Quartz	P	514	
6A	Quartz	P	458	
6A	Quartz	P	569	
6A	Quartz	P	>600	
6B	Quartz	P	>600	
6B	Quartz	P	458	

TABLE II. (con't)

Sample	Host Mineral	Type of Inclusion	Homogenization	
			Disappearance of	
			Vapor (^{O}C)	Liquid (^{O}C)
BARREN QUARTZ VEINS				
14A	Quartz	P	350	
14A	Quartz	P	334	
14A	Quartz	P	221	
14A	Quartz	P	355	
14A	Quartz	P	354	
14A	Quartz	P	344	
14A	Quartz	P	349	
14A	Quartz	P	362	
14A	Quartz	P		598
14A	Quartz	P		429
14A	Quartz	P		562
14B	Quartz	P	353	
14B	Quartz	P	341	
14B	Quartz	P	349	
14B	Quartz	P	345	
14B	Quartz	P	351	
14B	Quartz	P	346	
14B	Quartz	P	376	
14B	Quartz	P	348	
14B	Quartz	P	345	

TABLE III.   HOMOGENIZATION TEMPERATURES: TYPE C AND D INCLUSIONS
(All inclusions are primary inclusions from quartz)

| Sample | Phase Disappearance | | | Salinity Eq.wt.% |
	Vapor (^{o}C)	Halite (^{o}C)	Cryolite (^{o}C)	NaCl
	VERTICAL GREISEN VEINS			
1A	382	173		30.6
1A	393	173		30.6
1A	309	307		38.0
1A	358	348	419	
1A	256	476	>600	
1A	484	241		33.0
1A	309	277		36.0
1A	358	348		41.1
1A	313	393		45.0
1A	299	300		37.6
1A	258	342		40.1
1A	268	342		40.1
1A	288	299		37.5
1A	323	339		40.4
1B	261	438		49.3
1B	261	367		42.7
1B	354	367		42.7
1B	231	259		34.9
2A	368	489		54.9
2A	317	472		52.9
2A	324	499		56.0
2A	339	504		56.6
2A	319	499		56.6
2A	299	517		58.2
2B	321	359		42.0
2B	179	224		33.0
2B	221	324		39.3
2B	263	350		41.3
2B	249	345		40.9
2B	247	343		40.7
2B	283	349		41.2
2B	244	339		40.4
2B	246	344		40.8
3A	233	403		45.9
3A	320	424		47.9
3A	332	407		46.3
3A	273	509		57.2
3A	269	512		57.6
3A	288	514		57.8
3A	271	519		58.5

TABLE III.   (con't)

| Sample | Phase Disappearance | | | Salinity Eq.wt.% |
	Vapor (^{o}C)	Halite (^{o}C)	Cryolite (^{o}C)	NaCl
	VERTICAL GREISEN VEINS			
3A	269	517		58.2
3A	267	504		56.6
3A	265	524		59.1
3B	297	243		34.0
3B	305	283		36.4
3B	367	252		34.5
3B	303	254		34.6
3B	205	341		40.6
3B	206	339		40.4
3B	296	369		42.9
3B	226	414		46.9
5A	312	169		30.4
5A	331	291		36.9
5A	360	214		32.5
5A	278	484	>600	
5B	399	259		34.9
5B	415	153		29.8
5B	257	372		43.1
5B	347	232		33.4
5B	230	595	385	
N2A	241	384		44.6
N2A	303	479	349	
N2A	312	293		37.1
N2A	323	285		36.6
N2B	285	434		48.9
N2B	263	431		48.9
N2B	263	536		60.6
N2B	263	439	549	
N2B	329	285	539	
N2B	399	253		34.6
N2B	374	250		34.4
N2B	303	302		37.7
N2B	300	193		31.5
8B	289	299		37.5
8B	247	469		52.6
8B	207	224		33.0
8B	333	432		48.7
8B	301	481	449	
8B	327	473	327	
9A	340	306		38.0
9A	>600	200		31.8

TABLE III. (con't)

Sample	Phase Disappearance			Salinity Eq.wt.%
	Vapor (°C)	Halite (°C)	Cryolite (°C)	NaCl
VERTICAL GREISEN VEINS				
9A	595	306		38.0
9A	389	322		39.1
9A	419	277		36.0
9A	342	274		35.8
9A	532	454		51.0
9A	>600	232	>600	
9A	265	433	>600	
9A	265	476	>600	
9A	328	493		55.3
9A	292	432		48.7
9A	331	354		41.6
9A	224	293		37.1
9B	353	292		37.0
9B	281	489	324	
HORIZONTAL GREISEN VEINS				
4A	389	299		37.5
4A	319	228		33.2
4A	325	226		33.1
4A	327	207		32.1
4A	311	271		35.7
4A	217	519		58.5
4A	246	471		53.5
4A	255	436		49.1
4B	335	285		36.6
4B	219	504		56.6
4B	370	533		60.2
4B	349	387		44.4
10A	307	192		31.4
10A	318	162		30.4
11A	388	347		41.1
11A	365	332		39.9
11A	388	347		41.1
11A	365	332		39.9
11A	405	320		39.0
11A	418	348		41.1
11A	407	342		40.7
11A	372	353		41.5
11A	341	335		40.1
11A	448	232		33.4
11A	241	337		40.3
11A	237	333		39.9
11A	181	319		38.9
11A	232	329		39.7
11A	282	292		37.0

TABLE III. (con't)

Sample	Phase Disappearance			Salinity Eq.wt.%
	Vapor (^{O}C)	Halite (^{O}C)	Cryolite (^{O}C)	NaCl
HORIZONTAL GREISEN VEINS				
12A	385	401		45.7
12A	386	411		46.7
12A	353	353		41.5
12A	400	438		49.3
12B	285	344		40.8
12B	239	337		40.3
12B	272	279		36.2
12B	314	280		36.2
12B	278	219		32.7
18A	>600	344		40.8
18B	419	339		40.4
18B	399	309		38.2
18B	414	345		40.9
18B	261	283		36.4
18B	279	313		38.5
18B	200	270		35.6
18B	271	284		36.5
BARREN QUARTZ VEINS				
14A	363	384		44.2
14A	350	402		45.8
14A	352	399		45.5
14A	301	381		43.9
14A	303	379		43.7
14A	376	323		39.2
14B	352	371		43.0
14B	343	375		43.4
14B	315	379		43.7
14B	359	373		43.2

TABLE IV.   FLUID INCLUSION DATA FROM THE GRANITE
(All inclusions are primary inclusions
from quartz phenocrysts)

| Sample | Inclusion Type | Freezing Temp. ($^{\circ}$C) | Phase disappearance | | Salinity Eq.Wt.% |
			Vapor ($^{\circ}$C)	Halite ($^{\circ}$C)	NaCl
CHBRX	Liq.-rich	-15.8	>600		19.4
CHBRX	Liq.-rich	-16.9	449		20.3
CHBRX	Liq.-rich	-15.0	499		18.8
CHBRX	Liq.-rich	-15.3	501		19.0
CHBRX	Liq.-rich	-23.5	>600		25.0
CHBRX	Liq.-rich	-21.0	569		23.3
CHBRX	Liq.-rich	-14.0	573		17.9
CHBRX	Liq.-rich	-23.9	571		25.3
CHBRX	Liq.-rich	-14.5	>600		18.4
CHLV	Liq.-rich	-17.7			20.9
CHLV	Liq.-rich	-14.6	583		18.4
CHLV	Liq.-rich	-23.3	>600		24.9
CHLV	Liq.-rich	-16.5	451		20.0
CHLV	Liq.-rich	-21.7	>600		23.8
CHLV	Halite		242	495	55.6
CHLV	Halite		397	247	34.2
GM-1-80	Liq.-rich	-21.8	381		23.9
GM-1-80	Liq.-rich	-21.0	270		23.4
GM-1-80	Liq.-rich	-19.7	244		22.4
GM-1-80	Liq.-rich	-22.9	511		24.6
GM-1-80	Liq.-rich	-23.5	529		25.0
GM-1-80	Halite		329	303	37.8
GR-4-80	Halite		386	383	44.1
GR-4-80	Liq.-rich	-23.0	451		24.7
GR-4-80	Liq.-rich	-21.1	434		23.4
GR-4-80	Liq.-rich	-21.7	441		23.8
GR-4-80	Liq.-rich	-21.0	454		23.4
GR-4-80	Liq.-rich	-20.9			23.3
GR-4-80	Liq.-rich	-23.3	464		24.9
HGE-2-80	Halite		518	524	59.1
HGE-2-80	Halite		519	517	58.2
HGE-2-80	Halite		321	489	54.9
HGE-2-80	Halite		499	449	50.5
HGE-2-80	Halite		522	457	51.3
HGE-2-80	Halite		503	497	55.8
HGE-2-80	Halite		529	526	59.3

Liq.-rich = liquid-rich inclusion;
Halite = halite-bearing inclusion

REFERENCES

Ahmad, S.N., and Rose, A.W., 1980, Fluid inclusions in porphyry and skarn ore at Santa Rita, New Mexico: Econ. Geol., v. 75, no.2, pp. 229-250.

Allègre, C.J., and Minster, J.F., 1978, Quantitative models of trace element behavior in magmatic processes: Earth Planet. Sci. Lett., v. 38, pp. 1-25.

Armstrong, R.L., 1968, A model for the evolution of strontium and lead isotopes in a dynamic earth: Rev. Geophys. v. 6, pp. 175-199.

Barnes, H.L., 1979, Geochemistry of hydrothermal ore deposits, 2nd edition, John Wiley and Sons, New York, 798 p.

Barsukov, V.L., 1967, Source of ore substance of tin deposits (Abstract): in Trans. Inst. Min. Metal., Sect. B, v. 76, p. B220.

Bickford, M.E., and Mose, D.G., 1975, Geochronology of Precambrian rocks in the St-François Mountains, southeastern Missouri: Geol. Soc. America, Special Paper no. 165, 48 p.

Black, R., and Girod, M., 1970, Late Paleozoic to Recent igneous activity in West Africa and its relationship to basement structure: in African Magmatism and Tectonics, Clifford, T.N., and Gass, I.G., editors, Hafner Publishing Co, Darien, Conn., U.S.A., pp. 185-210.

Black, R., Jacobson, R.R.E., and Macleod, W.N., 1957, Ring complexes in the Younger Granite province of northern Nigeria: Geol. Soc. London, Pr. no. 1545, pp. 21-28.

Blaxland, A.B., van Breemen, O., Emeleus, C.H., and Anderson, J.G., 1978, Age and origin of the major syenite centers in the Gardar province of south Greenland: Rb-Sr studies: Geol. Soc. America Bull., v. 89, pp. 231- 244.

Brandvold, L.A., 1974, Atomic absorption methods for analysis of some elements in ores and concentrates: New Mexico Bur. Mines and Miner. Res., Circular 142, 22 p.

Brooks, C., 1966, The effect of mineral age discordancies in peralkaline and associated granites: Lithos, v. 7, pp. 15-21.

Brooks, C., and Compston, W., 1965, The age and initial 87Sr/86Sr of the Heemskirk granite, Western Tasmania: J. Geophys. Res., v. 70, no. 24, pp.6249-6262.

Brooks, C., James, D.E., and Hart, S.R., 1976, Ancient lithosphere: its role in young continental volcanism: Science, v. 193, pp. 1086-1094.

Buchanan, L.J., 1981, Precious metal deposits associated with volcanic environments in the Southwest: Arizona Geol. Soc. Digest, v. 14, pp. 237-262.

Burke, K., Dessauvagie, T.F.J., and Whiteman, A.J., 1971, Opening of the gulf of Guinea and geologic history of the Benue Depression and Niger delta: Nature Phys. Sci., v. 238, pp. 51-55.

Burnham, C.W., 1979, Magma and hydrothermal fluids: in Geochemistry of hydrothermal ore deposits (Barnes, H.L.,editor), 2nd edition, John Wiley and Sons, New York, pp. 71-136.

Butler, J.R., Bowden, P., and Smith, A.Z., 1962, K/Rb ratios in the evolution of the Younger Granites of northern Nigeria: Geochim. et Cosmochim. Acta, v.26, pp. 89-100.

Cahen, L., and Snelling, N.J., 1966, The Geochronology of Equatorial Africa, North Holland Publishing Co., Amsterdam, 195 p.

Cantagrel, J.M., Jamond, C., and Lasserre, M.,1978, Le magmatisme alcalin de la ligne du Cameroun au Tertiaire inférieur: données géochronologiques K/Ar: C.R. somm.,Soc. Géol. France, fasc. no. 6, pp. 300-303.

Condie, K.C., 1978, Geochemistry of Proterozoic granitic plutons from New Mexico, U.S.A.: Chemical Geology, v. 21, pp. 131-149.

Condie, K.C., and Hunter, D.R., 1976, Trace element geochemistry of Archean granitic rocks from the Barberton regions, South Africa : Earth Planet. Sci. Lett., v., pp. 389-400.

Condie, K.C., and Lo, H.H., 1971, Trace element geochemistry of the Louis Lake batholith of early Precambrian age, Wyoming: Geochem. et Cosmochim. Acta, v.35, pp. 1095-1120.

Cratchley, C.R., and Jones, G.P., 1965, An interpretation of geology and gravity anomalies of the Benue Valley, Nigeria: Geophys. Pap. Overseas Geol. Survs., v. 1 .

Dumort, J.C., 1968, Notice explicative sur la feuille Douala-Ouest, avec carte géologique au 1/500000, Imp. Nat., Yaoundé,Cameroun, 69 p.

El Bouseily, A.M., and El Sokkary, A.A., 1975, The relation between Rb, Ba, and Sr in granitic rocks: Chemical

Geology, v. 16, pp. 207-219.

Erwood, R.J., Kesler, S.E., and Cloke, P.L., 1979,
Compositionally distinct, saline hydrothermal
solutions, Naica Mine, Chihuahua, Mexico: Econ. Geol.,
v. 74, no. 1, pp.95-108.

Exley, C.S., 1957, Magmatic differentiation and alteration
in the St-Austell granite: Quat. Jour. Geol. Soc.
London, v.114, Part 2, pp.197-230.

Exley, C.S., 1976, Observation on the formation of kaolinite
in the St-Austell granite, Cornwall: Clay Minerals,
v.11, pp. 51-62.

Faure, G., 1977, Principles of isotope geology, John Wiley &
Sons,Inc., New York, 464 p.

Faure, G., and Powell, J.L., 1972, Strontium isotope geology,
Springer-Verlag, Berlin, 188 p.

Fourcade, S., and Allègre, C.J., 1981, Trace element
behavior in granite genesis: a case study: the calc-
alkaline plutonic association from the Quérigut
complex, (Pyrenées, France): Cont. Mineral. Petrol., v.
76, pp. 177-195.

Fullagan, P.D., Lemmon,R.E., and Ragland, P.C., 1971,
Petrochemical and geochronological studies of plutonic
rocks in the Southern Appalachians: Part I, The
Salisbury pluton: Geol. Soc. America Bull., v. 82,
pp. 409-416.

Gazel, J., Lasserre, M., Limasset, J., and Vachette, M.,
1963, Ages absolus des massifs granitiques ultimes et
de la minéralisation en étain du Cameroun central:
Acad. Sci., Paris, France, C.R., v. 255, no. 2, pp.
2875-2878.

Gazel, J., 1956, Geologic Map of Cameroon.

Gordon, G.E., Randle, K., Goles, G.G., Corliss, J.B.,
Beeson, M.H., and Oxley, S.S., 1968, Instrumental
activation analysis of standard rocks with
high-resolution Gamma-ray detectors: Geochim. et
Cosmochim. Acta, v. 32, pp. 369-396.

Gouhier, J., and Nougier, J. and D., 1974, Contribution à
l'étude volcanologique du Cameroun ("Ligne du Cameroun"
-Adamaoua): Ann. Fac. Sci., Univ. Yaoundé, Cameroun,
no. 17, pp. 3-48.

Gouhier, J., and Rollet, M., 1978, La structure annulaire de
Golda Zuelva (Cameroun), VI Réun. ann. sci. Terre,
Paris, p.189.

Haas, J.L., Jr., 1971, The effect of salinity on the maximum thermal gradient of a hydrothermal system at hydrostatic pressure: Econ. Geol., v. 66, pp. 940-946.

Harvey, P.K., Taylor, D.M., Hendry, R.D., and Bancroft, 1973, An accurate fusion method for the analysis of rocks and chemically related materials by X-ray fluorescence spectrometry: X-ray Spect., v. 2, pp. 33-44.

Haskin, L.A., Frey, F.A., Schmitt, R.A., and Smith, R.H., 1966, Meteoritic, solar, and terrestrial rare-earth distributions: Physics and chemistry of the Earth, v. 7, 316 p.

Haynes, F.M., and Titley, S.R., 1980, The evolution of fracture-related permeability within the Ruby Star granodiorite, Sierrita porphyry Cu deposit, Pima County, Arizona: Econ. Geol., v. 75, pp. 673-683.

Hemley, J.J., and Jones, W.R., 1964, Chemical aspects of hydrothermal alteration with emphasis on hydrogen metasomatism: Econ. Geol., v. 59, pp. 538-569.

Hollister, V.F., 1978, Geology of the Porphyry Copper Deposits of the Western Hemisphere: S.M.E., A.I.M.M.P.E., Inc., New York, 219 p.

Hosking, K.F.G., 1979, Tin distribution patterns: Geol. Soc. Malaysia, Bull. no. 11, pp.1-70.

Jackson, N.J., 1979, Geology of the Cornubian Tin field ´A Review´: Geol. Soc. Malaysia, Bull. no. 11, pp. 209-237.

Keevil, N.B., 1942, Vapor pressures of acqueous solutions at high temperatures: Jour. Amer. Chem. Soc., v. 64, pp. 841-850.

Kelly, W.C., and Rye, R.O., 1979, Geologic, fluid inclusion, and stable isotope studies of the tin-tungsten deposits of Panasqueira, Portugal: Econ. Geol., v. 74, no. 8, pp. 1721-1819.

Kelly, W.C., and Turneaure, F.S., 1970, Mineralogy, paragenesis and geothermometry of the tin and tungsten deposits of the eastern Andes, Bolivia: Econ. Geol., v. 65, no. 6, pp. 609-680.

Kistler, R.W., and Peterman, Z.E., 1973, Variations in Sr, Rb, U, Na, and initial 87Sr/86Sr in Mesozoic granitic rocks and intruded wall rocks in Central California: Geol. Soc. America Bull., v. 84, pp. 3489-3512.

Knapp, R.B., and Norton, D., 1981, Preliminary numerical analysis of process related to magma crystallization

and stress evolution in cooling pluton environments: American J. of Science, v. 281, pp. 35-68.

Koch, P., 1953, Carte géologique de reconnaissance du Cameroun, Feuille no. NB 32 NE-E41, Banyo,avec notice explicative, Imp. Nat., Paris.

Koch, P., 1959, Le Précambrien de la frontière occidentale du Cameroun Central: Bull. Dir. Mines et Géol., Cameroun, no. 3, pp. 160-164 and pp. 211-217.

Kosterin, A.V.,1959, The possible modes of transport of the rare earths by hydrothermal solutions: Geochemistry, no. 4, pp. 381-387.

Lameyre, J., Marot, A., Zimine, S., Cantagrel, J.M., Dosso, L., and Vidal, Ph., 1976, Chronological evolution of the Kerguelen Islands syenite-granite ring complex: Nature, v. 263, pp. 306-307.

Laplaine, L., 1969, Indices minéraux et ressources minérales du Cameroun: Bull. Dir. Mines et Géol., Cameroun, no. 5, pp. 63-73.

Lasserre, M., 1964, Mésures d´ages absolus sur les séries précambriennes et paléozoiques du Cameroun (Afrique équatoriale): C.R., Acad. Sci., Paris, France, v. 258, pp. 998-1000.

Lasserre, M., 1964, Etude géochronologique par la méthode rubidium-strontium de quelques échantillons en provenance du Cameroun: Ann. Fac. Sci., Univ. Clermont-Ferrand, no. 25, Géol. et Min., Fasc. no.8, Etudes géochronologiques I, pp. 53-67.

Lasserre, M., 1966, Confirmation de l´existence de granites tertiaires au Cameroun (Afrique équatoriale): Bull. B.R.G.M., France, no. 3, pp. 141-148.

Lasserre, M., 1975, Age libériens des formations à pyroxène du Sud-Cameroun: 3e R.A.S.T., Montpellier, p. 217.

Lasserre, M., 1978, Mise au point sur les granitoides dits "ultimes" du Cameroun: gisement, pétrographie et géochronologie: Bull. B.R.G.M., France, 2e série, Sect. IV, no. 2, pp. 143-159.

Lasserre, M., and Soba,Dj., 1976, Age libérien des granodiorites et des gneiss à pyroxène du Cameroun méridional: Bull. B.R.G.M., France, 2e série, sect. IV, no. 1, pp.17-32.

Lasserre, M., and Soba Dj., 1976, Ages cambriens des

granites de Nyibi et de Kongolo (Centre-Est Cameroun):
Acad. Sci. Paris, France, C.R., no. 283, Série D,
pp.1695-1698.

Lasserre, M., Tempier, P., and Suire, J., 1981, Age (Rb/Sr)
cambrien supérieur de quelques granites camerounais
situés au sein de la zone mobile de l'Afrique centrale:
Acad. Sci. Paris, France, C.R. no. 292, série II,
pp. 903-908.

Lowell, J.D., and Guilbert, J.M., 1970, Lateral and vertical
alteration-mineralization zoning in porphyry ore
deposits: Econ. Geol., v. 65, pp. 373-408.

Lyakhovich, V.V.,1970, Distribution of rare earths among the
accessory minerals of granites: Geochem. Int., v.4, p.
691-696.

Maaløe, S., and Wyllie, P.J., 1975, Water content of a
granite magma deduced from the sequence of
crystallization determined experimentally with water-
undersaturated conditions: Contrib. Mineral.
Petrol.,v. 52, pp. 175-191.

Martin, R.F., and Bowden, P., 1981, Peraluminous granites
produced by rock-fluid interaction in the Ririwai non-
orogenic ring-complex, Nigeria: Mineralogical evidence:
Canadian Mineralogist, v. 19, pp. 65-82.

Miller, C.F., and Mittlefehldt, D.W., 1979, Rare earth
element depletion accompanying differentiation of
felsic igneous rocks: Geol. Soc. America, Abstracts
with programs, v. 11, pp. 479-480.

Mitchell, A.H.G., 1979, Rift-, subduction- and collision-
related tin belts: Geol. Soc. Malaysia, Bull. no. 11,
pp. 81-102.

Moorbath, S., and Bell, J.D., 1965, Strontium isotope
abundance studies and rubidium-strontium age deter-
minations on Tertiary igneous rocks from the Isle of
Skye, NW Scotland: J. of Petrology, v. 6, part 1, pp.
37-66.

Morawietz, F.H., 1968, Etude des gisements de cassitérite et
de wolframite près de Mayo-Darlé, Cameroun: Salzgitter
n Industriebau Gesellschaft MBH, Salzgitter-Druette,
Allemagne Fédérale, 146 p.

McCall, G.J.H., and Hornung, G., 1972, A geochemical study
of Silali volcano, Kenya, with special reference of the
origin of the intermediate-acid eruptives of the
Central Rift Valley: in R.W. Girdler (ed), East
African Rifts, Tectonophysics, v. 15, no. 1/2, pp.
97-113.

McLennan, S.M., and Taylor, S.R., 1979, Rare earth element mobility associated with uranium mineralization: Nature, v. 282, pp. 247-250.

Norman, D.I., Holt, L.E., and Landis, G.P., 1979, Chemistry of post-magmatic fluids associated with alkalic intrusives, Oslo, Norway (abstract): Eos (Amer. Geophys. Union, Trans.), v. 60, no. 46, p. 488.

Norman, D.I., and Trangcotchasan, Y., 1982, Mineralization and fluid inclusion study of the Yod Nam tin mine, southern Thailand: in Metallization Associated with Acid Magmatism, Evans, A.M., ed., John Wiley & sons Ltd., pp. 261-272.

Norrish, K., and Hutton, J.T., 1969, An accurate X-ray spectrographic method for the analysis of a wide range of geological samples: Geochim. Cosmochim. Acta, v. 33, pp. 431-454.

Norton, D.L., and Cathles, L.M., 1973, Breccia pipes - products of exsolved vapor from magmas: Econ. Geol., v. 68, pp. 540-546.

Nougier, J., and Lameyre, J., 1973, Les nordmarkites des îles Kerguelen (T.A.A.F.) dans leur cadre structural. Problème de leur origine et de celle des domaines océaniques: Bull. Soc. Géol. France, (7), v. XV, no. 3-4, pp.306-312.

Petersen, U., Noble, D.C., Arenas, M.J., and Goodel, P.C., 1977, Geology of the Julcani mining district, Peru: Econ. Geol., v. 72, pp. 931-949.

Potter II, R.W., Clynne, M.A., and Brown, D.L., 1978, Freezing point depression of aqueous sodium chloride solutions: Econ. Geol., v. 73, no. 2, pp. 284-285.

Rehrig, W.A., and Heidrick, T.L., 1972, Regional fracturing in Laramide stocks of Arizona and its relationship to porphyry copper mineralization: Econ. Geol., v. 67, pp. 198-213.

Rivas, S., 1979, Geology of the principal tin deposits of Bolivia: Geol. Soc. Malaysia, Bull. no. 11, pp. 161-180.

Roedder, E., 1962, Studies of fluid inclusions I: Low temperatures application of a dual-purpose freezing and heating stage: Econ. Geol., v. 57, pp. 1045-1065.

Roedder, E., 1972, Composition of fluid inclusions: U.S. Geol. Survey Prof. Paper 440-JJ, 164 p.

Roedder, E., 1979, Fluid inclusions as samples of ore

fluids: in Geochemistry of hydrothermal ore deposits, 2nd edition (Barnes,H.L.,editor), John Wiley & Sons, New York, pp. 684-737.

Shcherba, G.N., 1970, Greisens: Int. Geol.Rev., v. 12, no. 2, pp. 114-151; pp. 239-254.

Sheppard, S.M.F., 1977, The Cornubian batholith, SW England: D/H and 18O/16O studies of kaolinite and other alteration minerals: J. Geol. Soc. London, v. 133, pp. 573-591.

Sillitoe, R.H., Halls, C., and Grant, J.N., 1975, Porphyry tin deposits in Bolivia: Econ. Geol., v. 70, pp. 913-927.

Sourirajan, S., and Kennedy, G.C., 1962, The system H2O-NaCl at elevated temperatures and pressures: Am. Jour. Sci., v. 260, pp. 115-141.

Stemprok, M., 1977, The source of tin, tungsten and molybdenum of primary ore deposit: in Symposium Metallization Associated with Acid Magmatism, (Stemprok, M., Burnol, L., Tischendorf,G.,editors), Geol. Survey-Prague 2., pp. 127-166.

Stuckless, J.S., and Miesch, A.T., 1981, Petrogenetic modeling of potential uranium source rock, Granite Mountains, Wyoming: U.S. Geol. Surv. Prof. Paper no. 1225, 34 p.

Taylor, R.G., 1979, Geology of tin deposits: Elsevier Scientific Publishing Co., New York, 543 p.

Tchoua, F., 1974, Contribution à l´étude géologique et pétrologique de quelques volcans de la ligne du Cameroun (Monts Manengouba et Bamboutos). Thèse Etat, Univ. Clermont, 347 p.

Tempier, P., and Lasserre, M., 1980, Géochimie des massifs "ultimes" du Cameroun: rapports entre l´évolution magmatique, l´âge et la position géographique. Comparaisons avec les "younger granites" du Nigeria: Bull. Soc. Géol. France, t. 12, no. 2, pp. 203-211.

Tischendorf, G., 1973, The metallogenic basis of tin exploration in the Erzgebirge: Trans. Inst. Min. and Met., Sect. B, v. 82, pp. B9-B24.

Tischendorf, G., 1977, Geochemical and petrographic characteristics of silicic magmatic rocks associated with rare-element mineralization: in Metallization Associated with acid magmatism, Geol. Survey Prague 2, pp. 41-96.

Titley, S.R.,1975, Geological characteristics and environment of some porphyry copper occurrences in the South-western Pacific: Econ. Geol., v. 70, pp.499-514.

Van Schmus, W.R., 1971, Ages of lamprophyre dikes of the Mongowin Pluton, north shore of Lake Huron, Ontario, Canada: Canadian Jour. Earth Sci., v. 8, pp.1203-1209.

Vera, R.H., and Van Schmus, W.R., 1974, Geochronology of some Precambrian rocks in the southern Front Range, Colorado: Geol. Soc. America Bull., v. 85, pp. 77-82.

Vidal, P., Dosso, L., Bowden, P., and Lameyre, J., 1978, Strontium isotope geochemistry in syenite-alkaline granite complexes: in Origin and distribution of the elements (Ahrens,L.H.,editor), Phys. Chem. Earth, v. 11, pp. 223-231.

Wilson, J.W.J., Kesler, S.E., Cloke, P.L., and Kelly, W.C., 1980, Fluid inclusion geochemistry of the Granisle and Bell porphyry copper deposits, British Columbia: Econ. Geol., v. 75, no. 1, pp. 45-61.

Wright, J.B., 1970, Controls of mineralization in the older and younger tinfields of Nigeria: Econ. Geol., v. 65, no. 8, pp. 945-951.

Wright, T.L., and Doherty, P.C., 1970, A linear programming and least-squares computer methods for solving petrologic mixing problems: Geol. Soc. America, Bull. no. 81, pp. 1995-2008.

York, D., 1966, Least-squares fitting of a straight line: Canadian Jour. Physics, v. 44, pp. 1079-1086.

This dissertation is accepted on behalf of the faculty of the

Institute by the following committee:

David J. Norman
Adviser

A. J. Budding

Scott C. Coulee

James M. Robertson

George Austin

29 April 1982
Date